

Chiral QCD phase in equilibrium with Hadron Gas and the location of the critical point

N. G. Antoniou*, F. K. Diakonos† and A. S. Kapoyannis‡

Faculty of Physics, University of Athens, GR-15784 Greece

August 15, 2023

Abstract

We develop a description of the equation of state of QCD matter with restored chiral symmetry, which is in thermal and chemical equilibrium with the hadronic phase. The hadron gas is described with thermodynamically consistent volume corrections. The chiral phase is composed of a set of few quark condensates, each of which corresponds to a family of hadrons with specific quark content. On the boundary between the two phases we apply the requirement of conservation of particle numbers per family. We use lattice calculations for temperatures below the transition curve to determine hadronic volumes. We find that the pion system plays decisive role in the shift of the transition from higher order (crossover) to first order. For four volume models we calculate the location of the critical point as function of critical temperature T_c at vanishing baryon density. Particularly, if we additionally impose the equality between the densities of quarks contained in mesons and baryons, we find a critical point residing in the interval of baryon chemical potential $\mu_B \simeq 233\text{-}267$ MeV and of temperature $T \simeq 153\text{-}158$ MeV.

Keywords: QCD critical point, Hadron gas, chiral phase

1 Introduction

The QCD phase diagram is a subject of intense research during the last years. This phase diagram describes the transition to hadronic matter at lower temperatures, a phase with equation of state (EoS) well described by different versions of the Hadron Gas (HG) model [1]. However, knowledge of the EoS of the phase at higher temperatures is accessible only through lattice calculations that are limited mainly to the zero baryon density regime [2]. The ideal quark-gluon plasma can, only, be reached at extremely high temperatures. The region which resides at temperatures higher than those determining the boundaries of the hadronic phase, is proposed to be associated with several exotic phases, like chiral-density waves, crystalline colour superconductivity, gluonic phase and quarkyonic matter [3]. The knowledge about this region is still developing and our work aims at this direction. We will focus on describing a model for the EoS at the high temperature region just above the transition to HG curve. The derivation of our model is based on a few useful, to our opinion, observations which are listed in the following:

*Dedicated to the memory of N. G. Antoniou (1939-2020)

†email: fdiakono@phys.uoa.gr

‡email: akapog@phys.uoa.gr

- (a) The chiral condensate, which acts as the order parameter of the chiral restoration, changes rather sharp with temperature. On the contrary deconfinement, connected with the renormalized Polyakov loop, needs a wider temperature interval to be completed [4]. This suggests that chiral restoration can be completed well before quarks are “dissolved” to independent entities ¹.
- (b) In [6] an equivalent description of the Lattice results at vanishing baryonic density has been carried out, using one particle states with mass and number of states calculated from the fit to these results. It was found that the quark-gluon interacting system, when crossing the critical temperature T_c , exhibits an abrupt decrease in the number of states and, also, in the respective mass. Moreover, the minimum value of the degeneracy factor, reached just above T_c , cannot be attributed to deconfined quark degrees of freedom, thus, leading to the conclusion that *these states should be still quark condensates*. Based on this observation, as well as the previous one (a), we will adopt in the present work the viewpoint that the quarks remain confined in hadronic type condensates even at temperatures above the QCD transition line.
- (c) In [7] a model has been developed which simulates the parity doubling of the nucleon. In this model chiral symmetry and an explicit mass term for the nucleon can coexist without contradiction. The nucleon has a partner of opposite parity. These particles have different masses in the broken symmetry phase (HG). However in the restored chiral phase these masses become degenerate. In [8], with the use of lattice simulations, a similar behaviour is found for opposite parity pairs of N , Δ and Ω baryons.
- (d) One of the proposed exotic phases, situated at high density and relatively low temperatures is the quarkyonic phase, which is valid for a system with a large number of colours N_c [9]. In the quarkyonic matter there are quarks forming a Fermi sea, but, also, baryons which occupy a Fermi surface. These baryonic particles are connected with phenomena like superconductivity and superfluidity. Likewise, here we assume that hadronic states can exist at densities and temperatures higher than those characterizing the hadronic phase.
- (e) Finally an important issue, which arises when considering the crossing of a transition curve to enter the HG phase from a higher temperature phase, is the conservation of quantum numbers (baryon number, strangeness, charge, etc.) which are carried by the quarks. This conservation is a necessary constraint additional to the continuity of chemical potentials and pressure [10], assuming thermal and chemical equilibrium between the two phases. However, these constraints alone are insufficient to determine how a certain number of quarks above the transition curve can be grouped to form certain number of hadrons below this curve. For example, the conservation of the net baryonic density $n_b - n_{\bar{b}}$, cannot insure the continuity of the multiplicities of proton and antiprotons separately. The latter can be explained by the sudden appearance or vanishing of quark-antiquark pairs upon crossing the transition line which change the number of quarks and antiquarks without altering the net baryon density. However, such a scenario should be excluded in the case of a smooth crossover.

Having presented the key observations which inspire our approach, we now proceed to suggest our working hypothesis in this paper:

¹Our argument rests on the width of the deconfinement transition not on the mean temperature of its occurrence. Indeed the mean temperature of the deconfinement and chiral transition can be the same [5], whereas the gradual nature of the deconfinement transition can have the effect that it is extended for a considerable temperature interval above the mean temperature. This temperature interval, which is due to the system’s finite size, may allow for the organization of the quarks in hadron-like particles.

A result of the partial chiral restoration is that the resonances with different masses and the same quark content, occurring below the critical temperature, become quasi-particle states (condensates), which are degenerate in mass, above the critical temperature.

The emerging picture we adopt is that the quark masses are reduced with the increase of temperature, while they are still interacting to form “hadronic-like” particles. This leads to an equivalent reformulation of the above hypothesis: *All the resonances with the same quark content at lower temperatures originate from the same quasi-particle state at higher temperatures.* As a consequence, since chiral symmetry breaking causes increase in the mass, we cannot allow the mass of a “hadronic-like” quasi-particle in the chiral phase to be greater than the mass of the lightest hadron in the broken symmetry phase. With this hypothesis we are able to solve the issue raised in remark (e) in a seamless way.

Another important point we are confronted with in this work is the fact that the exact position of the critical point depends crucially on the size of the hadronic volumes which encode the repulsive part of the strong interaction. To handle this uncertainty we estimate the hadronic volumes by fitting the Hadron Gas model with volume corrections for temperatures lower than the critical temperature to the lattice pressure with (2+1) flavours for zero [2] or finite [11] baryon-chemical potential. These, lattice QCD based, hadron volume determinations, together with the hypothesis of mass degeneration presented in the previous paragraph, constitute the backbone of the model we employ here to explore the QCD phase diagram region close to the boundary of the HG phase.

The structure of the following part of our paper is as follows. In section 2 we present in more detail the main ideas of our model. In section 3 we use them to propose a procedure for the determination of the critical point. In section 4 we investigate the effect on HG of volumes depending on temperature or chemical potentials and present results for hadron volumes calculated from fits to the lattice-pressure at zero baryon-density. In section 5 we use the results of sections 2, 3 and 4 to propose four different models for the description of the volume corrections leading to the determination of the critical point location in terms of T_c (critical temperature at zero baryonic density). The first model assumes a common radius for all hadrons which is independent from temperature and chemical potential. The second model assumes a common hadronic radius for all species which is varying with temperature. The third model assumes different hadronic radius for mesons which vary with temperature and for baryons which vary with baryon-chemical potential. The fourth model utilises again a common hadron radius which depends simultaneously on both temperature and baryon-chemical potential. In section 6 we investigate an additional condition for the determination of the critical point which ensures equality of the density of the quarks which are enclosed in mesons and baryons of the hadron gas. Finally, in section 7 we summarise our findings and record our concluding remarks.

2 Modelling the hadron-quark condensate transition

The HG phase, in its simplest form, can be described as point particles in the Boltzmann approximation with total particle density:

$$n_{HG,Bo}^{pt} = \frac{T}{2\pi^2} \sum_i \lambda_i \sum_j g_{ij} m_{ij}^2 K_2 \left[\frac{m_{ij}}{T} \right] , \quad (1)$$

where λ_i is the fugacity corresponding to a specific group of hadrons that have the same quark content and which will be called as “family”. Also, $\lambda_i = \lambda_B^k \lambda_S^l \lambda_Q^n$ if the particles of the family carry baryon number B equal to k , strangeness S equal to l and electric charge Q equal to n . The index j runs over all resonances of the i family. Since i runs over particles and antiparticles, g_{ij} is the degeneracy factor due only to the spin of the particle and m_{ij} is the respective mass. Equation

(1) easily shows that the HG partition function is a sum of terms, each of which corresponds to a specific fugacity.

Next we turn to the description of the QCD phase at temperatures just above the transition curve. In this phase the constituent quark masses are reduced due to the partial chiral restoration and in effect the mass of the corresponding quasi-particle is also reduced. Therefore, we shall call this phase in the following as “chiral” phase. We will, also, use the “tilde” ($\tilde{}$) symbol to denote all quantities associated with this phase. We consider it to be a sum of quark condensates which represent quasi-particles carrying fugacities λ_i and degeneracy factors \tilde{g}_i , where the index “ i ” runs over the families. Then the total particle density in the Boltzmann approximation for the chiral phase reads:

$$\tilde{n}_{Bo} = \frac{T}{2\pi^2} \sum_i \lambda_i \tilde{g}_i \tilde{m}_i^2 K_2 \left[\frac{\tilde{m}_i}{T} \right] . \quad (2)$$

If the condensates in the chiral phase have the same quark content as the particles of the HG phase, then the particle number conservation at an arbitrary point (T, λ_i) of the transition curve is converted to the conservation of the number of particles per family. For N existing families in the HG, this accounts to N equations, each denoted by the index i , of the form:

$$V_{HG} \sum_j g_{ij} m_{ij}^2 K_2 \left[\frac{m_{ij}}{T} \right] = \tilde{V} \tilde{g}_i \tilde{m}_i(T)^2 K_2 \left[\frac{\tilde{m}_i(T)}{T} \right] , \quad (3)$$

where $V_{HG}(\tilde{V})$ is the system volume in the HG (chiral) phase. Due to continuity criteria, in the crossover $V_{HG} = \tilde{V}$, while in the 1st order region $V_{HG} \neq \tilde{V}$. In order to fulfil eqs. (3), we allow the masses in the chiral phase to be functions of temperature, $\tilde{m}_i(T)$. In principle, the N equations in (3), since they do not depend on the fugacities, can be fulfilled at any point of a transition curve which may depend on fugacities.

Since chiral restoration is associated with the reduction of the quark masses, we expect the quasi-particle, which contains the relevant quarks, to reduce its mass. So we can associate the chiral state of each family with the ground mass state of the HG phase. This HG state will attribute the degeneracy factor $g_{i1} = \tilde{g}_i$ to the respective chiral phase state. However, one can easily see that eqs. (3) are impossible to be fulfilled if $\tilde{m}_i(T) = m_{i1}$ since the sum of several positive terms cannot be equal to the first term only. To overcome this inconsistency one should require:

$$0 < \tilde{m}_i(T) \leq m_{i1} . \quad (4)$$

Then, eqs. (3) could in principle be fulfilled, since the functions $K_2 \left[\frac{\tilde{m}_i(T)}{T} \right]$ are sensitive enough increasing exponentially with decreasing $\tilde{m}_i(T)$. The constraint (4) has a straightforward physical interpretation: the quasi-particle existing in the chiral restored phase will produce in the chiral broken (HG) phase, among other resonances, the ground state particle with the minimum mass among all resonances, m_{i1} . Since the breaking of chiral symmetry increases mass, the chiral mass cannot be greater than m_{i1} . So, we will set as the upper limit for the masses $\tilde{m}_i(T)$ the respective mass m_{i1} of the lightest hadron in the i family.

It can be checked that for some families eqs. (3) cannot be fulfilled for any value of mass $\tilde{m}_i(T)$ in the range of relation (4). This fact forces us to turn to a more realistic description of the HG phase. We have to take into account the hadron volume corrections which will effectively reduce all the particle number densities. For consistency reasons we will, also, use the correct quantum statistics (Bose-Einstein or Fermi-Dirac). The volume corrections in the HG have been accounted for in a thermodynamically consistent way which avoids negative contributions to the system volume [17]. The partial pressure of a point particle j belonging to the i family using the correct quantum

statistics is given by:

$$p_{ij}^{pt}(T, \mu_i) = \frac{g_{ij}}{2\pi^2} \int_0^\infty dk \frac{k^4}{(k^2 + m_{ij}^2)^{1/2}} f(k; m_{ij}, \mu_i, a) , \quad (5)$$

$$f(k; m_{ij}, \mu_i, a) \equiv \left[\exp \left(\frac{(k^2 + m_{ij}^2)^{1/2} - \mu_i}{T} \right) + \alpha \right]^{-1} , \quad (6)$$

where $\alpha = -1$ (+1) for bosons (fermions). If each particle carries volume v_{ij} , then the total HG pressure can be calculated from the partial pressures of the point particles. The relevant chemical potentials μ_i have to be replaced by the chemical potentials $\widehat{\mu}_i$ [17]:

$$p_{HG}(T, \dots, \mu_i, \dots) = p_{HG}^{pt}(T, \dots, \widehat{\mu}_i, \dots) = \sum_i \sum_j p_{ij}^{pt}(T, \widehat{\mu}_i) , \quad (7)$$

$$\widehat{\mu}_i = \mu_i - v_{ij} p_{HG}(T, \dots, \mu_i, \dots) . \quad (8)$$

Eq. (7) has to be solved numerically for the system pressure p_{HG} . The density for point particles in the Bose/Fermi statistics reads:

$$n_{ij}^{pt}(T, \mu_i) = \frac{g_{ij}}{2\pi^2} \int_0^\infty dk k^2 f(k; m_{ij}, \mu_i, a) . \quad (9)$$

Then we can proceed with the calculation of the particle densities with volume corrections:

$$n_{HG,ij}(T, \dots, \mu_i, \dots) = \frac{n_{ij}^{pt}(T, \widehat{\mu}_i)}{1 + \sum_r \sum_s v_{rs} n_{rs}^{pt}(T, \widehat{\mu}_r)} , \quad (10)$$

where the volume of the ij particle is connected to the corresponding radius [17] through:

$$v_{ij} = 4(4\pi/3)r_{ij}^3 \quad (11)$$

With the use of the volume corrections and the Bose/Fermi statistics, eqs. (3), for the equality of particle densities between the HG and the chiral phase, are replaced by:

$$V_{HG} \sum_j n_{HG,ij}(T, \mu_i) = \tilde{V} \tilde{n}_i(T, \mu_i) \Rightarrow$$

$$V_{HG} \frac{n_{ij}^{pt}(T, \widehat{\mu}_i)}{1 + \sum_r \sum_s v_{rs} n_{rs}^{pt}(T, \widehat{\mu}_r)} = \tilde{V} \frac{\tilde{g}_i}{2\pi^2} \int_0^\infty dk k^2 f(k; \tilde{m}_i(T, \mu_i), \mu_i, a) . \quad (12)$$

The fugacities in the densities do not factorize when the Bose/Fermi statistics are used. As a consequence, in eq. (12) the chiral states carry mass which is different between particles and antiparticles. This dependence, which will be denoted as $\tilde{m}_i(T, \mu_i)$, is not surprising since we are considering matter at positive baryon densities, and we are allowing the masses of baryons and antibaryons to change. Also, while in the Boltzmann approximation particles and antiparticles can be grouped together in the same family, in the Bose/Fermi statistics the particles have to form separate family from the respective antiparticles. However, as it will become evident in the next section, the mass difference between particles and antiparticles is low.

In the treatment of two QCD phases in equilibrium it is usual to apply the condition of the conservation of quantum numbers carried by the quarks [10]. Here we impose the more strict condition of the equality of the particle numbers per family. We assume that quarks have already been grouped in condensates at the chiral phase near the transition curve, which, after chiral

breaking, evolve to the hadronic spectrum of the specific family. The conservation of these particle numbers automatically insures the conservation of quantum numbers, e.g. for the baryon-number B :

$$N_{B,HG} = \sum_i k_i \sum_j V_{HG} n_{HG,ij}(T, \mu_i) = \sum_i k_i \tilde{V} \tilde{n}_i(T, \mu_i) = \tilde{N}_B \quad , \quad (13)$$

where k_i equals to the baryon-number carried in the particles of the i family, common to both the HG and the chiral phase and n refers to the particle number density.

To complete the set of requirements for equilibrium between the two phases we have to demand for the equality of pressures. In the chiral phase, apart from the quark condensates which contribute partial pressure \tilde{P}_q , also the gluons show considerable pressure, \tilde{P}_g , for $T > T_c$ [18,19]. Thus:

$$P_{HG} = \tilde{P}_q + \tilde{P}_g - B_v \quad , \quad (14)$$

where B_v accounts for the possible influence of the vacuum. Eqs. (12), (14) constitute the minimum requirements for two phases in equilibrium. Since the two phases are described by different partition functions, continuation of first and higher order derivatives cannot be fulfilled by these equations alone. We use, though, these equations assuming that the region for the transition between the HG states and the chiral states is small. This allows to consider the transition curve of the phase diagram as points of equilibrium between the HG and chiral phases. Indeed, in a more complete description the quantities \tilde{P}_g and B_v should be taken into account. Also, smoothing functions, like in [20], would have to be introduced in the crossover region to ensure continuation of the first and higher order derivatives. However, this procedure would increase the free parameters of the model in cost of physical insight.

To complete this section we refer to the families where we have grouped the hadronic particles. Related information is given in Table 1. The used states are the ones listed in the summary table of ‘‘Particle Data Group’’ [22]². For simplicity we have neglected the dependence of the particles on the electric charge ($\lambda_Q = 1$). For this reason, when the lightest HG states in a family are nearly degenerate we consider as lowest mass their average value (e.g. $m_{31} = (m_p + m_n)/2$). Notice that some information for the lowest mass states presented in Table 1 have been taken from the Quark Model classification scheme in [21] (see the relevant review ‘‘Quark Model’’ therein).

In family 2a, we, also, omit the $f_0(500)$ state. In the previous publications of Particle Data Group it was listed as σ particle with mass ~ 800 MeV. This particle is considered to be a two-pion state [23]. For this reason we omit it from the HG spectrum. There is not enough information of how to distribute the Light Unflavoured Mesons (L.U.M.) with Isotopic Spin $I = 0$ among families 2a and 2b. For this reason we consider the conservation of the inclusive particle numbers of both families, according to the formula:

$$V_{HG} \left[\sum_j n_{HG,2aj}(T) + \sum_j n_{HG,2bj}(T) \right] = \tilde{V} [\tilde{n}_{2a}(T) + \tilde{n}_{2b}(T)] \quad . \quad (15)$$

Last equation does not contain enough information for fixing both chiral masses. For this reason we assume the ratio of the chiral masses to be equal to the respective ratio of the lowest mass HG states:

$$\frac{\tilde{m}_{2a}(T)}{\tilde{m}_{2b}(T)} = \frac{m_{2a,1}}{m_{2b,1}} \quad . \quad (16)$$

This particular choice influences only the calculations concerning families 2a and 2b. In the following we shall consider families 2a and 2b as a common family 2. An additional comment is here in order: for the Ω family only two states are known, the Ω^- , which is considered as the ground state, the

²We include all particle states containing only u , d and s quarks.

i	Sym- bol	Name	Quark Content	Ground Mass State	m_{i1} (MeV)	g_{i1}	λ_i	α
1	π	L.U.M., $I = 1$	$u\bar{d}, (u\bar{u} - d\bar{d})/\sqrt{2}, d\bar{u}$ (flavour- antisymmetric)	$\pi^{+,0,-}$	138,03941	3	1	-1
2a	η	L.U.M., $I = 0$	$(u\bar{u} + d\bar{d})/\sqrt{2}$ (flavour-symmetric, no s -quark)	η	547,862	1	1	-1
2b	η'	L.U.M., $I = 0$	$c_1(u\bar{u} + d\bar{d}) + c_2s\bar{s}$ (flavour-symmetric, with s -quark)	$\eta'(958)$	957,78	1	1	-1
3	N	N Baryons ($I = 1/2$)	uud, udd	p, n	938,918747	4	λ_B	+1
-3	\bar{N}	N Antibaryons ($I = 1/2$)	$\bar{u}\bar{u}\bar{d}, \bar{u}\bar{d}\bar{d}$	\bar{p}, \bar{n}	938,918747	4	λ_B^{-1}	+1
4	Δ	Δ Baryons ($I = 3/2$)	uuu, uud, udd, ddd (flavour-symmetric)	$\Delta^{++,+,0,-}$	1232	16	λ_B	+1
-4	$\bar{\Delta}$	Δ Antibaryons ($I = 3/2$)	$\bar{u}\bar{u}\bar{u}, \bar{u}\bar{u}\bar{d}, \bar{u}\bar{d}\bar{d}, \bar{d}\bar{d}\bar{d}$ (flavour-symmetric)	$\bar{\Delta}^{--,-,0,+}$	1232	16	λ_B^{-1}	+1
5	K	Strange Mesons	$u\bar{s}, d\bar{s}$	K^+, K^0	495,644	2	λ_S	-1
-5	\bar{K}	Antistrange Mesons	$\bar{d}s, \bar{u}s$	\bar{K}^0, K^-	495,644	2	λ_S^{-1}	-1
6	Λ	Λ Baryons ($I = 0$)	uds	Λ	1115,683	2	$\lambda_B\lambda_S^{-1}$	+1
-6	$\bar{\Lambda}$	Λ Antibaryons ($I = 0$)	$\bar{u}\bar{d}\bar{s}$	$\bar{\Lambda}$	1115,683	2	$\lambda_B^{-1}\lambda_S$	+1
7	Σ	Σ Baryons ($I = 1$)	uus, uds, dds	$\Sigma^{+,0,-}$	1193,154	6	$\lambda_B\lambda_S^{-1}$	+1
-7	$\bar{\Sigma}$	Σ Antibaryons ($I = 1$)	$\bar{d}\bar{d}\bar{s}, \bar{u}\bar{d}\bar{s}, \bar{u}\bar{u}\bar{s}$	$\bar{\Sigma}^{+,0,-}$	1193,154	6	$\lambda_B^{-1}\lambda_S$	+1
8	Ξ	Ξ Baryons	uss, dss	$\Xi^{0,-}$	1318,285	4	$\lambda_B\lambda_S^{-2}$	+1
-8	$\bar{\Xi}$	Ξ Antibaryons	$\bar{d}\bar{s}\bar{s}, \bar{u}\bar{s}\bar{s}$	$\bar{\Xi}^{+,0}$	1318,285	4	$\lambda_B^{-1}\lambda_S^2$	+1
9	Ω	Ω Baryons	sss	Ω^-	1672,45	4	$\lambda_B\lambda_S^{-3}$	+1
-9	$\bar{\Omega}$	Ω Antibaryons	$\bar{s}\bar{s}\bar{s}$	$\bar{\Omega}^+$	1672,45	4	$\lambda_B^{-1}\lambda_S^{-3}$	+1

Table 1: The families where the hadrons are grouped when the Bose/ Fermi statistics are used. We list the difference in the quark content and the difference in the flavour wave function where it exists. Also, we list the lowest mass hadron in the HG phase, which is the upper limit for the respective mass in the chiral phase, according to eq. (4).

$\Omega(2012)^-$ and the $\Omega(2250)^-$. Thus, there are probably missing states in this family and this may influence family specific properties. In order to reduce the impact of this missing information in our analysis we will occasionally neglect the, anyway very small, contribution of this family (as well as $\bar{\Omega}$), when referring to family specific results.

3 A Procedure to locate the Critical Point

We first need a transition curve upon which we shall impose the equality of particle multiplicities of the two phases in equilibrium. Lattice results for the QCD pressure do not fix the transition temperature T_c at zero baryon-chemical potential. A lowest value of $T_c = 154$ MeV is suggested by [2]. A chemical freeze-out curve evaluated from heavy-ion collisions is suggested to end at $\mu_B = 0$ at a temperature $T_{ch,0} \simeq 166$ MeV in [24]. It is natural to assume that the HG state (in which the hadron particles exist) cannot be retained in higher temperatures than T_c , thus

$$T_{ch,0} \leq T_c \quad (17)$$

On the other hand the results in [2] and [24] obey $T_{ch,0} > T_c$ which can be compatible with the relation (17) only if

$$T_{ch,0} \simeq T_c \quad (18)$$

In fact such a condition is also compatible with the analysis presented in [33] ($T_c = 157.5 \pm 1.5$ MeV) and [25] ($T_{ch,0} \simeq 157$ MeV), which suggest that the critical QCD temperature and the freeze-out temperature at zero baryon-chemical potential are very close, if not identical. We will adopt this scenario in the following, assuming that the chemical freeze-out curve [24] coincides with the chiral transition curve. This curve is parametrised [24] as:

$$T(\mu_B) = 166 - 0.139 \cdot 10^{-3} \mu_B^2 - 0.053 \cdot 10^{-9} \mu_B^4, \quad (19)$$

with T and μ_B measured in MeV. Here, we will use a more general parametrization of (19) in order to implement the fact that T_c is not uniquely defined and to fulfil $T_{ch,0} = T_c$

$$T = T_c - A(T_c) \mu_B^2 - B(T_c) \mu_B^4 \Rightarrow T = f_{fr}(\mu_B; T_c), \quad (20)$$

$$A(T_c) = 3.25 \cdot 10^{-6} \cdot T_c - 4.005 \cdot 10^{-4}, \quad B(T_c) = (2.5 \cdot 10^{-2} \cdot T_c - 0.468) \cdot 10^{-9}$$

This parametrization is valid in the interval $T_{ch,0} = (154-166)$ MeV and it leads to the freeze-out curve of [24] for $T_{ch,0} = 166$ MeV. The curves of eq. (20) approach the curve in [24] at high values of baryon-chemical potential, while they differ from it at low values of baryon-chemical potential (each approaches a different value of $T_{ch,0}$ at zero density). In that sense, T_c remains in eq. (20) a free parameter. Upon this curve we shall apply the conservation of particle numbers between the HG and the chiral phase. In fact, any choice for a transition curve is able to accommodate the constraints of particle conservation. However, the numerical results for the densities and chiral masses will depend on the particular choice.

We, also, impose the strangeness neutrality

$$\langle S \rangle_{HG} = 0 \quad (21)$$

Equations (20), (21) can be solved for a given value of T_c and so the thermodynamic parameters of temperature T and strange quark chemical potential μ_s can be expressed as a function of the baryon chemical potential μ_B , $T = T(\mu_B; T_c)$, $\mu_s = \mu_s(\mu_B; T_c)$. Following this procedure, in the next equations of this section there will be no explicit dependence on the parameters T and μ_s .

We will now investigate whether solutions of eqs. (12) for given values of T_c , μ_B exist. In the crossover region, the equality of volumes, $V_{HG} = \tilde{V}$, leads to the equality of densities for the i family:

$$\sum_j n_{HG,ij}(\mu_B; T_c) = \tilde{n}_i(\mu_B; T_c) \Rightarrow f_{vc,i}(\mu_B; T_c) \sum_j n_{HG,ij}^{pt}(\mu_B; T_c) = \tilde{n}_i(\mu_B; T_c) \Rightarrow$$

$$f_{vc,i}(\mu_B; T_c) = \frac{\tilde{n}_i(\mu_B; T_c)}{\sum_j n_{HG,ij}^{pt}(\mu_B; T_c)} , \quad (22)$$

where we have written the HG particle density with volume corrections as the product of the corresponding point particle density times a volume correction factor $f_{vc,i}$:

$$f_{vc,i}(\mu_B; T_c) \equiv \frac{\sum_j n_{HG,ij}(\mu_B; T_c)}{\sum_j n_{HG,ij}^{pt}(\mu_B; T_c)} , \quad (23)$$

which represents the ratio of the density with volume corrections of the family i to the corresponding density for point particles at specific conditions.

Eq. (22) should hold in the crossover region and, according to eq. (4), it can be fulfilled as long as the chiral mass for each family is less than the maximum allowed value. So the limit of the crossover region (critical point) is reached if for some family i :

$$\tilde{m}_i = m_{i1} \quad (24)$$

When last equation holds, then the right hand side of eq. (22) becomes:

$$R_i(\mu_B; T_c) \equiv \frac{\tilde{n}_{i,min}(\mu_B; T_c)}{\sum_j n_{HG,ij}^{pt}(\mu_B; T_c)} = \frac{n_{HG,i1}^{pt}(\mu_B; T_c)}{\sum_j n_{HG,ij}^{pt}(\mu_B; T_c)} . \quad (25)$$

Here as R_i we define the ratio of the density of the least mass particle to the density of the whole family i for specific conditions. The nominator of this ratio equals the minimum allowed density at the chiral phase at these conditions, which is achieved for the maximum allowed mass. With this definition we are led to

$$f_{vc,i}(\mu_B; T_c) = R_i(\mu_B; T_c) \Rightarrow \sum_j n_{HG,ij}(\mu_B; T_c) = n_{HG,i1}^{pt}(\mu_B; T_c) , \quad (26)$$

i.e. the critical point is reached at the conditions where the density of a family (with volume corrections) becomes equal to the density of the point particle of the family with least mass.

The quantities $f_{vc,i}$ and R_i in the above equation, also, depend on μ_s which is calculated by solving eq. (21). Actually, μ_s is almost independent of the particle volumes in the Bose/Fermi statistics, while is completely independent in the Boltzmann approximation, since in this case the strangeness neutrality condition reduces to $\langle S \rangle^{pt} = 0$. To show that this dependence is negligible we depict in Fig. 1 the solution for the strange quark chemical potential $\mu_s = \mu_B/3 - \mu_S$ for the point particle case ($r_0 = 0$), as well as, for different values of the hadron radius r_0 and we observe that the results almost coincide. We present calculations for a high and a low value of T_c .

The only dependence of ratios R_i on particle volumes comes through μ_s . In turn, we have shown that μ_s weakly depends on particle volumes. Thus, we can draw our conclusions using R_i calculated for the $r_0 = 0$ case. The $f_{vc,i}$ we have defined, carry, then, almost all the dependence on the particle volumes corrections. Also, these volume correction factors are practically the same for all families, provided that the same radius r_0 is used for all hadrons. This property, which is ap-

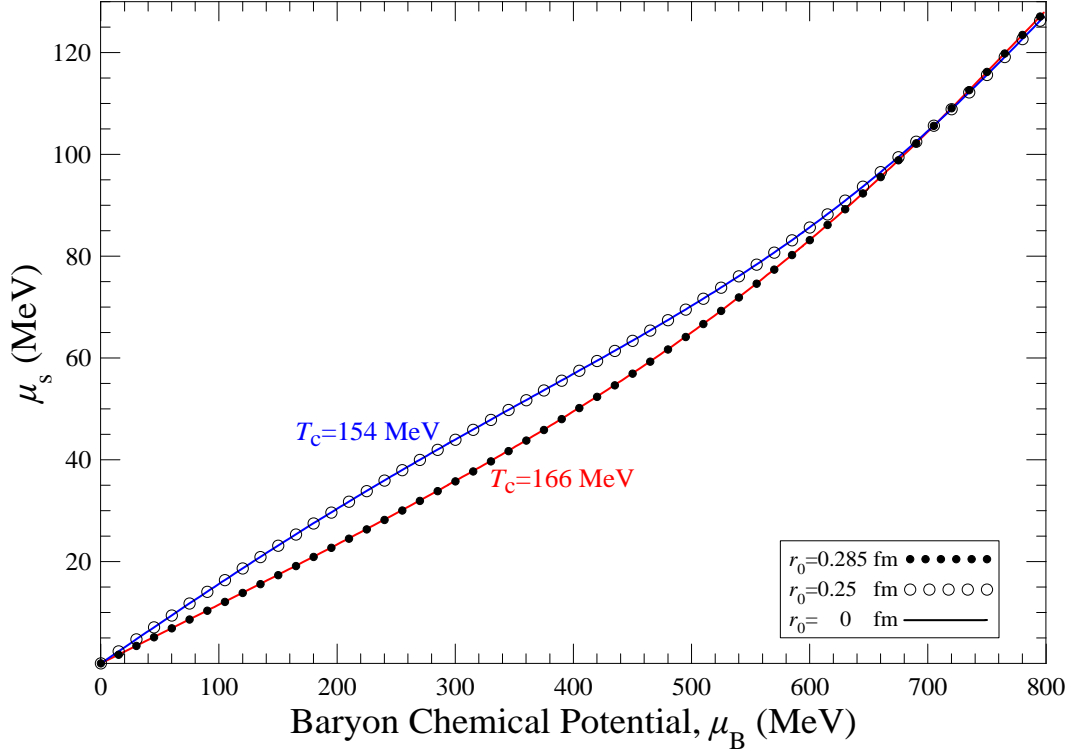


Figure 1: The dependence of the strange-quark chemical potential μ_s , which solves the $\langle S \rangle = 0$ equation for given hadronic radius r_0 , on the baryon chemical potential μ_B . Shown are two cases which correspond to a high value of $T_c = 166$ MeV (lower curves) and a low value of $T_c = 154$ MeV (upper curves) respectively. Continuous lines correspond to $r_0 = 0$ fm (point particle case), solid circles to $r_0 = 0.285$ fm and open circles to $r_0 = 0.25$ fm. It is evident that volume corrections practically do not affect the calculated value of μ_s .

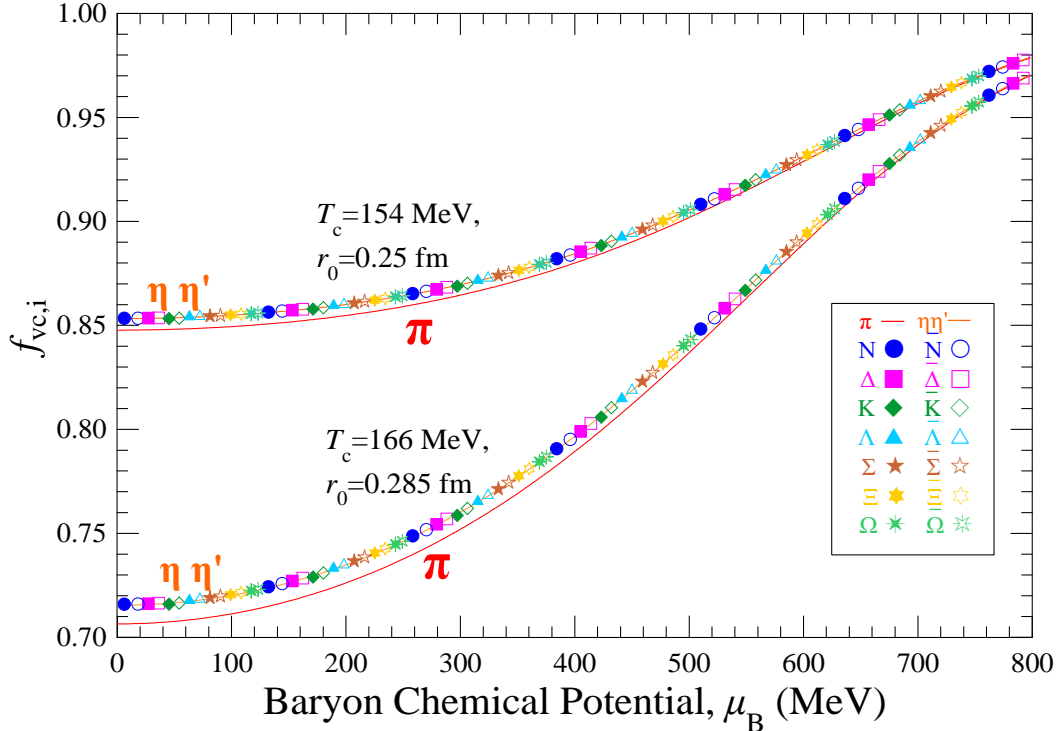


Figure 2: The volume correction factor f_{vc} for the hadronic families, with Bose/Fermi statistics for $T_c = 166$ MeV and radius $r_0 = 0.285$ fm (lower curves) and for $T_c = 154$ MeV and radius $r_0 = 0.25$ fm (upper curves), as function of the baryon chemical potential μ_B . Since the curves for all families except the pions are close we depict, instead of almost coinciding curves, calculations at distinct points of non-overlapping lattices.

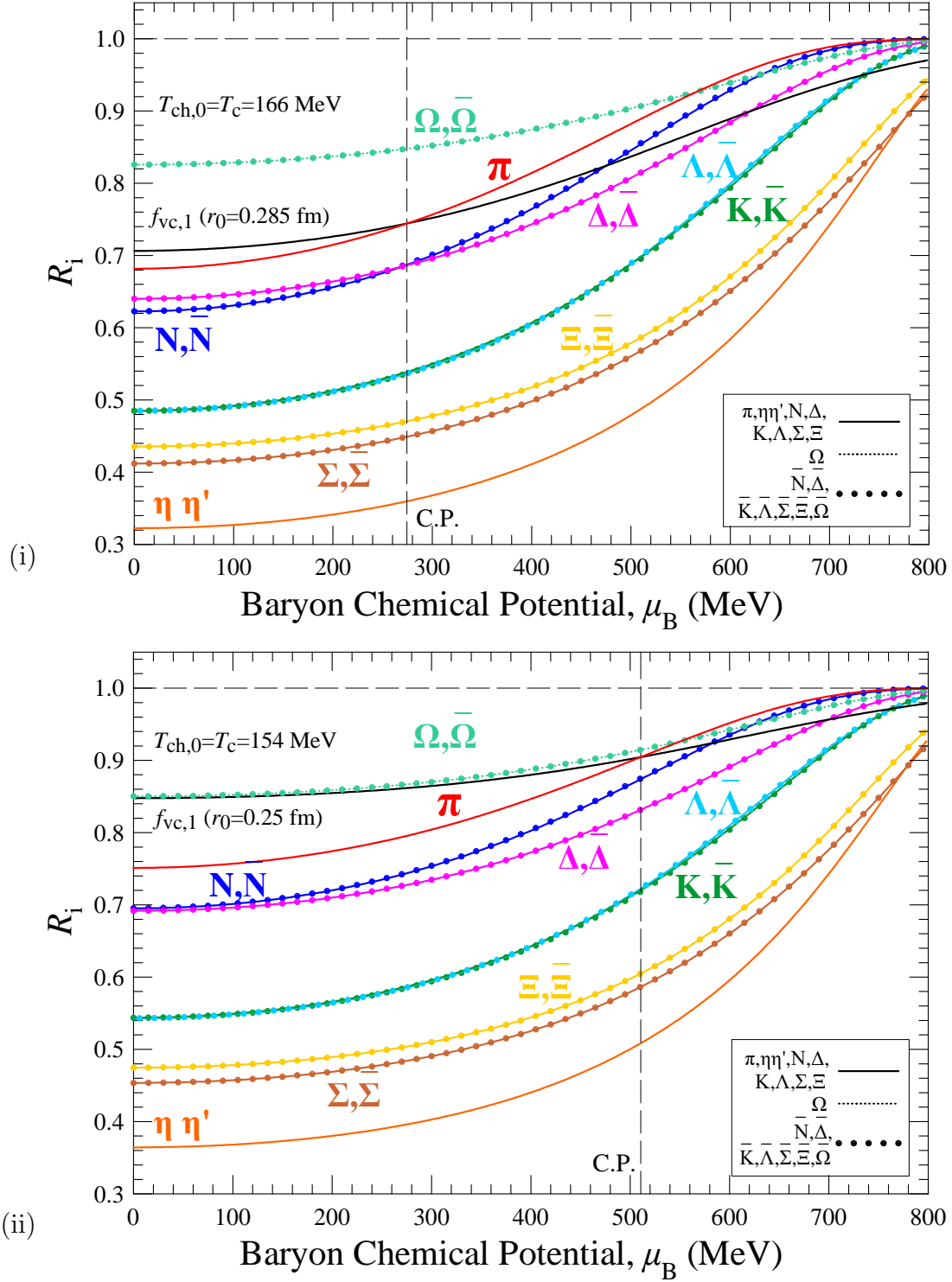


Figure 3: The ratios R_i along the transition curve for the families i as function of μ_B . These ratios are calculated for point particles and are equal to the density of the lowest mass particles of each family (equal to the minimum density of the chiral density at the same conditions) divided by the total particle density of the family. The ratios R_i here are calculated in the Bose/Fermi statistics and without volume corrections, since μ_s is practically unaffected by the hadron volumes, according to Fig. 1. In (i) we show calculations for a high value of $T_c = 166$ MeV. Also, it is shown the volume correction factor for the pion family, $f_{vc,1}$ for $r_0 = 0.285$ fm. The intersection of $f_{vc,1}$ with R_1 determines the position of the critical point (C.P.). In (ii) we show analogous calculations for a low value of $T_c = 154$ MeV and for $f_{vc,1}$ for $r_0 = 0.25$ fm. The pion family retains for all values of T_c the higher value of ratio R . The second important family is the nucleon family which, almost everywhere, retains, the second higher value of ratio R . The ratio for the Ω family is shown with dotted line to represent the artificially high value of the $\Omega, \bar{\Omega}$ families which are due to the absence of unknown resonances.

proximate in the Bose/Fermi statistics, holds exactly in the Boltzmann description. Indeed, for equal hadron volumes, v_0 , eq. (23) reduces to:

$$f_{vc,i}(\mu_B; T_c) = \frac{\exp[-v_0 P]}{1 + v_0 \exp[-v_0 P] \sum_i \sum_j n_{HG,ij}^{pt}} . \quad (27)$$

To verify that the dependence of the correction factor on the family is weak, we plot in Fig. 2 the factor f_{vc} in the Bose/Fermi statistics for the different families i and for two hadron volumes (which correspond to the radii $r_0 = 0.285$ fm and $r_0 = 0.25$ fm respectively). It is evident from the graph that the values of this ratio are very close for all the families. We have to point out, though, that if different radii r_i are used for different families, then the corresponding factors $f_{vc,i}$ will differ.

After these considerations, we plot in Fig. 3 the values of the ratios R_i for each family, calculated along the transition curves which correspond to the two extreme values of $T_c \simeq 166$ MeV in (i) and $T_c \simeq 154$ MeV in (ii). In this figure we see, firstly, that the differences between families which contain particles and antiparticles are small. Secondly, we notice that the ratio for the $\Omega, \bar{\Omega}$ families is artificially high as a consequence of unknown resonances in these families. Neglecting this discrepancy, the ratio R_i for the π family for certain value of baryon chemical potential has the highest value of all the families. Thus, if we apply the volume corrections for r_0 equal for all hadrons, the π 's will be the first family (i.e. for the lower value of μ_B) which satisfies the condition that its chiral mass acquires the maximum allowed value:

$$\tilde{m}_1(\mu_{Bcr}) = m_\pi = m_{11} . \quad (28)$$

Equivalently, last equation can be written as:

$$f_{vc,1}(\mu_{Bcr}) = R_1(\mu_{Bcr}) \Rightarrow \sum_j n_{HG,1j}(\mu_{Bcr}) = n_{HG,11}^{pt}(\mu_{Bcr}) . \quad (29)$$

Eqs. (28),(29) enable us to calculate the critical point position at baryon-chemical potential μ_{Bcr} .

For values $\mu_B \leq \mu_{Bcr}$ the crossover conditions (22) can be fulfilled not only for the π family, but also for all the families (since $R_i(\mu_B) < R_1(\mu_B), i \neq 1, 9, -9$). For $\mu_B > \mu_{Bcr}$ the chiral mass of the pion family remains equal to the maximum allowed pion mass. The conservation of the particle number of the pion family can no longer be fulfilled through the reduction of the mass and, thus, it has to be fulfilled through the alteration of the system volume, $V_{HG} > \tilde{V}$. So we are in the region of the 1st order transition. To ensure the conservation of particle number for the pion family we impose the condition:

$$V_{HG} \sum_j n_{HG,1j}(\mu_B) = \tilde{V} n_{HG,1}^{pt}(\mu_B) \Rightarrow v_{er} \equiv \frac{V_{HG}}{\tilde{V}} = \frac{n_{HG,1}^{pt}(\mu_B)}{\sum_j n_{HG,1j}(\mu_B)} . \quad (30)$$

We have defined as v_{er} the volume expansion ratio. This ratio is determined by eq. (30) for $\mu_B > \mu_{Bcr}$, while it remains equal to 1 in the crossover. Consequently, v_{er} is inherited to the rest of the families. The conservation for the particle number in these families is ensured by:

$$v_{er} \sum_j n_{HG,ij}(\mu_B) = \tilde{n}_i(\mu_B) , i \neq 1 . \quad (31)$$

The last equation determines the chiral masses $\tilde{m}_i(\mu_B)$ for the particle families different than the pion family. However, it has to be checked for consistency reasons that the condition

$$\tilde{m}_i(\mu_B) \leq m_{i1} , i \neq 1 , \quad (32)$$

continues to hold in the region of the 1st-order transition, as well.

It is evident from this description that the pions with the associated spectrum of resonances play fundamental role. The position of the critical point is determined by the knowledge of the pion family particle spectrum. The particle spectrum of the rest of the families does not influence the critical point position. The addition of currently unknown resonances in the spectrum of these families will further reduce the ratios R_i , depicted in Figs. 3.

In Figs. 3 we, also, present graphical solutions of eq. (29) – for the transition curves which correspond to $T_c \simeq 166$ and 154 MeV – determining the position of the critical point. To this end we plot the volume correction factors for the relevant value of hadron radii r_0 . The intersection of these factors with the pion ratios, R_1 , determine the critical baryon chemical potential, μ_{Bcr} . The factors $f_{vc,i}$ are almost the same for all the families i for equal hadron volumes, according to Fig. 2. Thus, the fact that the ratio R_1 retains the higher value among all R_i ensures that the intersection of the curves $f_{vc,1}$ and R_1 will occur first (at lower μ_B). Also, it is evident from Fig. 2 that $f_{vc,1}$ is slightly lower than the rest of the volume correction factors. This further confirms our conclusion that the pion family will reach first the relative maximum mass at the chiral phase. However, we have to point out that the factors $f_{vc,i}$ will differ if different particle volumes are used.

This description is consistent with the fact that in the low baryon density area the HG state is dominated mainly by mesons and the pion is the meson with the lower mass. Thus, its production is favoured at this territory, which leads to enhanced pion multiplicities. Also, we observe that the family with R_i closest to the pion family is the nucleon family N . Indeed, the nucleon family contains the nucleons, protons and neutrons, which are the lightest hadrons carrying baryon number. Thus, these particles, with their family, should play important role as the baryonic density increases and their multiplicity becomes enhanced. So, the next family to the pions which may play important role are the nucleons.

In this section for simplicity we have used volume correction factors for the case of constant volumes equal for all hadrons. If different volumes are introduced for specific hadron species these factors will differ among these species. Additionally, for volumes depended on chemical potentials the volume correction factors may differ between particles and antiparticles (according to eq. (43)). In each case we have to ensure that the pion family is the family for which the volume correction factor meets the corresponding ratio R_i at the lower value of baryon-chemical potential.

4 Constrains of Lattice QCD on hadron volumes - Thermodynamic implications

The hadron densities in the HG state depend on the eigenvolume of each particle, which incorporate the effect of the repulsive part of the strong interaction. In the previous section, to show the effect of the hadron volumes on our model, we used arbitrary values, which where not subject to any constraint. In this section we take a step further and we try to acquire knowledge of the values of these particle volumes by a fit on the Lattice QCD results. We consider here the QCD pressure P_L as a function of temperature for vanishing baryon chemical potential which is calculated in [2]. Our results will depend on the critical temperature T_c for zero density. Below T_c the system exists in the Hadron Gas (HG) state. We will consider both scenarios: (i) constant eigenvolumes (independent of temperature and baryon chemical potential), as well as, (ii) eigenvolumes depending on temperature and baryon chemical potential.

4.1 Constant Eigenvolumes

We start our investigation with the scenario of constant eigenvolumes. In Fig. 4 we present the normalised lattice pressure $3P_L/T^4$ as function of temperature for three values of T_c : 154 MeV (which is the preferred one in [2]), 161 MeV and 166 MeV (lines, (1)-(3)). We focus on the temperature region $T \geq 100$ MeV, since the lattice results may not be accurate for $T \ll T_c$. As it is evident from Fig. 4, the increase of T_c causes the lattice pressure to decrease for the same temperature. With line (4) we depict the normalised HG pressure for point particles in the Boltzmann approximation. However, line (4) lacks two additional requirements for a correct HG description, quantum statistics and volume corrections. So, with line (5) we depict the HG pressure with Bose/Fermi statistics for point particles. We observe that this addition shifts the HG pressure to higher values. This line still produces lower pressure values than the lattice $T_c = 154$ MeV curve. The insertion of finite hadron volume will shift line (5) to even lower values. So the lattice $T_c = 154$ MeV curve cannot be fitted by physical hadron volumes. On the contrary the increase of T_c moves the lattice pressure curve to lower values than line (5). The addition of the volume corrections causes even more decrease in the HG pressure (line (6)). So, to shift the lattice pressure to values compatible to the HG case, an increase of T_c is needed.

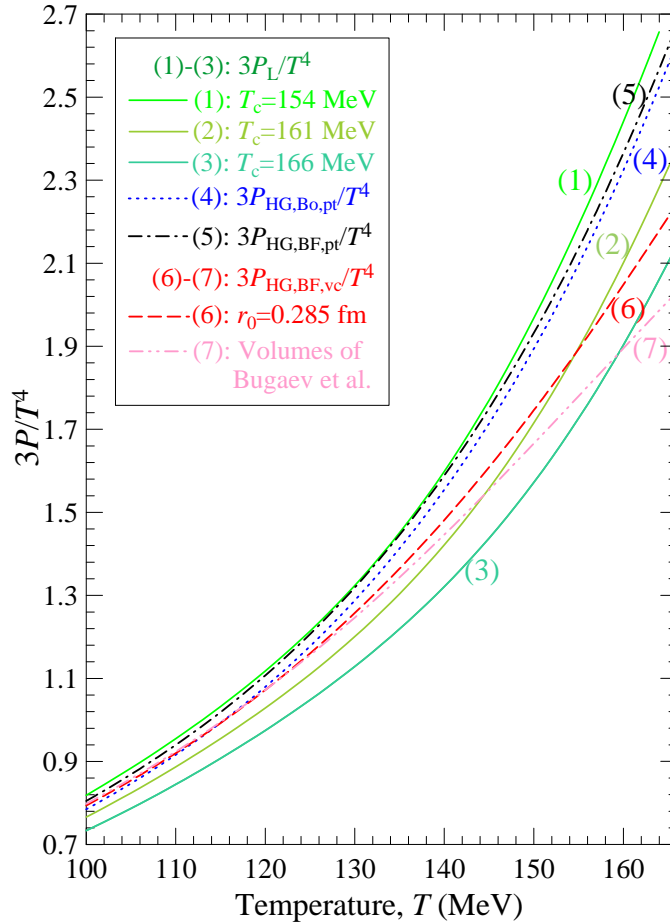


Figure 4: Normalised pressures, $3P/T^4$, as function of temperature, T : Lattice QCD of [2] (continuous lines) corresponding to $T_c = 154$ MeV (line (1)), 161 MeV (line (2)) and 166 MeV (line (3)). Hadron Gas for point particles in Boltzmann approximation (dotted line (4)). Hadron Gas for point particles with Bose/Fermi statistics (slashed-dotted line (5)). Hadron Gas for extended particles, with common radius $r_0 = 0.285$ fm (slashed line (6)) and with radii fixed at the values cited in [34] (slashed-double dotted line (7)).

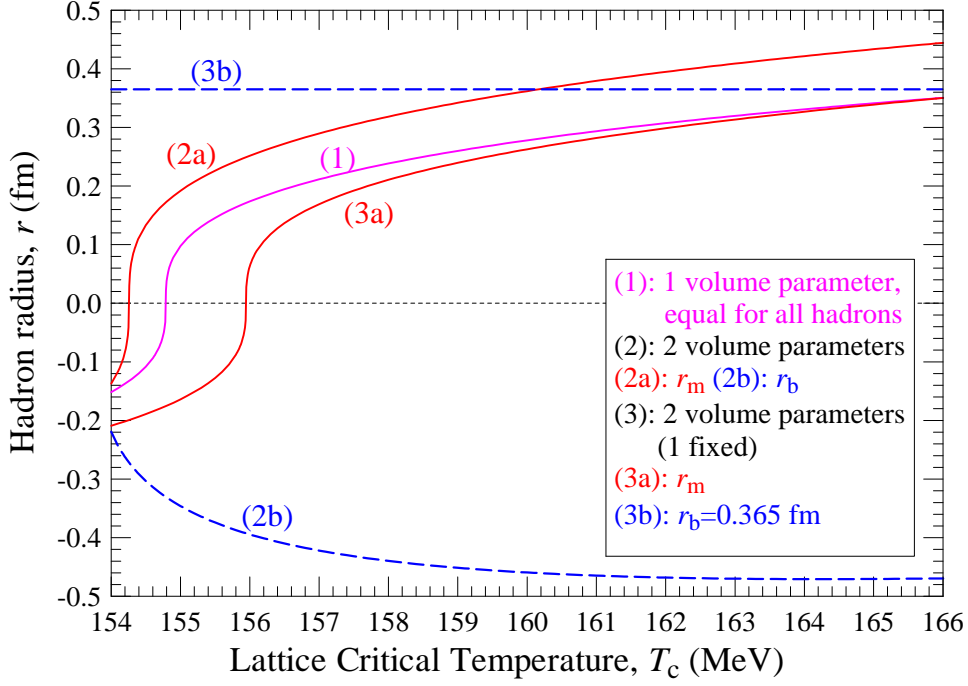


Figure 5: The constant hadron radii in HG model which best fit the lattice QCD pressure, as function of the critical QCD temperature, T_c . Line (1): a common radius for all hadrons. Lines (2): Continuous line (2a): the radius for all mesons, r_m . Slashed line (2b): the radius for all baryons, r_b (lying completely to the unphysical negative territory). Lines (3): Continuous line (3a): the radius for all mesons, r_m . Slashed line (3b): the radius for all baryons, held fixed $r_b = 0.365$ fm (as in [34]).

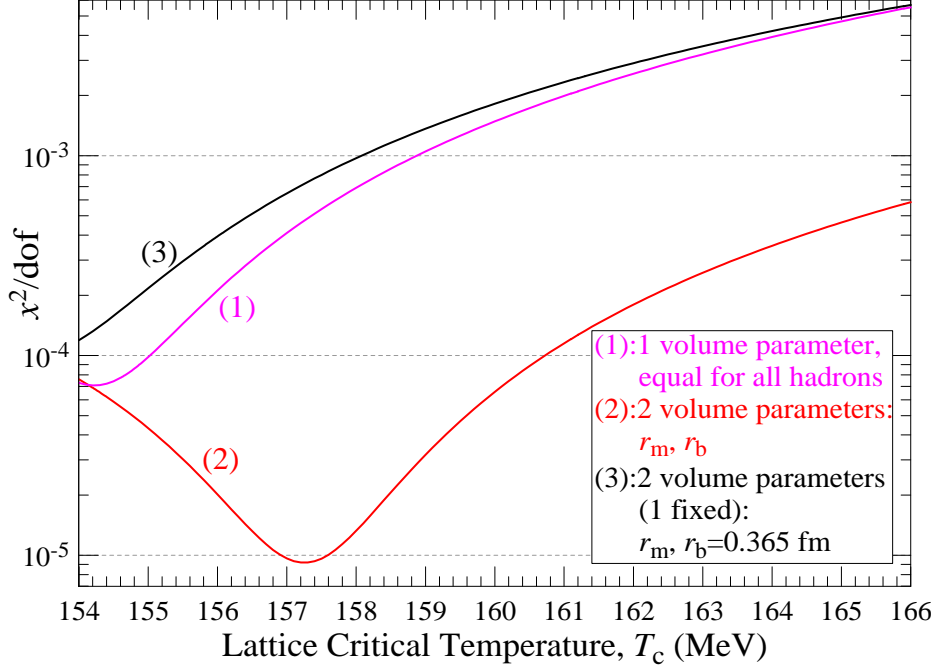


Figure 6: The quality, χ^2/dof , of the fits performed with constant hadron radii in HG model so as to fit the lattice QCD pressure, as function of the critical QCD temperature T_c . Since the errors are taken ad hoc $s_i = 1$, the graph serves to compare the relevant quality between the different cases. Line (1): a common radius for all hadrons determined by the fit. Line (2): two radii determined by the fit one for mesons, r_m , and one for baryons, r_b . Line (3): the radius for baryons is held fixed $r_b = 0.365$ fm (as in [34]) and only the meson radius, r_m , is determined by the fit.

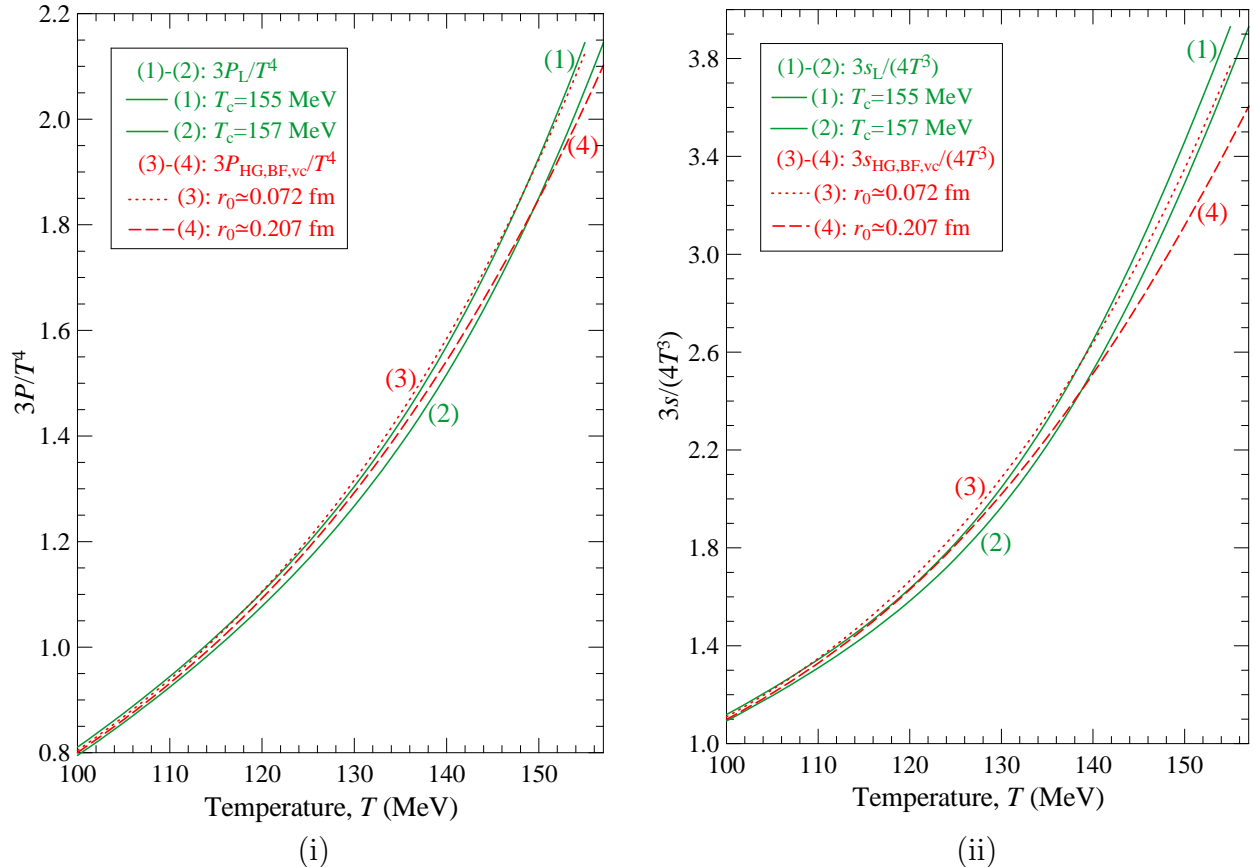


Figure 7: (i) Comparison of lattice normalised pressures with HG normalised pressures, as function of temperature, for two values of $T_c = 155$ MeV and 157 MeV. The relevant HG pressures correspond to common radius determined by the fit, $r_0 = 0.072$ fm and 0.207 fm, respectively. The choice of T_c 's represent an optimised interval: below $T_c = 154.5$ MeV r_0 falls into unphysical negative values and above $T_c = 157$ MeV the quality of the fit worsens (the fit for $T_c = 157$ MeV is worse than the one for $T_c = 154$ MeV). (ii) Comparison of lattice normalised entropy densities with HG normalised entropy densities, as function of temperature, for the parameters in (i). Although, the pressures are fitted quite well in (i), the entropy densities here fail to do so.

We, then, attempt to fit the lattice pressure with constant values of volumes. First we employ the same volume parameter, v_0 , for all the hadrons. We determine this volume by a fit on the lattice pressure [2], P_L , so that the quantity:

$$\chi^2 = \sum_{i=1}^N \left\{ \frac{3}{T_i^4} \frac{[P_L(T_i; T_c) - P_{HG}(T_i, \{\mu\} = 0; v_0)]}{s_i} \right\}^2. \quad (33)$$

is minimized. The $N = 20$ temperature points, T_i , are taken at equal intervals in the range $(100 \text{ MeV} - T_c)$, while the errors are all taken equal $s_i = 1$. The degrees of freedom are $dof = N - k$, where k is the number of the volume parameters we shall determine by the fit. The value of s_i certainly affects any conclusion about the quality of the fit, however we are only interested in the relative success of the different fits we shall perform. In Fig. 5 we show the results of this fit in line (1), which represents the radius r_0 common to all hadrons as a function of T_c . It is clear that for $T_c < 155$ MeV the value of this radius is negative, thus unphysical. This is in accordance to the observation that the $T_c = 154$ MeV lattice pressure curve lies above the Bose/Fermi HG pressure for point particles. Consequently, the unphysical negative hadron volume is necessary to mathematically fit the lattice results, since it increases the point-particle pressure, instead of suppressing it. However, above $T_c \simeq 155$ MeV, we find physical positive values for the hadron radius. We observe a tendency for saturation as the maximum value of $T_c = 166$ MeV is approached.

In Fig. 6 we present results of the quality of the fit. From this graph, it is evident that the quality worsens as T_c increases. Returning to Fig. 4, where we have plotted the normalised HG pressures for the fitted radius value which corresponds to $T_c = 161$ MeV, we observe that the lattice pressure is fitted poorly by the one volume parameter (line (6)). For comparison we have also plotted the HG pressure for the hadron volumes of [34] (line (7)). It is evident that it does not fit well the lattice pressure. Only between the values $T_c = 155-157$ MeV we find the relative best fit, with the universal hadron volume in the range $r_0 = 0.07-0.21$ fm. We use this interval because for $T_c < 154.5$ MeV, r_0 is unphysical and the quality of the fit worsens as T_c rises.

We then attempt to fit the lattice pressure with two volume parameters, one for the mesons, v_m and one for the baryons, v_b , which are both left free to be determined by the fit. The procedure entails to determine these two parameters by minimizing the quantity χ^2 of eq. (33, which now involves HG pressure depending on $v_m, v_b, P_{HG}(T_i, \{\mu\} = 0; v_m, v_b)$). The results for the fitted hadron radii are shown in Fig. 5 with lines (2a) and (2b) and in Fig. 6 with line (2). This fit achieves better quality than the one parameter case, as it is shown in Fig. 6. This is expected due to the use of an extra parameter. However, the baryon volumes are shifted, completely or partly, to unphysical negative volumes for all values of T_c . This is also understandable, because for zero baryon density the HG is composed mainly by mesons, while the baryon content remains relatively small. Thus, small variations to the mesonic radius produce large variations to the meson multiplicities. On the contrary, to obtain comparable variations to the baryon multiplicities the respective radius has to vary considerably. Since the parameters in the performed fit are treated without constraints, the baryon radius is easily shifted to negative values whenever there is a tendency for the reduction of this parameter. To avoid this behaviour, while keeping two volume parameters in the HG description, we decided to fit the lattice pressure varying only the mesonic radius r_m . During the fitting procedure the baryon radius remains fixed to the value $r_b = 0.365$ fm given in [34]. Our results for r_m are shown in Fig. 5 with lines (3a) and (3b) and in Fig. 6 with line (3). From Fig. 5 we find that r_m acquires physical values for $T_c \geq 156.5$ MeV. The quality of the fit remains worst than the one volume parameter case (Fig. 6, line (3)) for all T_c .

We end this subsection by showing representative fits with common particle eigenvolumes for both mesons and baryons. We concentrate on this case since the fit with the two free volume parameters leads to unphysical results and the one parameter fit has better quality than the one with the fixed baryon volume. Thus, we present in Fig. 7(i) results of the HG pressure corresponding to $T_c = 155$ and 157 MeV. The best fit (at $T_c = 155$ MeV) corresponds to rather low value for hadron volume, while the fit starts to deteriorate at 157 MeV. In any case the HG model fails to fit sufficiently the lattice entropy density, which is the temperature derivative of the pressure. In Fig. 7(ii) we compare the entropy densities of lattice and HG for the parameters of Fig. 7(i). It is clear that the best constant HG volume parameters which fit quite well the lattice pressure are not adequate to fit the lattice entropy density.

4.2 Varying hadron eigenvolumes

Since the constant particle eigenvolumes are inadequate to fit the Lattice results (pressure and entropy density) we turn now to the use of volumes which depend on temperature and chemical potentials. However, this approach affects certain thermodynamic quantities. The total HG pressure can be calculated by eqs. (7)-(8).

For simplicity we use, here, only one index i for a specific particle, without reference to the family it belongs to. If the particle volumes remain fixed, then the particle densities and the system entropy density read, respectively:

$$n_{HG,j}^v(T, \{\mu\}) = \left. \frac{\partial P_{HG}(T, \{\mu\})}{\partial \mu_j} \right|_{T, \{\mu\}_j} \quad (34)$$

$$s_{HG}^v(T, \{\mu\}) = \left. \frac{\partial P_{HG}(T, \{\mu\})}{\partial T} \right|_{\{\mu\}}, \quad (35)$$

where the upper index v denotes constant particle volumes $v_1, v_2, \dots \equiv \{v\}$ and we have defined $\mu_1, \dots, \mu_{j-1}, \mu_{j+1}, \dots \equiv \{\mu\}_j$, i.e. the group of all the items without the j -th one.

The last two equations can be worked out to give the known results [17]:

$$n_{HG,j}^v(T, \{\mu\}) = \frac{n_j^{pt}(T, \widehat{\mu}_j)}{1 + \sum_i v_i n_i^{pt}(T, \widehat{\mu}_i)}, \quad (36)$$

$$s_{HG}^v(T, \{\mu\}) = \frac{s^{pt}(T, \widehat{\mu})}{1 + \sum_i v_i n_i^{pt}(T, \widehat{\mu}_i)}, \quad (37)$$

where the upper index ‘‘pt’’ denotes the point-particle case.

Then we examine the effect of having volumes which are *not constant* with respect of temperature and/or chemical potentials. We use the notation $\dots, v_{j-1}, v_{j+1}, \dots \equiv \{v\}_j$. Then we calculate

$$\begin{aligned} \left. \frac{\partial P_{HG}(T, \{\mu\}; \{v\})}{\partial v_j} \right|_{T, \{\mu\}, \{v\}_j} &= \sum_i \frac{\partial P_i^{pt}}{\partial \widehat{\mu}_i} \frac{\partial \widehat{\mu}_i}{\partial v_j} = \\ \sum_i \frac{\partial P_i^{pt}}{\partial \widehat{\mu}_i} \left(-\delta_{ij} P_{HG} - v_i \frac{\partial P_{HG}}{\partial v_j} \right) &= -P_{HG} \frac{\partial P_j^{pt}}{\partial \widehat{\mu}_j} - \frac{\partial P_{HG}}{\partial v_j} \sum_i v_i \frac{\partial P_i^{pt}}{\partial \widehat{\mu}_i} \Rightarrow \\ \frac{\partial P_{HG}}{\partial v_j} &= \frac{-P_{HG} \frac{\partial P_j^{pt}}{\partial \widehat{\mu}_j}}{1 + \sum_i v_i \frac{\partial P_i^{pt}}{\partial \widehat{\mu}_i}} = \frac{-P_{HG} n_j^{pt}(T, \widehat{\mu}_j)}{1 + \sum_i v_i n_i^{pt}(T, \widehat{\mu}_i)} \Rightarrow \\ \frac{\partial P_{HG}}{\partial v_j} &= -P_{HG} n_{HG,j}^v \end{aligned} \quad (38)$$

If the particle volumes depend on temperature, $v_i = v_i(T)$, then, using eq. (38), we determine the entropy density

$$\begin{aligned} s_{HG}(T, \{\mu\}; \{v\}) &= \left. \frac{\partial P_{HG}(T, \{\mu\}; \{v\})}{\partial T} \right|_{\{\mu\}} = \left. \frac{\partial P_{HG}(T, \{\mu\}; \{v\})}{\partial T} \right|_{\{\mu\}, \{v\}} + \sum_i \frac{\partial P_{HG}}{\partial v_i} \frac{dv_i}{dT} \Rightarrow \\ s_{HG} &= s_{HG}^v - P_{HG} \sum_i n_{HG,i}^v \frac{dv_i}{dT}, \end{aligned} \quad (39)$$

where with s_{HG}^v we denote the part of the HG entropy density which is calculated with constant volumes, according to eq. (37).

If the particle volumes depend on chemical potentials, $v_i = v_i(\{\mu\})$, then, using eq. (38), we calculate the particle densities

$$\begin{aligned} n_{HG,j}(T, \{\mu\}; \{v\}) &= \left. \frac{\partial P_{HG}(T, \{\mu\}; \{v\})}{\partial \mu_j} \right|_{T, \{\mu\}_j} = \left. \frac{\partial P_{HG}(T, \{\mu\}; \{v\})}{\partial \mu_j} \right|_{T, \{\mu\}_j, \{v\}} + \sum_i \frac{\partial P_{HG}}{\partial v_i} \frac{\partial v_i}{\partial \mu_j} \Rightarrow \\ n_{HG,j} &= n_{HG,j}^v - P_{HG} \sum_i n_{HG,i}^v \frac{\partial v_i}{\partial \mu_j}, \end{aligned} \quad (40)$$

where with $n_{HG,j}^v$ we denote the part of the HG density of the particle j , which is calculated with constant volumes, according to eq. (36).

At this point we want to have the same result if we evaluate the density for two particle species i, j and then add them and if we evaluate the density of the two particles together

$$n_{HG,j} + n_{HG,k} = n_{HG,j+k} . \quad (41)$$

For example we can imagine that we have a family with two particle species j and k and common volume v and we evaluate each density separately with chemical potentials μ_j, μ_k . Then we evaluate the density for the whole family $j + k$ with chemical potential $\mu_j = \mu_k$. If the index i in eq. (40) runs to all the hadrons of the system, then eqs. (40) and (41) cannot hold simultaneously. So we make the *choice* that the dependence of a hadron volume on chemical potentials is restricted to the chemical potential of the specific hadron

$$\frac{\partial v_i}{\partial \mu_j} = \delta_{ij} \frac{\partial v_j}{\partial \mu_j} . \quad (42)$$

Then eq. (40) results in

$$n_{HG,j} = n_{HG,j}^v - P_{HG} n_{HG,j}^v \frac{\partial v_j}{\partial \mu_j} = n_{HG,j}^v \left(1 - P_{HG} \frac{\partial v_j}{\partial \mu_j} \right) . \quad (43)$$

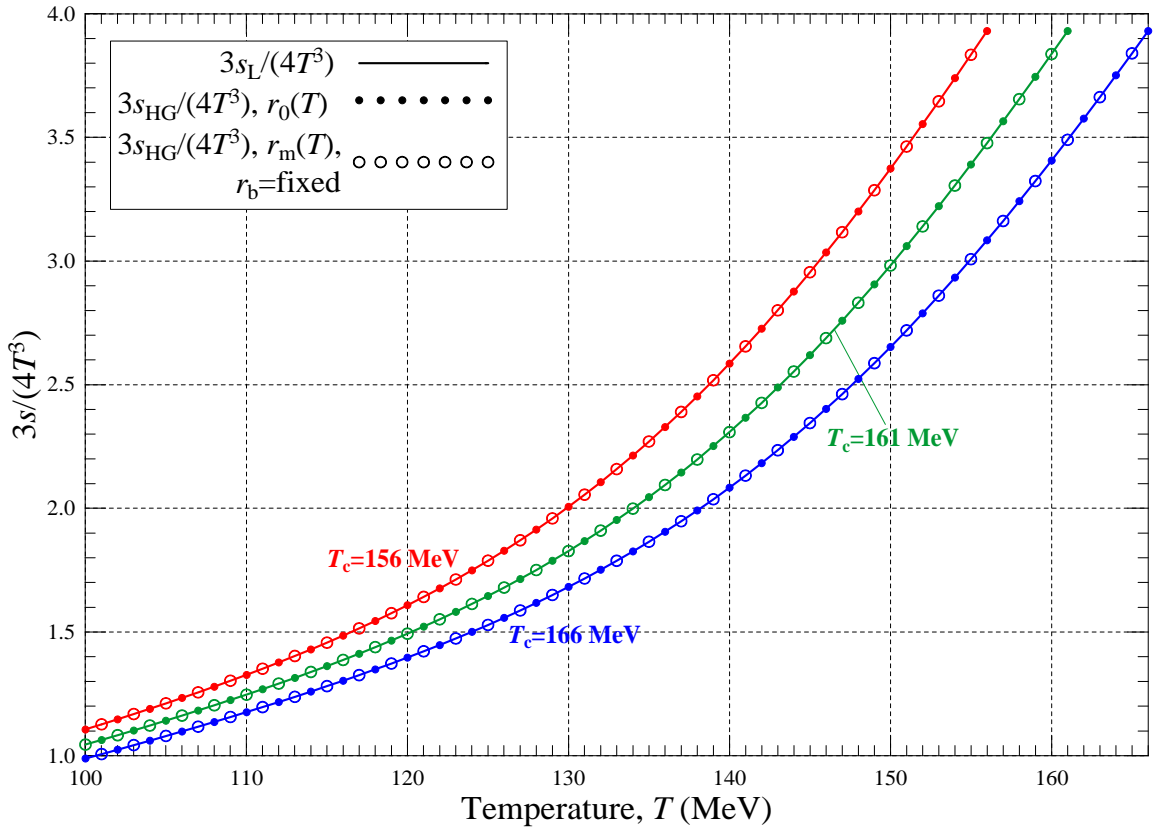
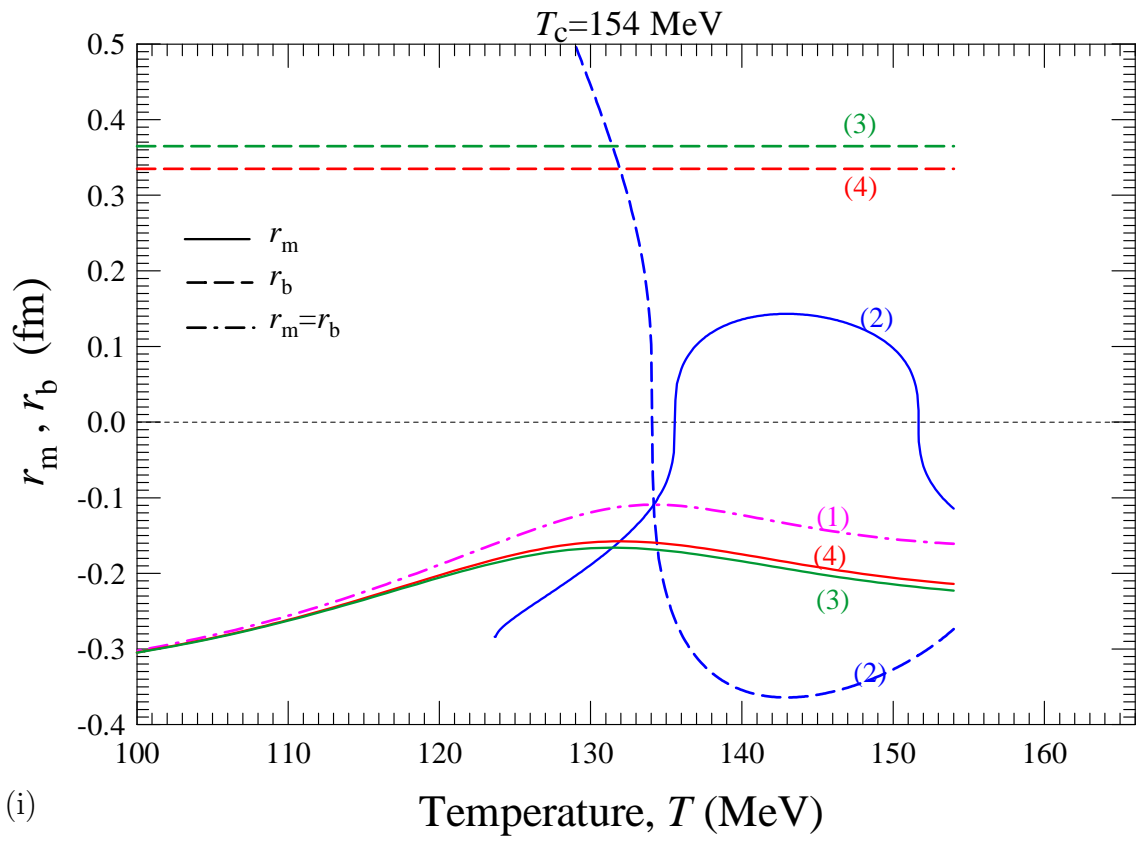
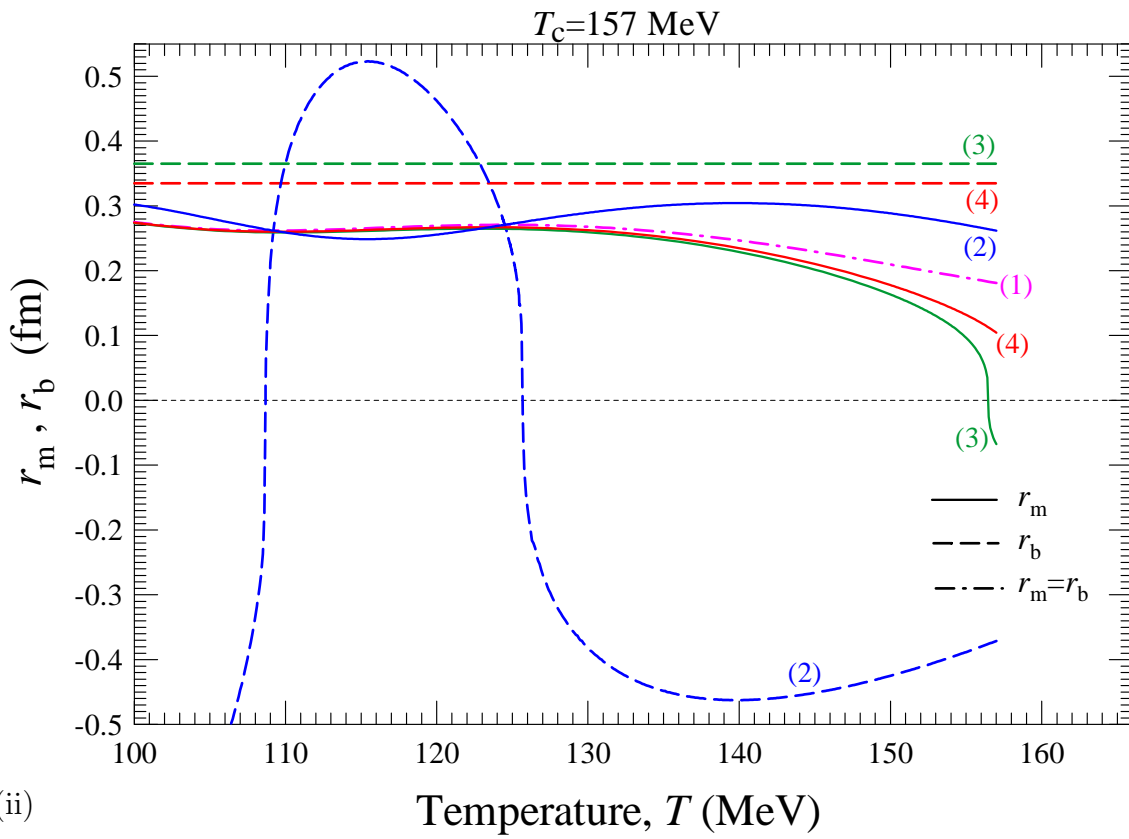


Figure 8: Comparison between the normalised entropy density, $3s/(4T^3)$, from Lattice (continuous lines) and from Hadron Gas (symbols). The entropy density of the Hadron Gas has been calculated by eq. (39) with a radius dependent on temperature which is calculated by a fit on the lattice pressure. With filled circles is shown the case of a unique radius, $r_0(T)$, for all hadrons. With open circles we depict the case of a radius $r_m(T)$ for mesons, while the radius for baryons is held fixed ($r_b=0.20$ fm for $T_c=156$ MeV and $r_b=0.3655$ fm for $T_c=161$ and 166 MeV). It is evident that the parameters which fit the lattice pressure, also fit exactly the lattice entropy density.



(i)



(ii)

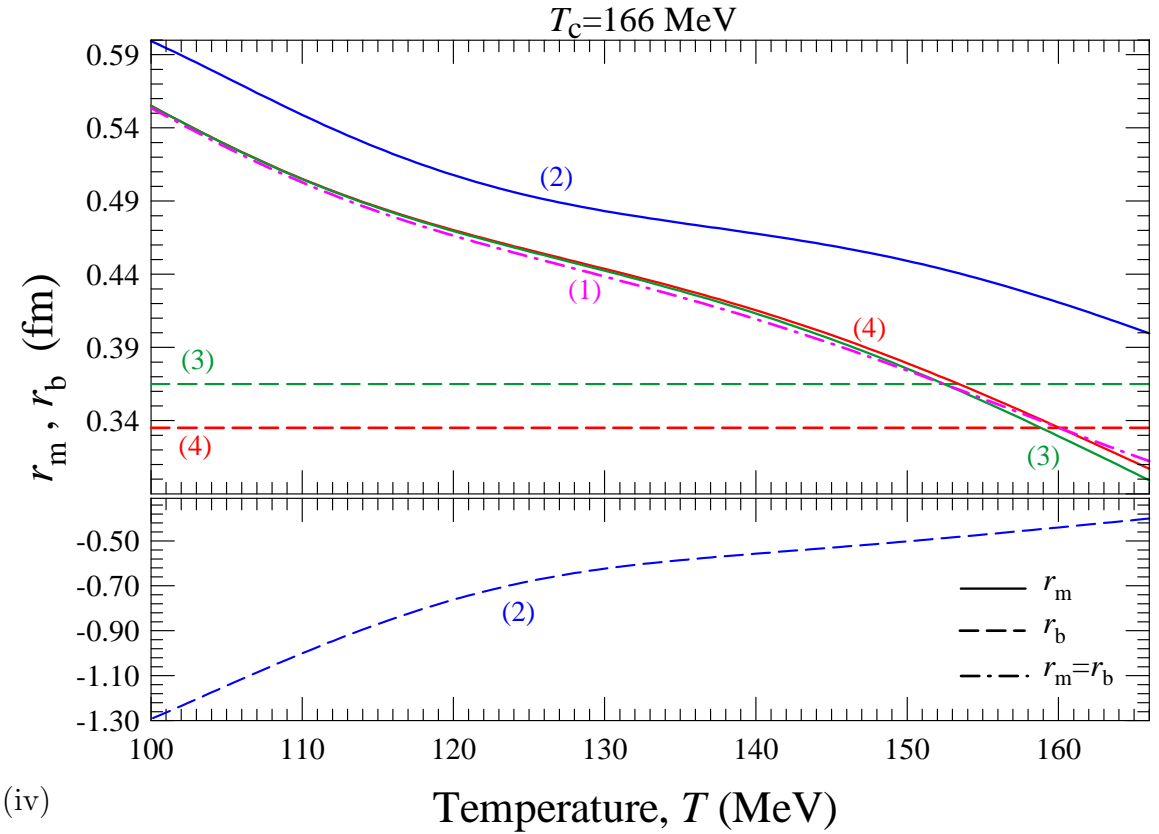
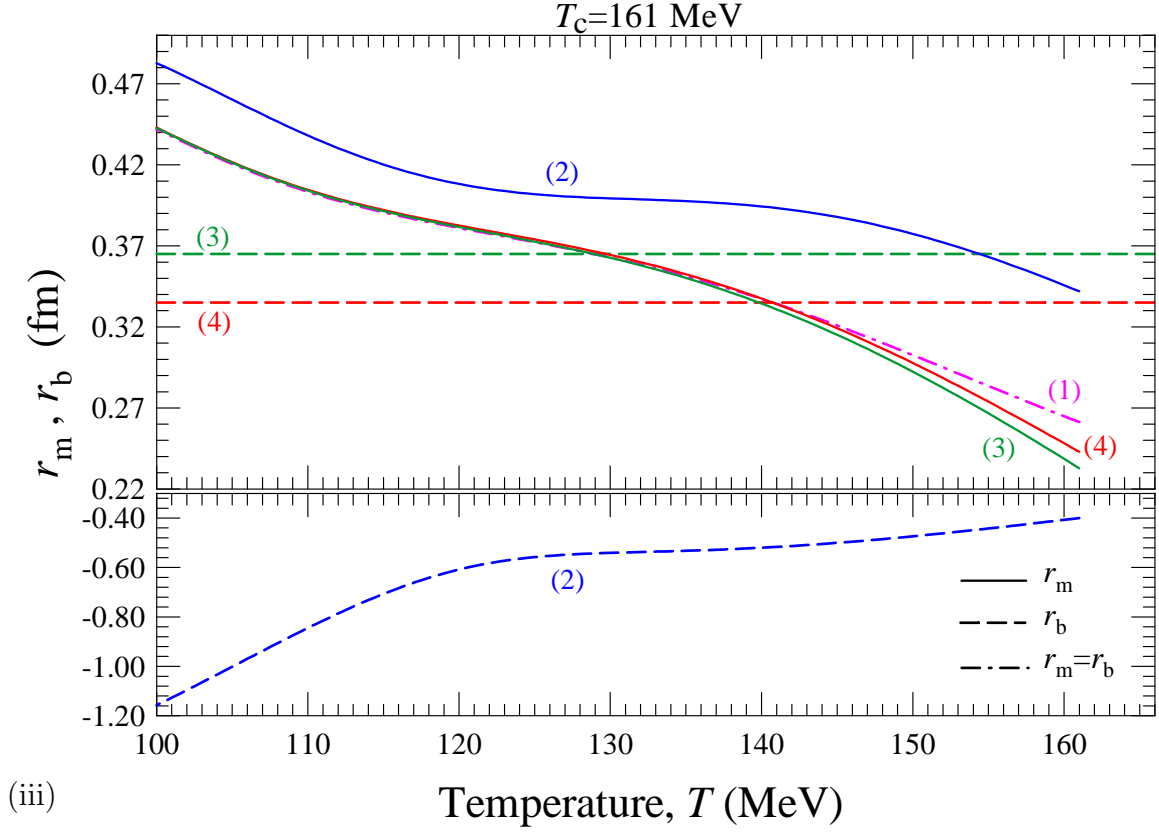


Figure 9: The solutions $r_m(T)$ and $r_b(T)$ obtained by setting the pressure and entropy density between HG and Lattice QCD equal. Dotted-slash line (1), case A: a common radius for all hadrons. Lines (2), case B: Continuous line: the radius for all mesons, $r_m(T)$. Slashed line: the radius for all baryons, $r_b(T)$. Lines (3), case C: Continuous line: the radius for all mesons, $r_m(T)$. Slashed line: the radius for all baryons, held fixed at $r_b = 0.365$ fm (as in [34]). Lines (4), case C: the same as green lines (3), but baryon radius is fixed at $r_b = 0.335$ fm. Each graph corresponds to a specific value for the critical QCD temperature T_c : (i) $T_c = 154$ MeV, (ii) $T_c = 157$ MeV, (iii) $T_c = 161$ MeV and (iv) $T_c = 166$ MeV.

After evaluating the effect of the varying volumes on entropy density and particle densities, we shall use this type of volumes to fit the Lattice results. Obviously, the Lattice Pressure at vanishing baryon density depends only on temperature. Thus, the hadron volumes we will use in the fitting procedure depend only on temperature, as well. This, indeed, will allow us to produce a HG curve which completely coincides with the lattice pressure curve. Also, it will be possible to reproduce exactly the lattice entropy density curve with the use of eq. (39).

Our first attempt (case A) is to use one volume parameter, $v_0(T)$, for all hadrons. This volume is determined for every T if we solve the equation:

$$\frac{3P_L(T; T_c)}{T^4} - \frac{3P_{HG}(T, \{\mu\} = 0; v_0(T))}{T^4} = 0 . \quad (44)$$

Then, the corresponding HG entropy density can be calculated by eq. (39), where only one volume parameter is available:

$$s_{HG} = s_{HG}^v - P_{HG} \frac{v_0(T + \delta T) - v_0(T - \delta T)}{2\delta T} \sum_i n_{HG,i}^v , \quad (45)$$

where δT is infinitesimal, i runs over all hadrons and in the approximate calculation of the derivative $dv_0(T)/dT$ we have used terms up to the order of δT^2 .

The HG entropy density of eq. (45) fits exactly s_L , as it is evident from Fig. 8. Also, because $s_L > s_{HG}^v$, $P_{HG} > 0$ and $n_{HG,i}^v > 0$, we must have $dv_0(T)/dT < 0$. Thus, the hadron volume decreases with the increase of temperature. In Fig. 9 we present the results for the hadronic radii calculated from the fit to the Lattice results for specific critical temperatures T_c : in (i) $T_c=154$ MeV, in (ii) $T_c=157$ MeV, in (iii) $T_c=161$ MeV and in (iv) $T_c=166$ MeV. In each graph the result corresponding to a common radius for all hadrons is shown with line (1).

Our second try (case B) utilises two separate volume parameters, one for mesons $v_m(T)$ and one for baryons $v_b(T)$. We determine these two parameters for every T , so that the HG pressure and entropy density equals the relevant quantities of the lattice. Thus, we simultaneously solve the equations:

$$\frac{3P_L(T; T_c)}{T^4} - \frac{3P_{HG}(T, \{\mu\} = 0; v_m(T), v_b(T))}{T^4} = 0 . \quad (46)$$

$$\frac{3s_L(T; T_c)}{4T^3} - \frac{3s_{HG}^v(T, \{\mu\} = 0; v_m(T), v_b(T))}{4T^3} = 0 . \quad (47)$$

This case is interesting because the HG entropy density for these specific volumes has the same functional dependence on the hadron eigenvolumes as the HG entropy density with constant volumes, that is $s_{HG}^v(T, \{\mu\} = 0; v_m(T), v_b(T)) = s_{HG}(T, \{\mu\} = 0; v_m(T), v_b(T))$. Consequently, in view of eq. (39), this leads to:

$$n_{HG,m}^v \frac{dv_m}{dT} + n_{HG,b}^v \frac{dv_b}{dT} = 0 , \quad (48)$$

where $n_{HG,m}^v$ ($n_{HG,b}^v$) is the density of all mesons (baryons) in HG calculated for constant eigenvolumes. The last equation suggests that when, at certain temperature intervals, $\frac{dv_m}{dT} > 0$, then $\frac{dv_b}{dT} < 0$ and vice versa. Also, when $\frac{dv_m}{dT} = 0$, then $\frac{dv_b}{dT} = 0$, meaning that $v_m(T)$ and $v_b(T)$ should reach simultaneously maximum or minimum values. Our results for this case are shown with lines (2) in graphs 9, where the properties of $v_m(T)$ and $v_b(T)$ which are inferred by eq. (48) can be observed.

Our last effort (case C) is again with two volume parameters, but only with the meson volume depending on temperature, e.g. $v_m(T), v_b$. The baryon eigenvolume is held fixed and the meson eigenvolume is determined by solving the equation

$$\frac{3P_L(T; T_c)}{T^4} - \frac{3P_{HG}(T, \{\mu\} = 0; v_m(T), v_b)}{T^4} = 0 . \quad (49)$$

The HG entropy density can be calculated by eq. (39) and equals to the corresponding lattice quantity. The results of this case are shown in graphs 9 with lines (3), where the baryon radius is fixed at $r_b = 0.365$ fm (which is the mean baryon radius cited in [34]) and with lines (4), where the baryon radius is fixed at $r_b = 0.335$ fm (which is the lower baryon radius cited in [34]).

Comparing, now, the results from cases A-C, we see that case B leads to baryon volumes which are negative in almost all the temperature range and for all T_c . Thus, we have to drop this case as a plausible scenario. These results are similar to the case of fits with constant (with respect to T) baryon volumes. Again we find that if v_b is left as a free parameter, it is easily shifted to negative, unphysical values. So we have to reject this approach. On the contrary, fixing the baryon volume at a certain (positive) value, independently of our choice, allows us to solve for the meson volume $v_m(T)$, so that the HG pressure equals the Lattice pressure at every temperature point. The relevant entropy density can be calculated by eq. (45), where i runs over mesons only. In Fig. 8 it is shown that the Hadron Gas entropy density fits exactly the lattice entropy density, as well. Moreover, it is evident that for $T_c = 154$ MeV the parameters fall, for cases A-C, almost completely in the unphysical negative domain. Thus, lattice results for this critical temperature cannot be fitted by HG. This picture changes dramatically if T_c is raised by an amount of the order of 1 MeV. Additionally, when $T_c = 166$ MeV the volume parameters acquire rather high values, disfavoured by phenomenology.

5 Locating the Critical Point through volume models guided by lattice QCD

In this section we will utilise HG models, using hadronic volumes extracted from Lattice QCD results, in order to describe the transition of the hadron phase to the chiral phase in the entire baryon chemical potential- temperature plane. Our goal is to determine the location of the critical endpoint of the first order transition line indicating the entrance into the smooth crossover region.

5.1 Critical Point with single Constant Hadron Volume

We first consider the model which assumes that all particles have the same eigenvolume v_0 , connected with the hard-core particle radius r_0 , which is constant with respect to temperature and chemical potentials. Its value, however, will be determined, for a specific choice of T_c , by a fit on the Lattice Pressure curve, as in section 4 (through minimisation of χ^2 given by eq. (33)). We will refer to this choice as volume model (a).

The use of a single volume parameter for all hadrons has, also, been used elsewhere. In [26–28] the eigenvolume was taken equal for all baryons and mesons. In these works the radius for baryons was given by the hard-core repulsive interaction as extracted from nucleon-nucleon scattering [29], while radius values for other baryons were taken similar. For mesons, in the absence of detailed information on their interactions at short distance, it was assigned the same radius value, based on the similarity of the meson charge radii compared to baryons and on the energy dependence of the pion-nucleon phase shifts [30].

The choice of eq. (20) as the transition curve, fixes the temperature, T , for given T_c, μ_B . To determine the strange quark chemical potential we apply the zero strangeness condition in the HG phase:

$$\langle S \rangle_{HG}(T, \mu_B, \mu_s; T_c) = 0 \quad . \quad (50)$$

Last equation can be solved to determine μ_s for given values of T_c, T and μ_B . Eqs. (20),(50) enable us to depict our calculations as function of μ_B alone, for a specific value of T_c . The conservation of particle numbers insures the strangeness neutrality in the chiral phase, as well.

We proceed by considering the dependence of the position of the critical point on T_c , i.e. the Lattice QCD critical temperature at $\mu_B = 0$. In Fig. 10(i) we plot the calculated radius r_0 as function of T_c . In Figs. 10(ii)-(iv) we show the position of the critical point ($T_{cr}, \mu_{B,cr}, \mu_{s,cr}$, respectively) as a function of T_c . In Fig. 10(v) we depict the location of the critical point in the (T, μ_B) plane. We observe that for values $T_c \simeq 161.5$ MeV ($r_0 \simeq 0.301$ fm) the critical point is located at zero baryon chemical potential, while it disappears for higher T_c (or r_0) values. Decrease of T_c (and the radius r_0) shifts the critical point at higher values of chemical potential μ_B .

We have to impose the condition that the solution for the chiral masses is positive for all the families. The lowest values for these masses are found for $\mu_B = 0$ and these values decrease with decreasing T_c (or r_0). We find that the chiral mass of the pion family reaches the zero value, as T_c decreases, while the rest of the chiral masses are still positive. This imposes a constraint on T_c , leading to the lowest allowed value of $T_c \simeq 155.7$ MeV ($r_0 \simeq 0.157$ fm), which in turn gives an upper value for the position of the critical point at $\mu_{B,cr} \simeq 709$ MeV. These findings provide a lower limit for the critical temperature $T_{cr} \simeq 84.8$ MeV. Thus, our treatment excludes scenarios with very low critical temperatures [32]. In Fig. 10(v) we present the solution at zero baryon density for the chiral mass of each family (as the ratio to the higher allowed chiral mass of the family) with varying T_c .

In summary, for a universal hadronic volume, which remains constant with temperature, the critical point can be located in the range of μ_B (0-709) MeV, which corresponds to range of $T_c \sim (162-156)$ MeV or mean hadronic radius in the range of $r_0 \sim (0.16-0.30)$ fm. Also in Figs. 10 we depict by open circle the critical point, determined by the criterion which will be presented in detail in the next Section 6. This critical point corresponds to $T_c \simeq 160.8$ MeV ($r_0 \simeq 0.291$ MeV) and it is located at $\mu_B \simeq 249.1$ MeV and $T \simeq 153.0$ MeV.

We shall finish this subsection by presenting full calculations of the quantities involved for the solution for this critical point. In Fig. 11(i) we present the ratios R_i . The intersection of the volume correction factor of the pion family, $f_{vc,1}$, with the corresponding ratio, R_1 , determines the position of the critical point. In Fig. 11(ii) we present the masses that solve eq. (12) for every family i . Since the masses differ considerably among the families, we choose to depict the ratio of the chiral mass to the respective mass of the HG ground state. As it can be observed, the chiral mass of the pion family starts at its minimum value at zero baryon chemical potential, it reaches the maximum value at $\mu_{B,cr}$ and then remains constant. The chiral masses of the rest of the families in general increase with the increase of μ_B . A general observation is that all the masses tend, for zero temperature (maximum value of μ_B), to the physical mass of the lowest mass hadron in each family. Another observation is that the solution for the particle family differs slightly from antiparticle family solution.

In Fig. 11(iii) we present the calculations for the densities of each family in the HG and chiral phase. To display values in wide range, the family densities are divided by the respective minimum density (maximum value of chiral mass) at the chiral phase for the same conditions of temperature and chemical potentials, $\tilde{n}_{i,min}$. For $\mu_B < \mu_{Bcr}$ (crossover region) the densities of the HG and the chiral phase are equal (the slashed and continuous lines are identical at this region). For $\mu_B > \mu_{Bcr}$ (1st order transition) the density in the HG phase is lower than the density in the chiral phase, since the volume expands as the system crosses from chiral to HG phase. This is evident by the fact that the HG curves (slashed lines) are lower than chiral curves (continuous lines). The densities between particle-antiparticle (with the respective normalization) are almost equal. All the densities for low temperatures tend to the respective $\tilde{n}_{i,min}$.

Also, Figs. 11(ii)-(iii) confirm that the $\Omega, \bar{\Omega}$ families exhibit irregular behaviour: the chiral masses of these families attain higher values than the maximum allowed ones and the HG densities for these families at the crossover region are lower than the minimum chiral density values. Both of these facts would be remedied if additional mass spectrum were present in the $\Omega, \bar{\Omega}$ families.

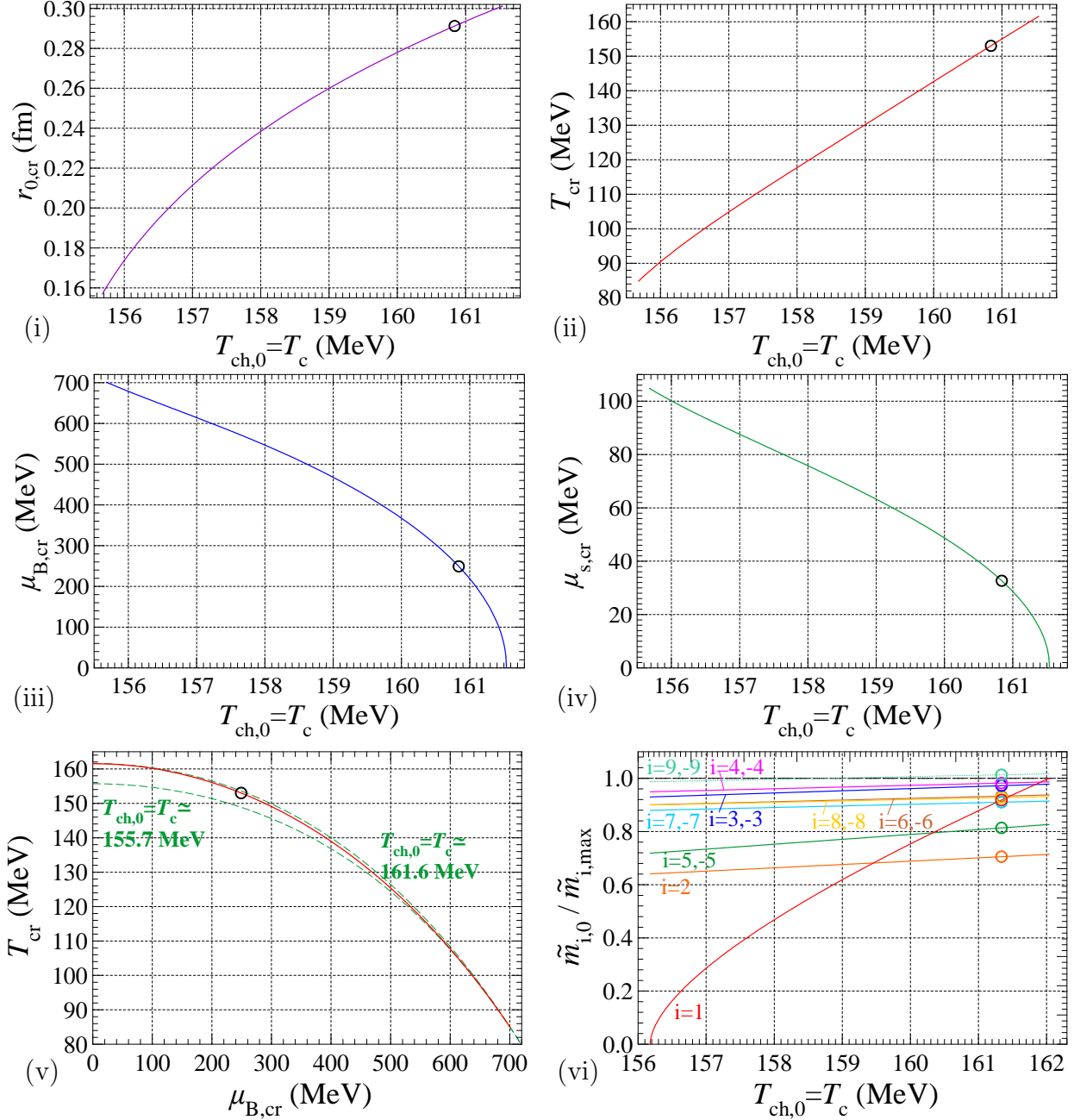
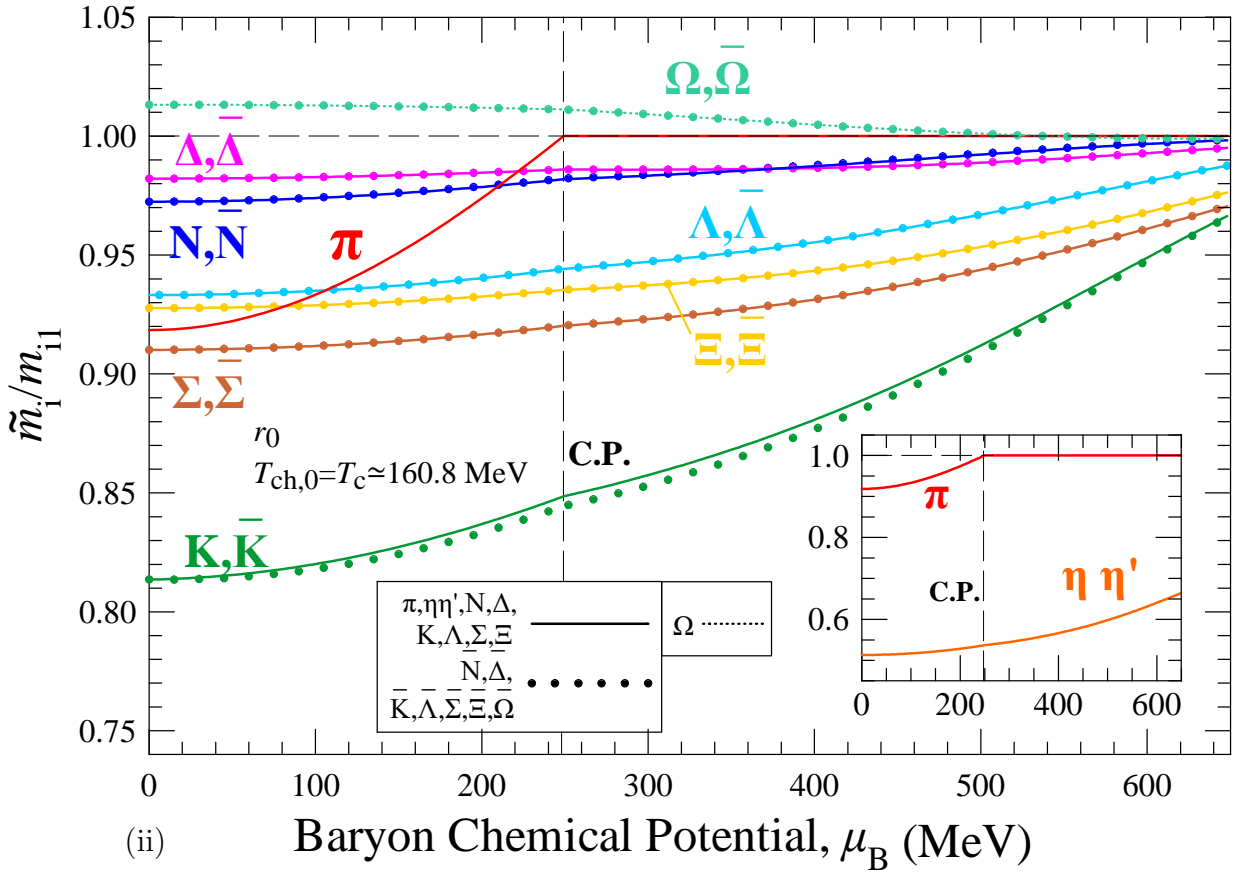
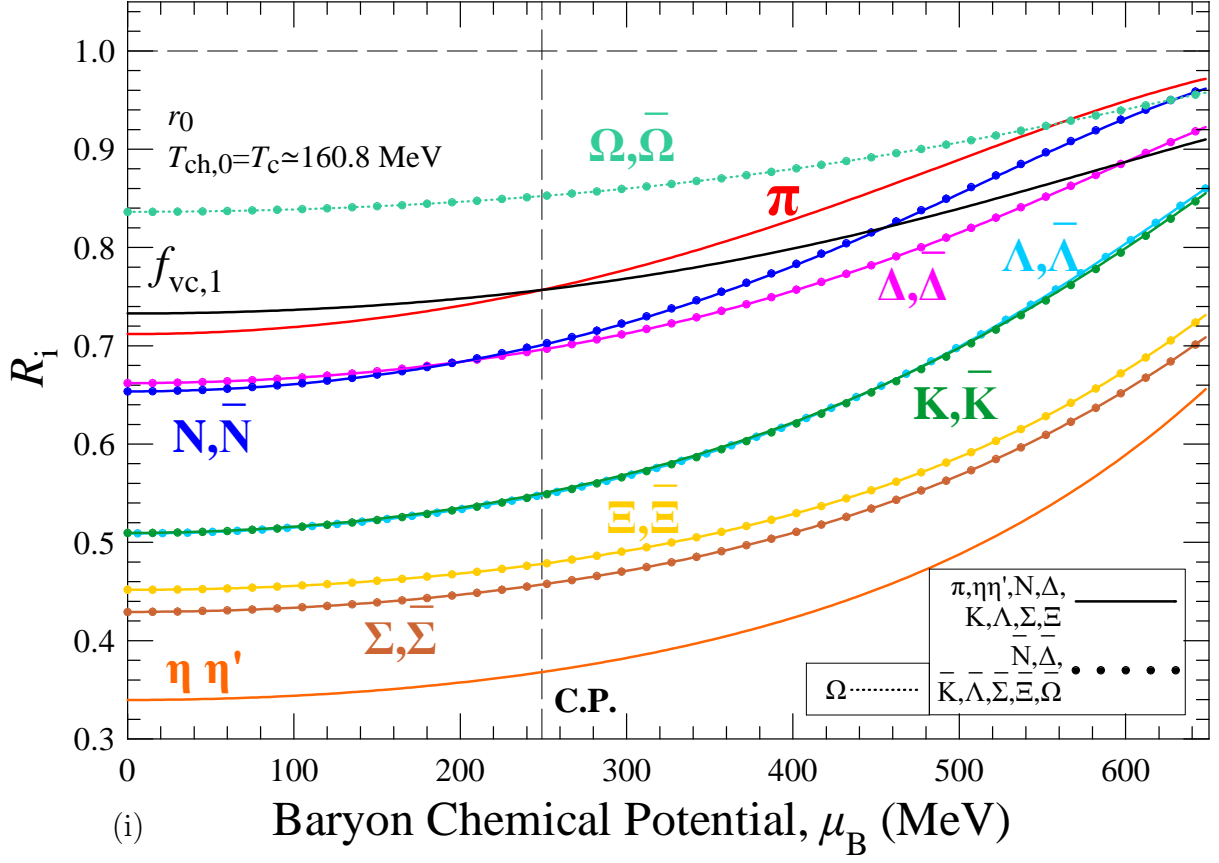
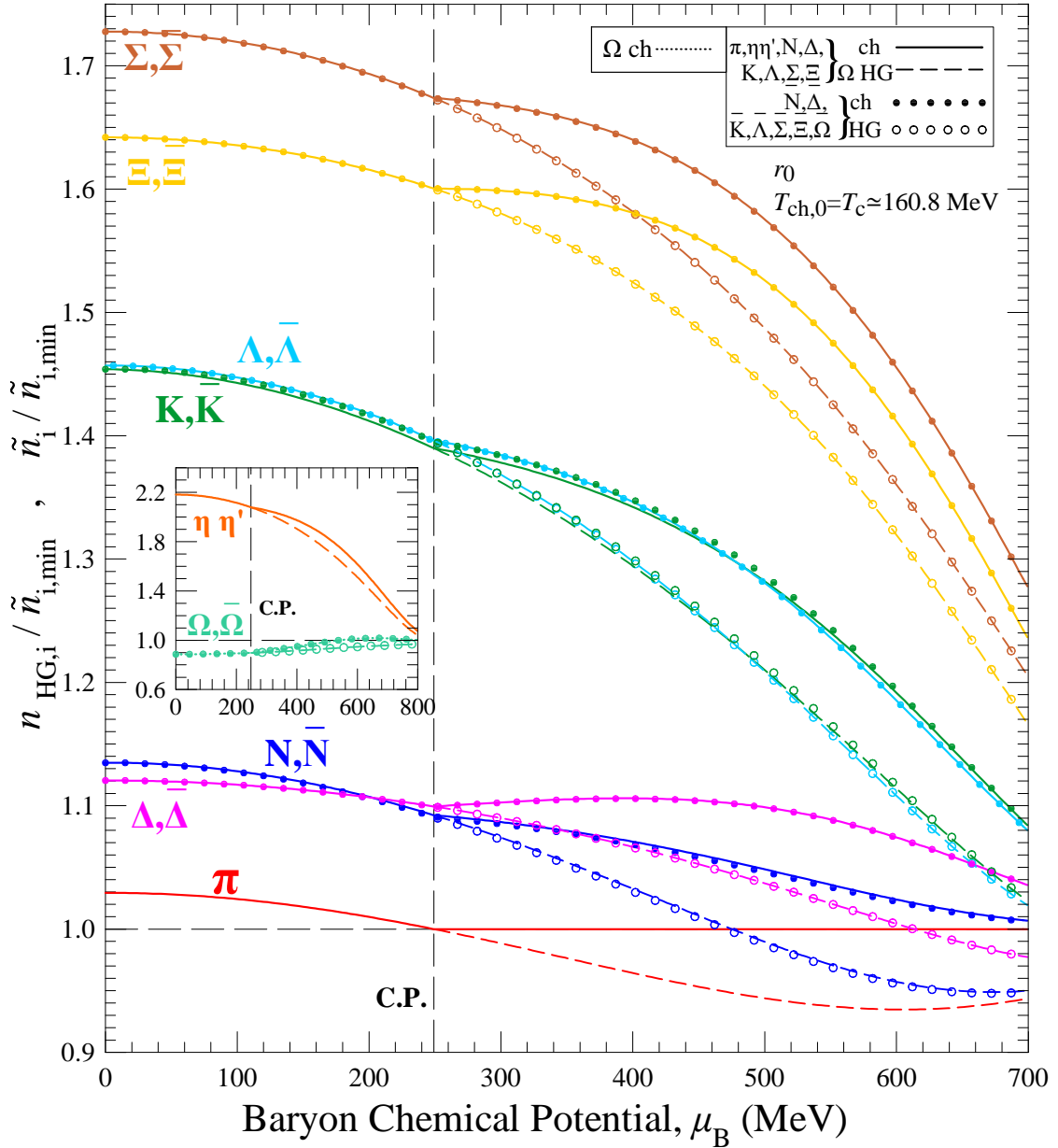


Figure 10: The position of the critical point determined for different values of critical lattice temperatures, T_c , which is always taken equal to the freeze-out temperature at $\mu_B = 0$, $T_{ch,0}$. Calculations are carried out in the interval $T_c \simeq (155.7-161.5)$ MeV. The critical point always resides on the corresponding freeze-out curve. Calculations involve constant common hadron radius r_0 , determined by the lattice pressure at $\mu_B = 0$ (volume model (a)). (i) The value of the common hadron radius on the critical point, r_0 , as function of $T_c = T_{ch,0}$. (ii) The temperature of the critical point, T_{cr} , as function of $T_c = T_{ch,0}$. (iii) The baryon-chemical potential of the critical point, $\mu_{B,cr}$, as function of $T_c = T_{ch,0}$. (iv) The strange quark-chemical potential of the critical point, $\mu_{s,cr}$, as function of $T_c = T_{ch,0}$. (v) The location of the critical point, $T_{cr} - \mu_{B,cr}$, for different values of $T_c = T_{ch,0}$. The freeze-out curves which correspond to the maximum value of $T_c = 161.5$ MeV and the minimum value of $T_c = 155.7$ MeV are shown. (vi) The solution for the chiral mass for each family at $\mu_B = 0$ MeV as function of $T_c = T_{ch,0}$. This chiral mass for the pion family becomes zero at $T_c = 155.7$ MeV and so, no real solutions exists for lower values of T_c . In all graphs with circle we present the critical point which additionally fulfils the criterion described in section 6.





(iii)

Figure 11: Calculations for $T_c = T_{ch,0} \simeq 160.8$ MeV and constant common hadron radius, $r_0 = 0.291$ fm, determined by the lattice pressure for $\mu_B = 0$. (i) The ratios R_i for the families i as function of μ_B , calculated exactly for these specific values of T_c and r_0 . Also, shown the volume correction factor for the pion family, $f_{vc,1}$, which intersects with R_1 at $\mu_B \simeq 249.1$ MeV and produces at this location the critical point. (ii) The ratio of the chiral mass for the i family to the respective maximum allowed value, as function of μ_B . With continuous lines we depict calculations for particle families, while with solid circles we depict calculations for antiparticle families. (iii) The ratio of the hadron gas or chiral family density to the minimum chiral density for the same conditions as function of μ_B . In the crossover region the hadron gas and chiral densities are equal, corresponding, thus, to the same curve, while they differ in the 1st order transition regime. Densities of particle families are depicted with lines, continuous for the chiral case and slashed for the HG case. Densities of antiparticle families are depicted with circles, solid for the chiral case and open for the HG case. The case of the Ω family is shown with dotted line to represent the irregular behaviour of the $\Omega, \bar{\Omega}$ families (in (i),(ii) everywhere and in the (iii) the chiral case).

5.2 Critical Point with single temperature dependent hadron volume

The common hadron volume we used in the previous section fails to fit exactly the Lattice QCD pressure and entropy density, as it was discussed in subsection 4.1. In this section we shall use the approach of subsection 4.2 and we shall try to locate the critical point using the same radius for all hadrons, which now depends on temperature, $r_0(T)$. This radius is fixed by the fit on the Lattice Pressure at vanishing baryon density. However, the assumption that $r_0(T)$ is independent of the chemical potentials enable us to transfer the value we have determined from the Lattice results at $\mu_B = 0$ to every value of baryon chemical potential. This will be referred to as volume model (b).

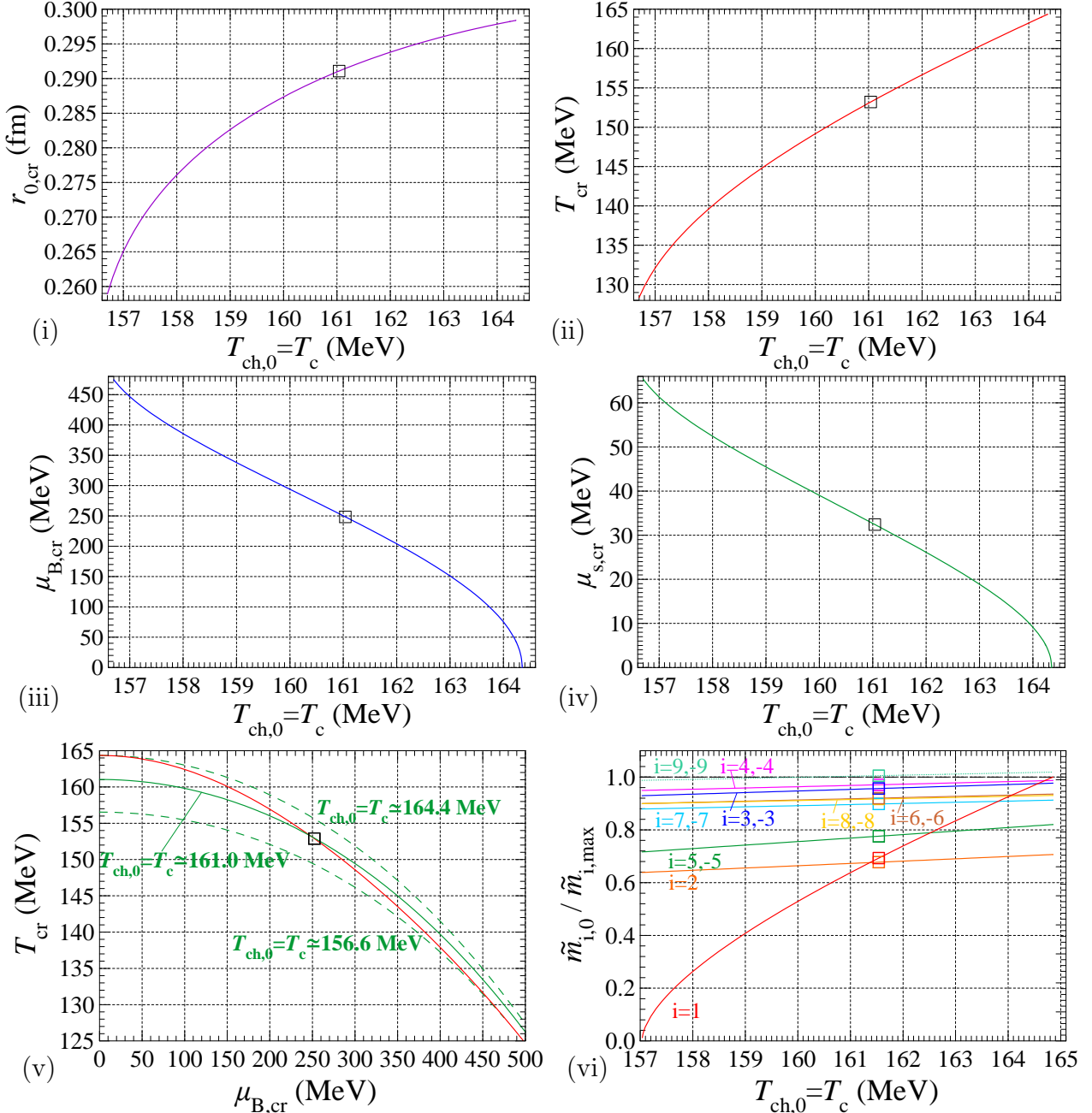
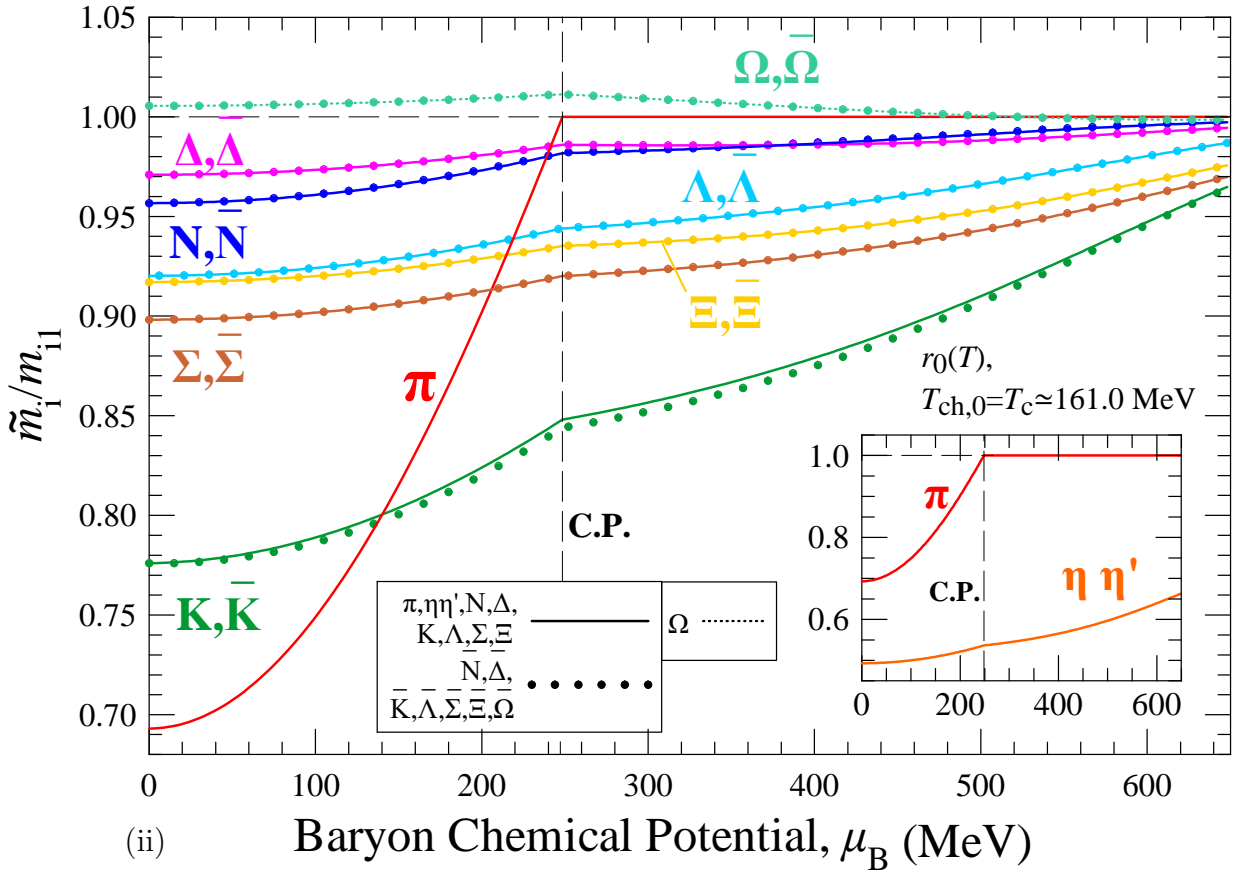
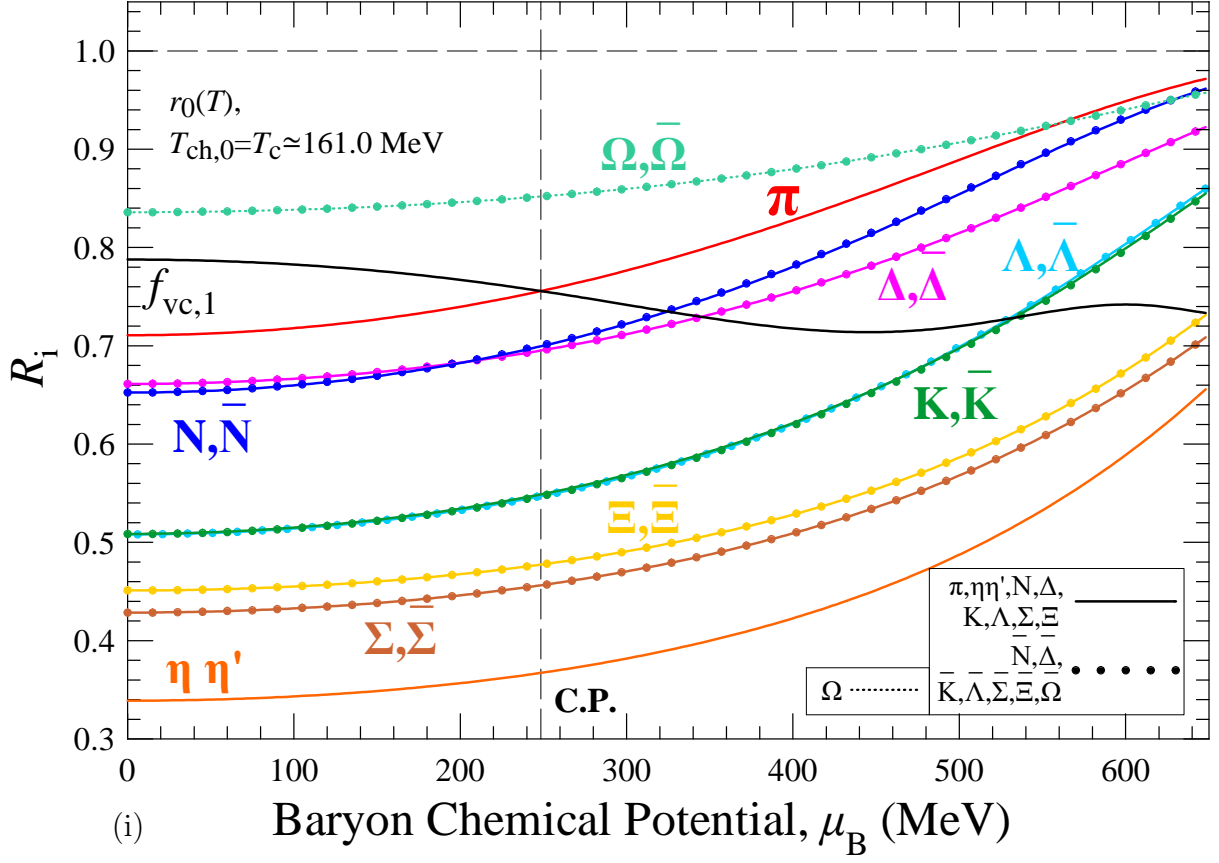


Figure 12: Graph similar to Fig. 10. Calculations are carried out in the interval $T_c \simeq (156.5-164.4)$ MeV. and involve common hadron radius which depends on temperature, $r_0(T)$, determined by the lattice pressure at $\mu_B = 0$ (volume model (b)). In (v) the freeze-out curves which correspond to the maximum value of $T_c = 164.4$ MeV, the minimum value of $T_c = 156.5$ MeV and the value of $T_c = 161.0$ MeV which produces the C.P. depicted with open square are shown. In all graphs with open squares we present the critical point which additionally fulfils the criterion of section 6.



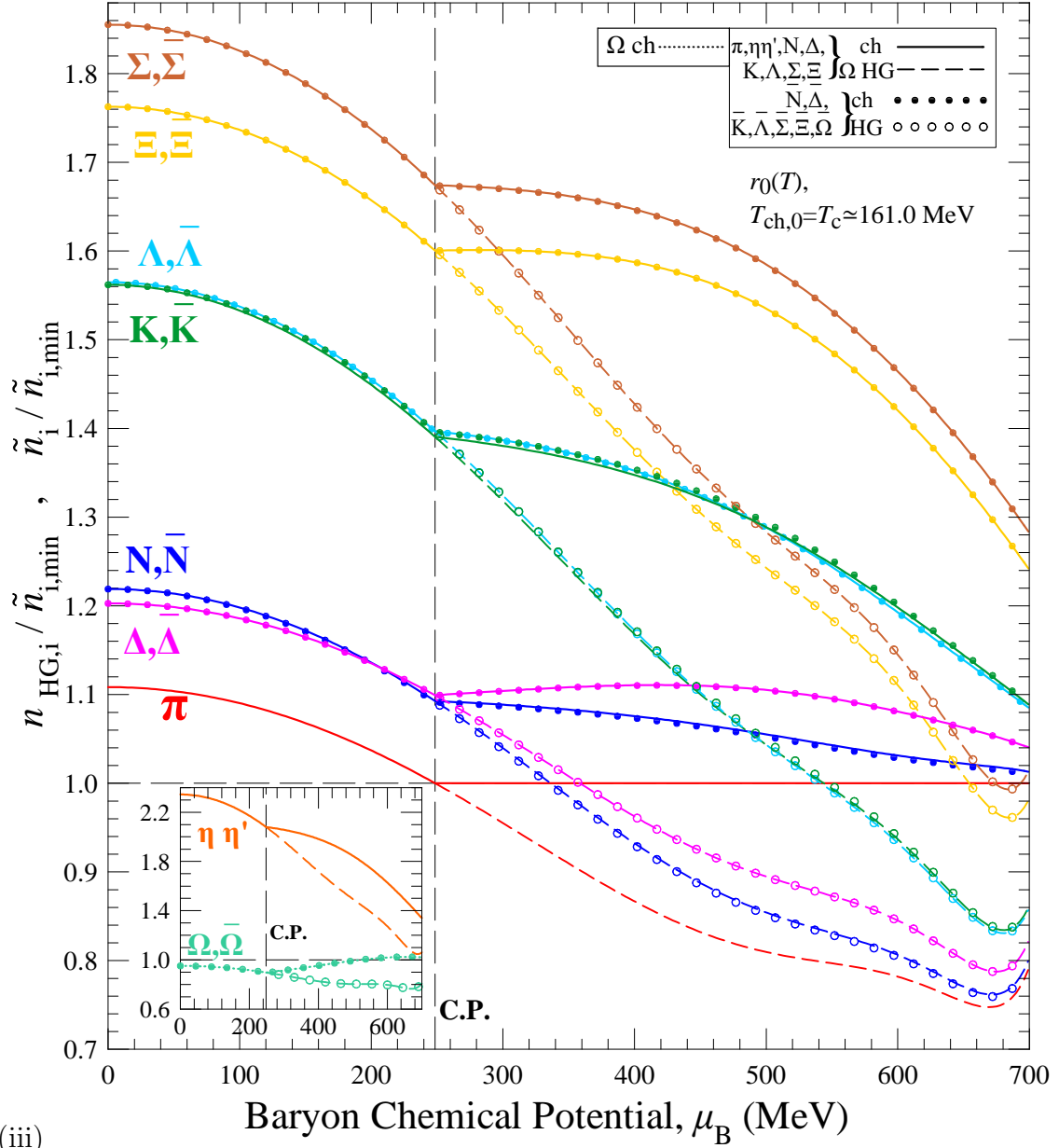


Figure 13: Graph similar to Fig. 11. Calculations are carried out for $T_c = T_{ch,0} \simeq 161.0$ MeV and temperature dependent common hadron radius, $r_0(T)$, determined by the lattice pressure for $\mu_B = 0$. In (i) the shown volume correction factor for the pion family, $f_{vc,1}$, intersects with R_1 at $\mu_B \simeq 248.4$ MeV to produce at this location the critical point.

For the transition curve we use the parametrisation of eq. (20), leaving T_c as a free parameter.

We calculate the position of the critical point, i.e. the value of the critical parameters $(T_{cr}, \mu_{B,cr}, \mu_{s,cr})$ by solving the following set of equations:

$$P_L(T; T_c) = P_{HG}(T, \mu_B = 0, \mu_s = 0; r_0(T)) \quad (51)$$

$$\sum_j n_{HG,1j}(T, \mu_B, \mu_s; r_0(T)) = n_{HG,11}^{pt}(T, \mu_B, \mu_s; \tilde{m}_1 = m_\pi) \quad (52)$$

$$T = f_{fr}(\mu_B; T_c) \quad (53)$$

$$\langle S \rangle (T, \mu_B, \mu_s) = 0 \quad (54)$$

However, we find that the lower value of T_c that results in a real solution for the chiral pion mass is $T_c \simeq 156.5$ MeV. Also, for $T_c \simeq 164.4$ MeV the critical point is located at zero baryon density. In Fig. 12 we show our results for the position of the QCD critical point for all the accepted values of $T_c = 156.5 - 164.4$ MeV. In Fig. 12(i) we plot the calculated radius $r_0(T)$ which corresponds to the temperature of the critical point as a function of T_c . In Figs. 12(ii)-(iv) we depict the position of the point $(T_{cr}, \mu_{B,cr}, \mu_{s,cr})$, respectively, with varying T_c . In Fig. 12(v) we show the solution at zero baryon density for the chiral mass of each family (as the ratio to the higher allowed chiral mass of the family) for different values of T_c . Our findings are similar to the results of the hadronic radius which is independent of the temperature. However, the higher value of μ_B that allows for a critical point is shifted to lower values. Thus, the critical point can be located in the range of $\mu_B \sim (0-498)$ MeV, which corresponds to mean hadronic radius at the critical point $r_{0,cr}(T)$ in the range of $(0.253-0.298)$ fm. Also in Figs. 12 we depict by open square the critical point which is determined by the criterion discussed in the next section 6. This corresponds to $T_c \simeq 161.04$ MeV and it is located at $\mu_B \simeq 248.41$ MeV and $T \simeq 153.21$ MeV.

In Figs. 13 we show results for this value of T_c . In (i) we show the ratios R_i for the different families. The intersection of the pion family with the volume correction factor determines the position of the critical point. In (ii) we show the corresponding solutions for the chiral masses for each family and in (iii) we present the densities in the HG and chiral phases for all families.

5.3 Critical Point with meson and baryon radii

Turning to a more realistic scenario for the hadron volumes, we introduce separate volume radii for the mesons, r_m and for the baryons, r_b . Different hadron volumes have, also, been used through the bag-model where the volume varies with the hadron mass [20, 35] or energy [20]. In [34] different eigenvolumes have been used for several groups of hadrons. Here we assume that the mesonic radius only depends on the temperature, $r_m(T)$ and the baryonic radius only depends on the baryon-chemical potential, $r_b(\mu_B)$. We, also, assume that r_b remains constant at the crossover region with respect to μ_B . So, the baryon-chemical potential begins to affect the baryonic volume at the first order transition region, where the baryonic density has increased above a certain level. Having r_b fixed, we determine the radius $r_m(T)$ from a fit on the Lattice Pressure for a specific value T_c . Then, these two values are passed on to the whole crossover region. Moreover, the fact that the radii are independent on the baryon-chemical potential ($\frac{dv_b}{d\mu_B} = 0$) allows us to calculate densities through eq. (36), instead of eq. (43), for values of baryon-chemical potential up to the critical point. This will be referred to as volume model (c).

In the 1st order transition curve the baryon volume *does* depend on μ_B . Applying eq. (43), we have for mesonic families $\frac{\partial v_j}{\partial \mu_j} = 0$, so:

$$n_{HG,j} = n_{HG,j}^v, \quad j = 1, 2, 5, -5 \quad (55)$$

For the baryonic and antibaryonic families eq. (43) can be rewritten as

$$n_{HG,j} = n_{HG,j}^v \left(1 - P \frac{\partial v_j}{\partial \mu_B} \frac{\partial \mu_B}{\partial \mu_j} \right) \quad (56)$$

For baryons we have $\mu_j = \mu_B + n\mu_S$ with $n = 0, -1, -2, -3$, so $\frac{\partial \mu_B}{\partial \mu_j} = 1$. Similarly, for the antibaryons we have $\frac{\partial \mu_B}{\partial \mu_j} = -1$. Thus, eq. (56) is transformed to

$$n_{HG,j} = n_{HG,j}^v \left(1 - cP \frac{\partial v}{\partial \mu_B} \right), \quad (57)$$

$$c = 1(j = 3, 4, 6, 7, 8, 9), \quad c = -1(j = -3, -4, -6, -7, -8, -9)$$

In the last equation for this model (c) the volume is the common volume to all baryons and antibaryons $v = v_b(\mu_B)$, which is connected to the respective radius r_b .

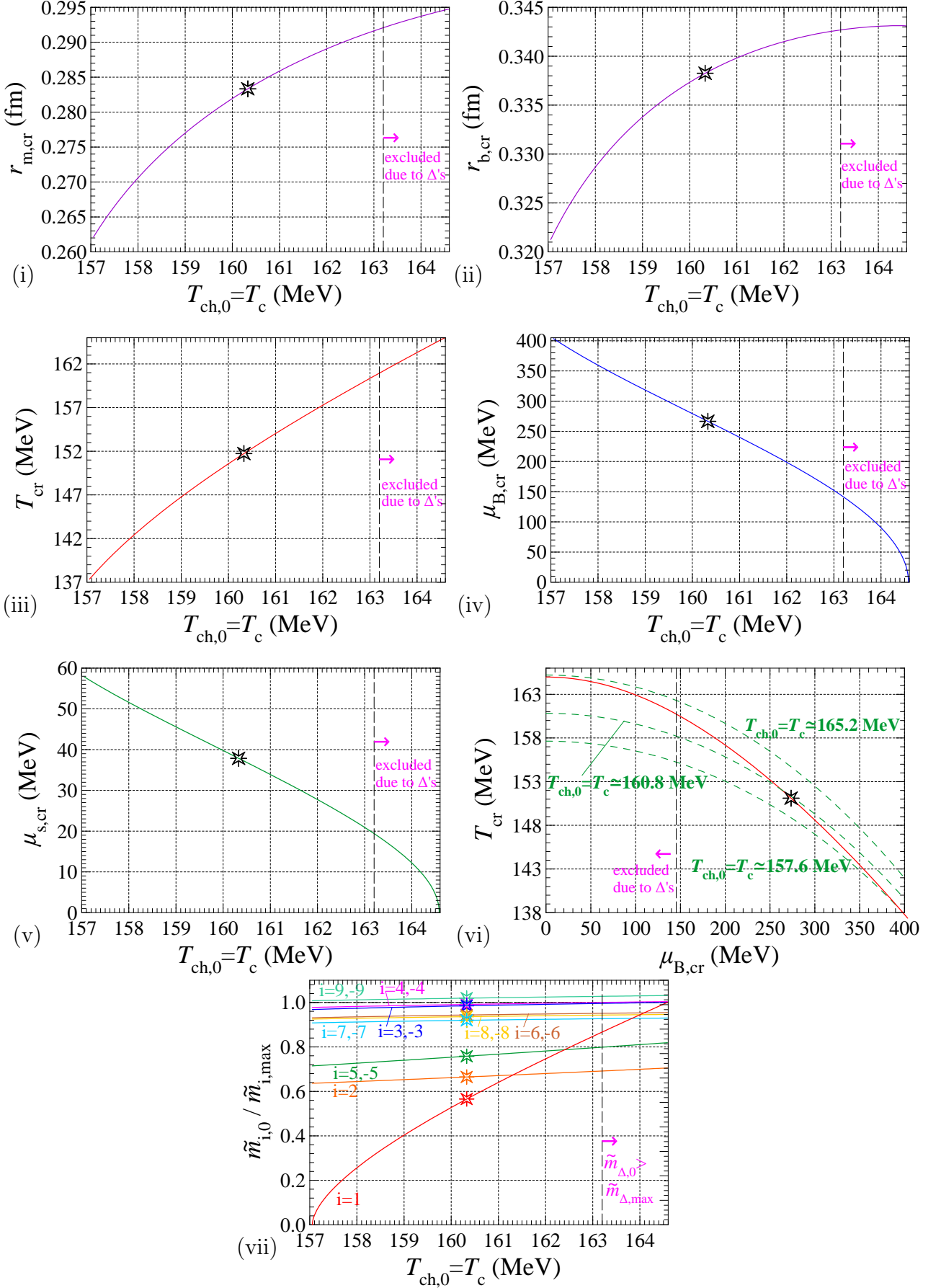


Figure 14: Graph similar to Fig. 10. Calculations are carried out in the interval $T_c \simeq (157.5-165.0)$ MeV and involve a meson radius which depends on temperature, $r_m(T)$ and a baryon radius which depends on baryon-chemical potential, $r_b(\mu_B)$. The radius $r_m(T)$ is determined by the lattice pressure at $\mu_B = 0$ for the value of r_b at the critical point (volume model (c)). In (i),(ii) we depict the value of the meson, baryon radius on the critical point, $r_{m,cr}$, $r_{b,cr}$, as a function of $T_c = T_{ch,0}$, respectively. Graphs (iii)-(vii) correspond to graphs Fig. 10(ii)-(v), respectively. In (vi) we show the freeze-out curves which correspond to the maximum value of $T_c = 165.0$ MeV, the minimum value of $T_c = 157.5$ MeV together with the curve for $T_c = 160.7$ MeV (corresponding to the C.P. which is depicted with a star). In all graphs with stars we present the critical point which additionally fulfils the criterion described in section 6. Also, we include in all graphs a region where the Δ family acquires slightly higher chiral mass than the maximum allowed value.

The extra parameter for the baryon radius, r_b , allows us to impose the constraint that the chiral masses of both the pion and nucleon families acquire their maximum values at the critical point. For a specific choice of $T_c = T_{ch,0}$ we have a freeze out curve which links the freeze out temperature with the baryon-chemical potential. So, in order to calculate the position of the critical point we have to evaluate the value of the critical parameters $(T_{cr}, \mu_{Bcr}, \mu_{scr})$, as well as, the values of the meson radius, r_m and baryon radius, r_b . This is accomplished by solving, for given T_c , the following set of five equations:

$$P_L(T; T_c) = P_{HG}(T, \mu_B = 0, \mu_s = 0; r_m(T), r_b) \quad (58)$$

$$n_{HG,1}^v(T, \mu_B, \mu_s; r_m(T), r_b) = \tilde{n}_1(T, \mu_B, \mu_s; \tilde{m}_1 = m_\pi) \quad (59)$$

$$n_{HG,3}^v(T, \mu_B, \mu_s; r_m(T), r_b) = \tilde{n}_3(T, \mu_B, \mu_s; \tilde{m}_3 = m_n) \quad (60)$$

$$T = f_{fr}(\mu_B; T_c) \quad (61)$$

$$\langle S \rangle_{HG}(T, \mu_B, \mu_s; r_m(T), r_b) = 0 \quad (62)$$

We find that for $T_c = T_{ch,0} \gtrsim 157.5$ MeV there is real solution for the chiral pion mass and that for $T_c \simeq 165.0$ MeV the position of the critical point is located at zero baryon chemical potential. However, for $T_c \gtrsim 163.6$ MeV the Δ family develops a chiral mass which is slightly above the maximum allowed value (at most 0.4%). To stay on the safe side we exclude these cases for the solution of a critical point. Thus, the critical point is located in the interval $\mu_B \simeq 142-404$ MeV and the area in μ_B which is allowed for the critical point is further suppressed compared to the case of the common hadronic radius. In Fig. 14 we show our results for the position of the QCD critical point for the values for $T_c = 157.5-165.0$ MeV. In Figs. 14(i)-(ii) we plot the calculated mesonic radius r_m and baryonic radius r_b which correspond to the conditions of the critical point as function of T_c . In Figs. 14(iii)-(v) we depict the position of the critical point $(T_{cr}, \mu_{B,cr}, \mu_{s,cr})$, respectively as a function of T_c . In Fig. 14(vi) we illustrate the solution at zero baryon density for the chiral mass of each family (as the ratio to the higher allowed chiral mass of the family) with varying T_c . Also, in Figs. 14 we show by a star the critical point which further fulfils the criterion described in the next Section 6. This corresponds to $T_c \simeq 160.73$ MeV and it is located at $\mu_B \simeq 266.56$ MeV and $T \simeq 151.74$ MeV.

Next we can evaluate the thermodynamic variables on the crossover curve, for a given value of T_c . The value of r_b remains fixed to the value which was found from the equations that determined the critical point for this value of T_c . So we obtain $(T, \mu_s; r_m)$ for every value of μ_B by solving equations (58),(61) and (62), while the chiral masses for all families are calculated by eq. (12) with $V_{HG} = \tilde{V}$.

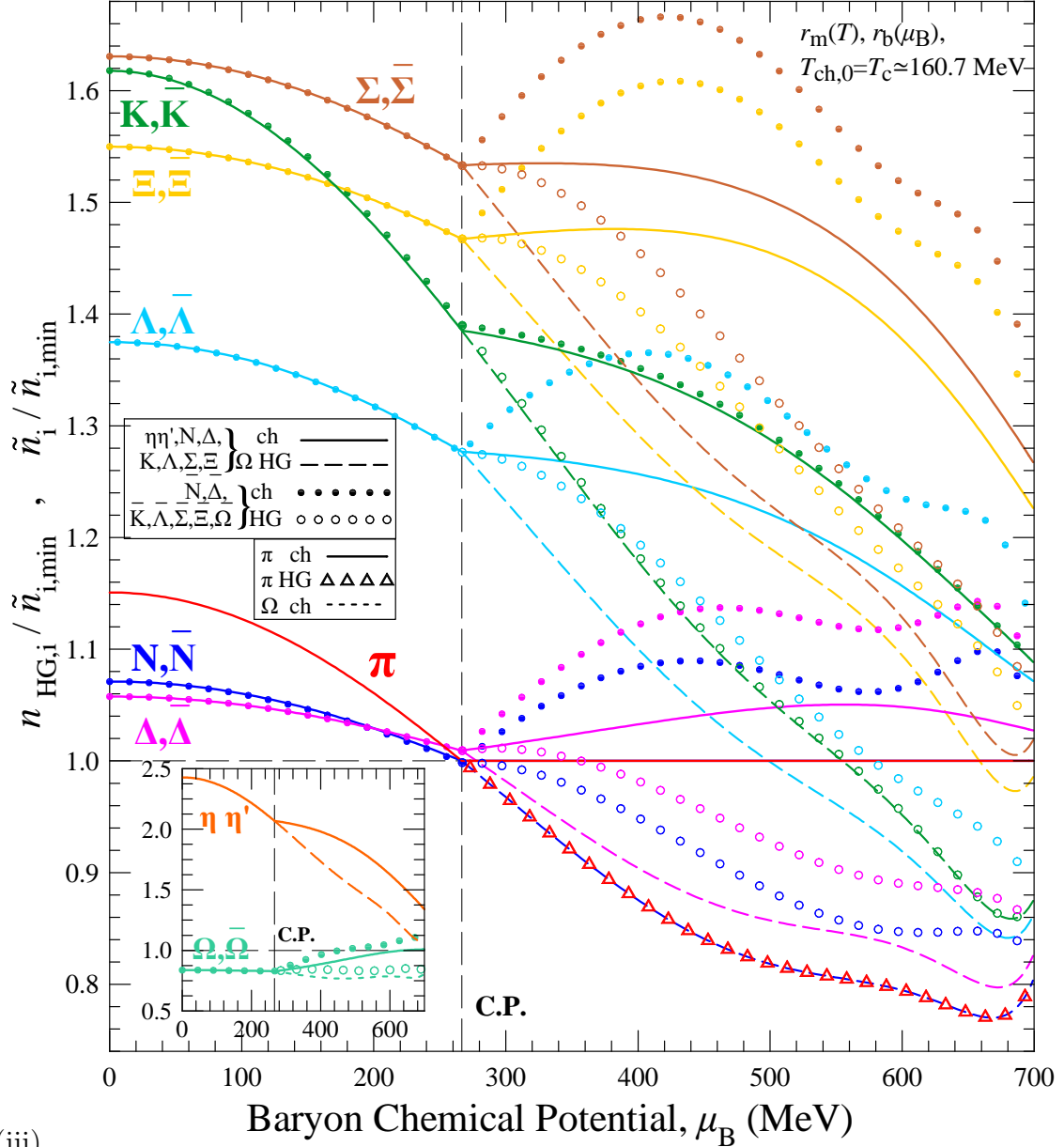


Figure 15: Graph similar to Fig. 11. Calculations are carried out for $T_c = T_{ch,0} \simeq 160.73$ MeV and different meson $r_m(T)$ and baryon $r_b(\mu_B)$ radii, determined by the lattice pressure for $\mu_B = 0$. In (i) the shown volume correction factors for the pion family, $f_{vc,1}$, and the nucleon family, $f_{vc,3}$, simultaneously intersect with R_1 and R_3 , respectively, at $\mu_B \simeq 266.56$ MeV and produce at this location the critical point.

Turning, then, to the first order transition line, we have to evaluate for specific T_c the set of variables $(T, \mu_s, v_{er}; r_m, r_b)$, since now, we allow r_b to change. Given a value of r_b , we determine $r_m(T)$ from the lattice pressure curve for zero baryon density. The chiral masses of the pion and the nucleon family remain fixed at their corresponding maximum values. Since we allow the baryon radius to depend on μ_B and the meson radius does not depend on μ_B , we have to replace eqs. (59) and (60) by the equations:

$$n_{HG,1}^v = v_{er}^{-1} \tilde{n}_{1,min} \Rightarrow v_{er}^{-1} = \frac{n_{HG,1}^v}{\tilde{n}_{1,min}} \quad (63)$$

$$n_{HG,3} = v_{er}^{-1} \tilde{n}_{3,min} \Rightarrow n_{HG,3}^v \left(1 - P_{HG} \frac{\partial v}{\partial \mu_B} \right) = v_{er}^{-1} \tilde{n}_{3,min} \Rightarrow$$

$$P_{HG} \frac{\partial v}{\partial \mu_B} = 1 - v_{er}^{-1} \frac{\tilde{n}_{3,min}}{n_{HG,3}^v} \Rightarrow \frac{\partial v}{\partial \mu_B} = \frac{1}{P_{HG}} \left(1 - \frac{n_{HG,1}^v \tilde{n}_{3,min}}{n_{HG,3}^v \tilde{n}_{1,min}} \right), \quad (64)$$

where $v = v_b(\mu_B)$. The zero strangeness condition has to be imposed, as well, which in view of eqs. (55) and (57), acquires the form:

$$\langle S \rangle_{HG} = 0 \Rightarrow n_{HG,S} = 0 \Rightarrow n_{HG,S}^v + P \frac{\partial v}{\partial \mu_B} n_{HG,|S|,b+\bar{b}}^v = 0, \quad (65)$$

where the subscript $|S|, b + \bar{b}$ denotes the absolute strangeness enclosed in the baryonic and antibaryonic families, i.e.

$$n_{HG,|S|,b+\bar{b}}^v = n_{HG,6}^v + n_{HG,-6}^v + n_{HG,7}^v + n_{HG,-7}^v + 2(n_{HG,8}^v + n_{HG,-8}^v) + 3(n_{HG,9}^v + n_{HG,-9}^v). \quad (66)$$

Eqs. (58),(61), (63)-(65) form a system of five equations which allows us to determine the set of variables $(T, \mu_s, v_{er}; r_m, r_b)$, for a given value of μ_B . The situation is simplified since eqs. (61), (63) allow us to solve for T and v_{er} directly. So, eqs.(58),(64) and (65) form a subset of three equations (one of which is a differential equation, though), which allows to evaluate r_m, r_b and μ_s . The chiral masses for all families except the pion ($i = 1$) and the nucleon family ($i = 3$) are calculated by eq. (12) with $V_{HG} = v_{er} \tilde{V}$.

In Fig. 15 we depict all the calculations (as a function of μ_B) for a specific value of $T_c \simeq 160.7$ MeV which, also, fulfils the criterion described in section 6. In (i) we plot the ratios R_i , where the simultaneous intersections of the volume correction factors for the pion and the nucleon family with the corresponding ratios R_i determine the position of the critical point. In (ii) we plot the chiral masses of the hadronic families, where, at the first order transition line, the chiral masses of the pion and the nucleon families remain constant, retaining their maximum allowed values. In (iii) we display the densities of the families, with suitable normalisation, at the hadronic and chiral phases. We observe that in the 1st order transition curve, where the baryon volume depends on μ_B , the densities of the baryon families exhibit different behaviour than the corresponding antibaryon families due to the different sign that enters eq. (57).

5.4 Critical Point from Lattice QCD at finite baryon-chemical potential

Lattice calculation at finite values of baryon chemical potential have been carried out in [11–16]. We use the results of the pressure p/T^4 as function of temperature T for fixed values of $\hat{\mu}_B \equiv \mu_B/T$ from 0 to 3.5 with 0.5 MeV step from [11]. These values are determined for vanishing strangeness chemical potential, μ_s . The temperature values of interest are in the range 125 – 170 MeV. The lower value is given by the presented calculations and the upper is an approximate upper bound for the critical Lattice temperature for $\mu_B = 0$, which sets an upper temperature bound in the existence of the Hadron Gas. The values from the graph are then fitted with a 4th degree polynomial (as function of T) to produce a curve that fits the pressure points for each value of fixed $\hat{\mu}_B$. Totally, we have 8 such curves, which give us the pressure as function of T at specific values of $\hat{\mu}_B$. Then, each time we need the pressure at a given point $(T_1, \hat{\mu}_{B,1})$, we evaluate from these 8 curves the pressure values for temperature T_1 and 8 values of $\hat{\mu}_B$. On these 8 values we perform a fit with a 6th degree polynomial, but only with the even powers present (since the pressure has to be an even function of $\hat{\mu}_B$). This procedure gives us the pressure as function of chemical potential for the specific temperature T_1 and we can just read the value for the specific $\hat{\mu}_{B,1}$.

We, also, need to allow the critical temperature at $\mu_B = 0$, $T_{0,c} \equiv T_c(0)$ to vary. In such case we define the dimensionless temperature $t \equiv \frac{T}{T_{0,c}}$. If the critical temperature is shifted to $T'_{0,c}$ the

temperature T' for which t stays unchanged is

$$t = t' \Rightarrow \frac{T}{T_{0,c}} = \frac{T'}{T'_{0,c}} \Rightarrow T' = T \frac{T'_{0,c}}{T_{0,c}} \Rightarrow T' = Ta \quad (67)$$

where we have defined

$$a \equiv \frac{T'_{0,c}}{T_{0,c}} = \frac{T'}{T} \quad (68)$$

For vanishing baryon chemical potential we demand that the dimensionless pressure $\hat{P} \equiv \frac{P}{T^4}$ stays the same at the same t , so

$$\hat{P}'(t') = \hat{P}(t) \Rightarrow \hat{P}'(T') = \hat{P}\left(\frac{T'}{a}\right) \Rightarrow P'(T') = a^4 P\left(\frac{T'}{a}\right) \quad (69)$$

This was the case for volume models (a), (b) and (c).

In [36, 37] the critical temperature is taken to be $T_c = 158$ MeV. For finite baryon chemical potential the critical temperature changes as ([36, 37]):

$$T_c(\mu_B) = T_{0,c} \left[1 - k_2 \left(\frac{\mu_B}{T_{0,c}} \right)^2 \right]. \quad (70)$$

Demanding eq. (70) to stay unchanged, if we change the critical temperature from $T_{0,c}$ to $T'_{0,c}$, amounts to

$$T'_c(\mu'_B) = T'_{0,c} \left[1 - k_2 \left(\frac{\mu'_B}{T'_{0,c}} \right)^2 \right] \quad (71)$$

Since $T'_c(\mu'_B)$ is the temperature that corresponds to the lattice with $T'_{0,c}$, it should be related to $T_c(\mu_B)$ through eq. (67). Combing eqs. (67)-(71) we get

$$T'_c(\mu'_B) = T_c(\mu_B) \frac{T'_{0,c}}{T_{0,c}} \Rightarrow \frac{\mu'_B}{T'_{0,c}} = \frac{\mu_B}{T_{0,c}} \Rightarrow \frac{\mu'_B}{T'} = \frac{\mu_B}{T} \Rightarrow \hat{\mu}'_B = \hat{\mu}_B. \quad (72)$$

Thus, for eq. (70) to remain unchanged the baryon chemical potential has to be shifted to

$$\hat{\mu}'_B = \hat{\mu}_B \Rightarrow \mu'_B = \mu_B \frac{T'_{0,c}}{T_{0,c}} \Rightarrow \mu'_B = \mu_B a \quad (73)$$

We assume the same behaviour for any other chemical potential describing the system:

$$\hat{\mu}'_U = \hat{\mu}_U \quad (74)$$

Generalising eq. (69) for the pressure as function of any set of chemical potentials, as well, we get

$$P'(T', \dots, \mu'_B, \dots) = a^4 P\left(\frac{T'}{a}, \dots, \frac{\mu'_U}{a}, \dots\right) \Rightarrow \hat{P}'(T', \dots, \hat{\mu}'_U, \dots) = \hat{P}(T, \dots, \hat{\mu}_U, \dots) \quad (75)$$

Assuming that for a quantity \hat{f} the following relation holds:

$$\hat{f}'(T', \dots, \hat{\mu}'_U, \dots) = \hat{f}(T, \dots, \hat{\mu}_U, \dots), \quad (76)$$

then we have

$$\left. \frac{\partial \hat{f}'(T', \dots, \hat{\mu}'_U, \dots)}{\partial \hat{\mu}'_U} \right|_{T', \dots} = \left. \frac{\partial \hat{f}(T'/a, \dots, \hat{\mu}'_U, \dots)}{\partial \hat{\mu}'_U} \right|_{T'/a, \dots} = \left. \frac{\partial \hat{f}(T, \dots, \hat{\mu}_U, \dots)}{\partial \hat{\mu}_U} \right|_{T, \dots}. \quad (77)$$

Applying the above procedure to any kind of chemical potentials and any order of derivatives we get that for any susceptibility

$$\chi'_{ijk}{}^{BSQ}(T', \hat{\mu}'_B, \hat{\mu}'_S) = \chi_{ijk}{}^{BSQ}(T, \hat{\mu}_B, \hat{\mu}_S) \quad (78)$$

Using equations (76)-(77) for the dimensionless pressure, we find for the dimensionless baryon density $\hat{n}_B \equiv \frac{n_B}{T^3}$

$$\hat{n}'_B(T', \hat{\mu}'_B) = \hat{n}_B(T, \hat{\mu}_B) \quad (79)$$

After dealing with derivatives of chemical potentials, we turn to temperature derivatives. Assuming that we have defined a new dimensionless quantity:

$$\hat{h}(T, \dots, \hat{\mu}_U, \dots) \equiv T^k \left. \frac{\partial^k \hat{f}(T, \dots, \hat{\mu}_U, \dots)}{\partial T^k} \right|_{\dots, \hat{\mu}_U, \dots}, \quad (80)$$

then (76) leads to:

$$T'^k \left. \frac{\partial^k \hat{f}'(T', \dots, \hat{\mu}'_U, \dots)}{\partial T'^k} \right|_{\dots, \hat{\mu}'_U, \dots} = T'^k \frac{1}{a^k} \left. \frac{\partial \hat{f}(T'/a, \dots, \hat{\mu}'_U, \dots)}{\partial (T'/a)^k} \right|_{\dots, \hat{\mu}'_U, \dots} \quad (81)$$

So

$$\hat{h}'(T', \dots, \hat{\mu}'_U, \dots) = \hat{h}(T, \dots, \hat{\mu}_U, \dots) \quad (82)$$

Also, for a dimensionless entropy density $\hat{s} \equiv \frac{s}{T^3}$, we have:

$$T \frac{\partial \hat{P}}{\partial T} = -4\hat{P} + \hat{s} \quad (83)$$

Identifying in (80) $\hat{f} = \hat{P}$ and $k = 1$ and using (82), (83) and (75) we arrive at:

$$\hat{s}'(T', \dots, \hat{\mu}'_U, \dots) = \hat{s}(T, \dots, \hat{\mu}_U, \dots) \quad (84)$$

In Fig. 16 (i)-(ii) we have plotted the Lattice QCD results for the normalised pressure \hat{P} for vanishing value of strangeness chemical potential ($\mu_S = 0$) extracted from Fig. 4 in [11] depicted as solid rhomboid points. These correspond to the value of $T_c = 158$ MeV. On the same graphs we present our reconstruction which is carried through the fit on these points. Also, we plot the corresponding results of the Ideal Hadron Gas (IHG), i.e. Hadron Gas with zero hadron volumes. It is evident that the Lattice QCD pressure for $T_c = 158$ MeV at certain domains rises above the IHG pressure. This means that at these domains, if we try to have a Hadron Gas description for the Lattice results, we will get a negative hadron volume which is physically impossible. However, if we shift the Lattice results to a higher temperature, using eqs. (67), (74) and (75), e.g. $T_c = 161$ MeV, we find that the Lattice pressure is lower than the IHG pressure, meaning that a positive solution for the hadron volume can make the two pressures identical.

We proceed by evaluating a volume parameter equal for all hadrons which depends on temperature and baryon chemical potential so that the Lattice QCD and Hadron Gas pressure be equal at any point of the $\mu_S = 0$ plane. This amounts to solving, for specific T_c , the equation:

$$P_L(T, \mu_B, \mu_S = 0; T_c) = P_{HG}(T, \mu_B, \mu_S = 0; r(T, \mu_B)) \quad (85)$$

where $r(T, \mu_B)$ is the radius of the common hadron volume. At this point we make the assumption that the common hadron volume does not depend on the strangeness chemical potential, so we use the calculated from eq. (85) radii as input to evaluate our Hadron Gas model (called model (d)) for any point (T, μ_B, μ_S) .

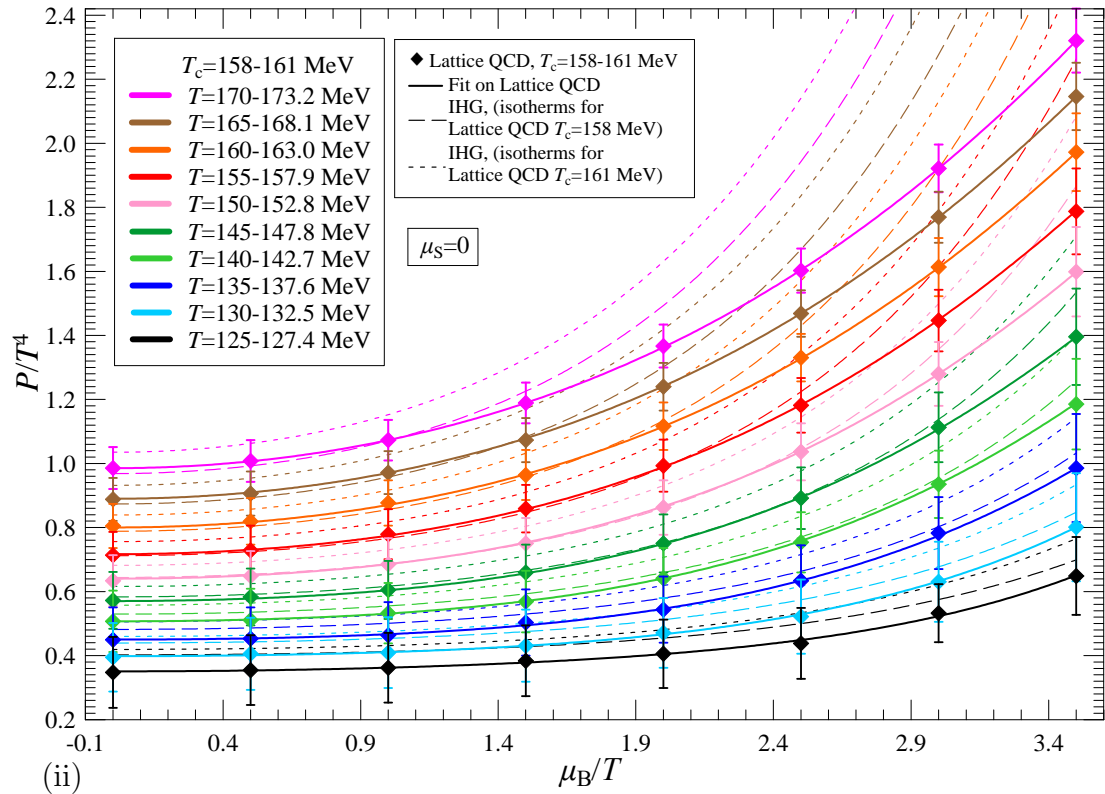
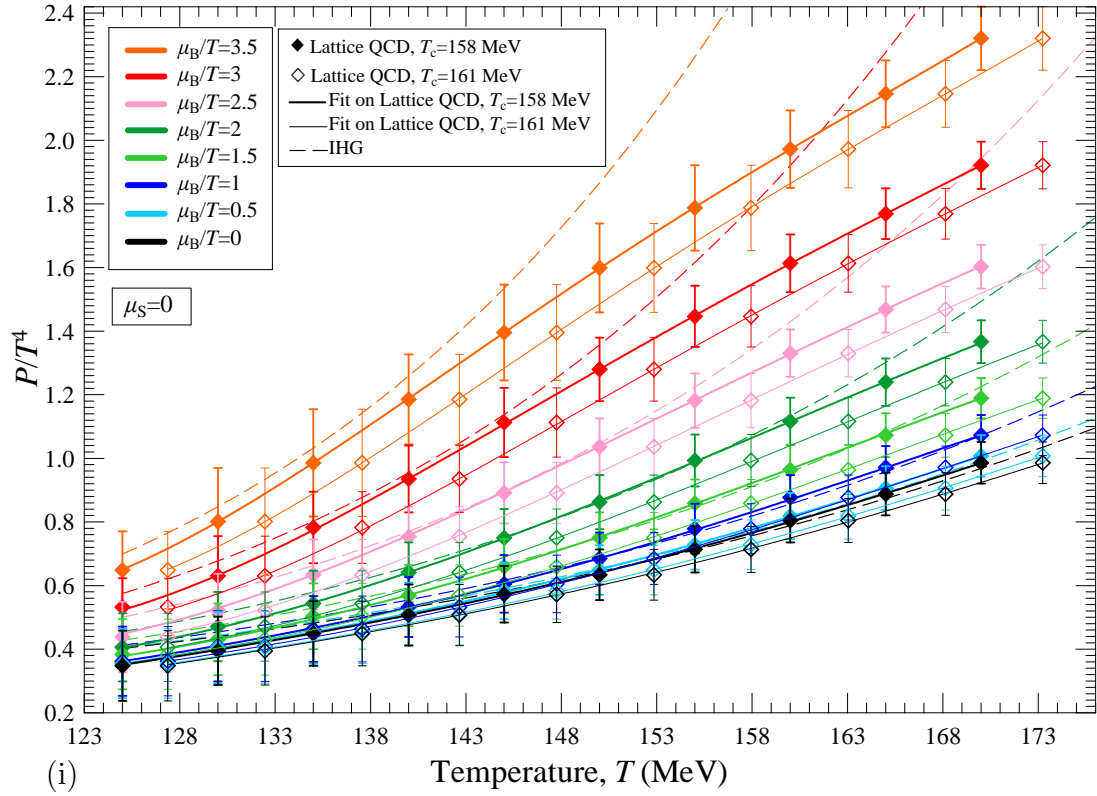


Figure 16: (i) The pressure P/T^4 for constant μ_B/T as function of temperature. Lattice QCD calculations extracted from Fig. 4 of [11] at $T_c = 158(161)$ MeV appear with closed (open) rhomboid points. Our fits on these points are depicted with thick (thin) continuous lines. Corresponding Ideal Hadron Gas (IHG) calculations appear with slashed lines (one set of curves since IHG formalism does not depend on T_c). (ii) The pressure P/T^4 for constant temperature as function of μ_B/T . Since the quantity P/T^4 remains the same as function of $\hat{\mu}_B$ under the shift of T_c (eq. (75)), the Lattice QCD calculations and the corresponding fits are unchanged for the two values of T_c which are considered, however, they correspond to different isotherms, according to the displayed legend. The IHG curves which correspond to Lattice curves of $T_c = 158(161)$ MeV are displayed with slashed (dotted) lines. All calculations in (i) and (ii) are carried out at vanishing strangeness chemical potential ($\mu_S = 0$). Each set of curves from lower to higher values of pressure correspond to gradually increasing values of μ_B/T in (i) and T in (ii).

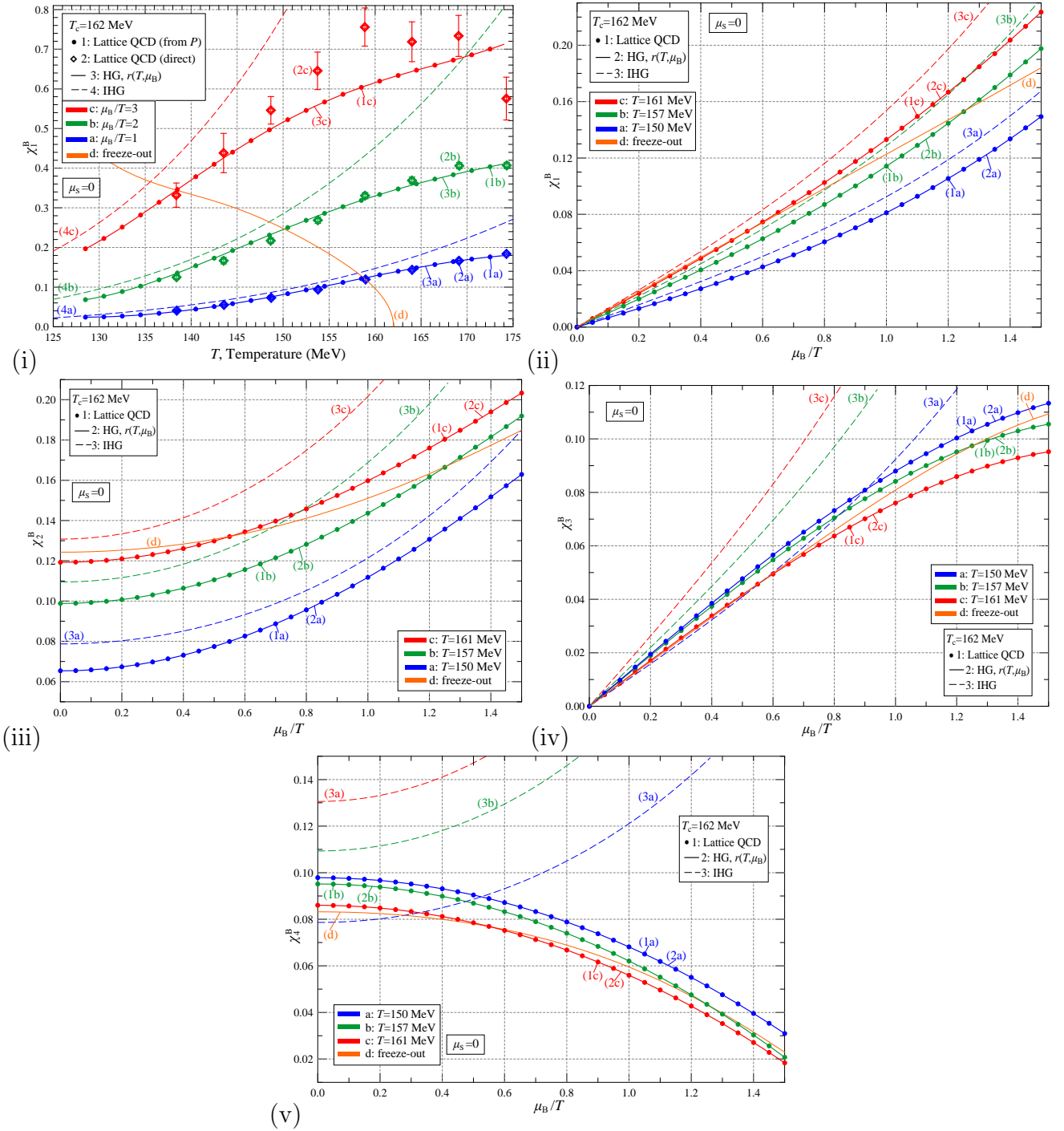


Figure 17: Baryon susceptibilities $\chi_j^B = \left(\frac{\partial}{\partial \mu_B}\right)^j \frac{P(T, \mu_B)}{T^4}$, $j = 1, 2, 3, 4$ for $T_c = 161$ MeV. Solid circles are evaluations from the fits on the Lattice QCD pressure from Fig. 4 of [11], while continuous thick lines are the susceptibilities from our HG model which uses hadron volumes with radius $r(T, \mu_B)$ evaluated from eq. (85). We plot with thin continuous lines the boundaries set by the freeze-out curve within which the HG needs to hold. We, also, show the respective IHG calculations. In (i) we include as open rhomboid points direct calculation of χ_1^B from Fig. 1 of [11] (N²LO points).

In Fig. 17 we depict the baryon susceptibilities. For the Lattice QCD we can only evaluate these susceptibilities for $\mu_s = 0$ (solid lines on the graphs). The corresponding susceptibilities from the HG (circular points) show a calculation consistency for our model. In Fig. 17(i) we also include direct evaluation of χ_1^B from [11]. We note that the HG model needs to hold only for temperatures lower than the freeze-out curve described by eq. (20). For comparison we include the susceptibilities

of the Ideal HG.

To locate the critical point for specific $T_c = T_{ch,0}$, apart from eqs. (85) and (61), we have to solve the set of equations:

$$n_{HG,1}(T, \mu_B, \mu_s; r(T, \mu_B)) = \tilde{n}_1(T, \mu_B, \mu_s; \tilde{m}_1 = m_\pi) \quad (86)$$

$$\langle S \rangle_{HG}(T, \mu_B, \mu_s; r(T, \mu_B)) = 0 \quad (87)$$

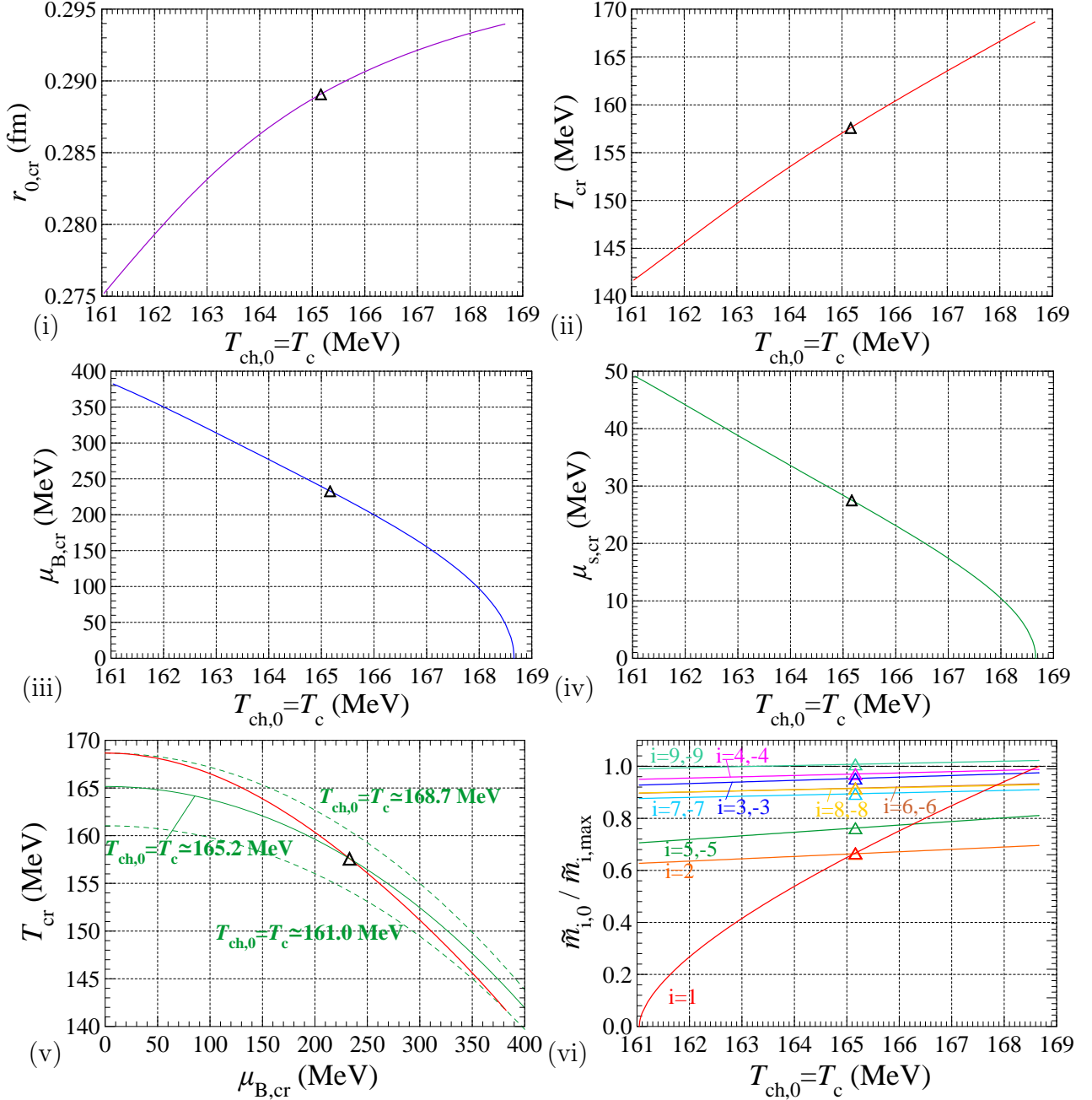
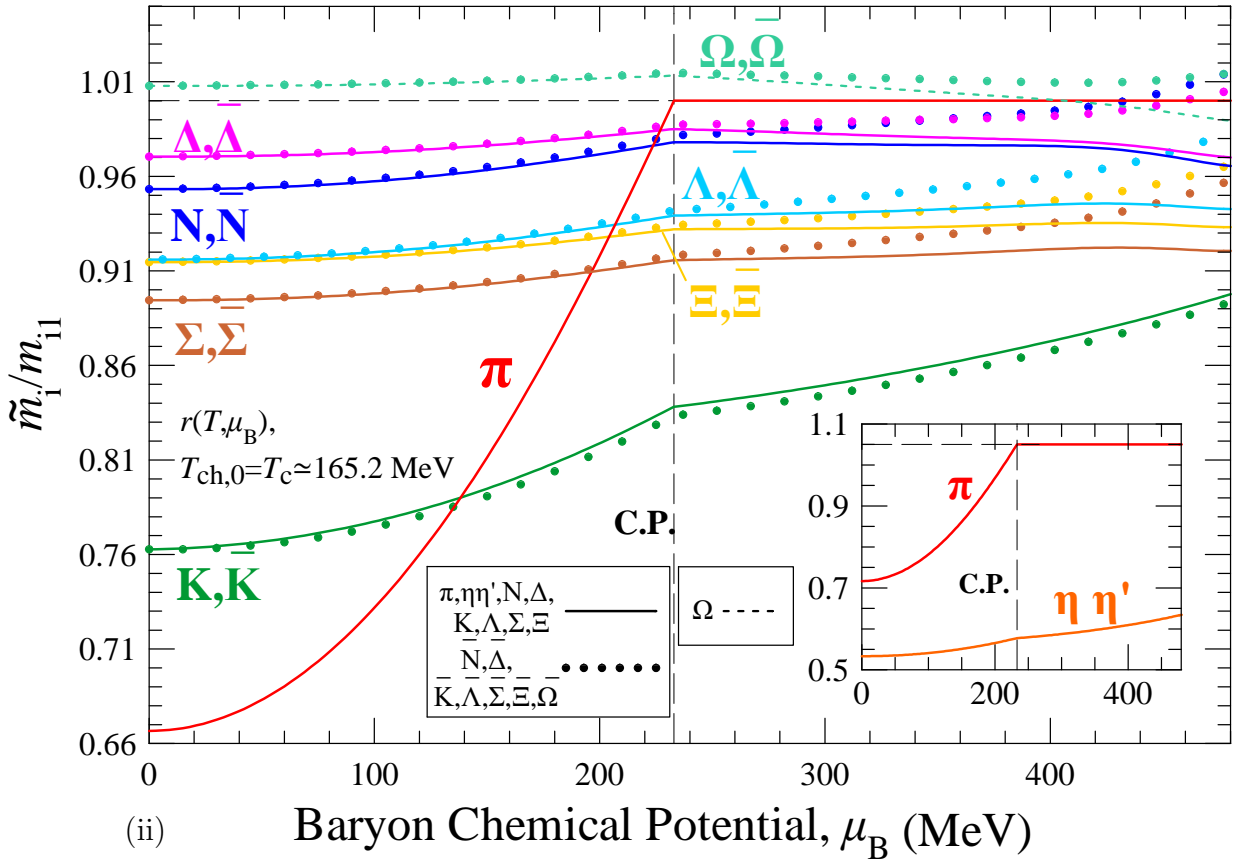
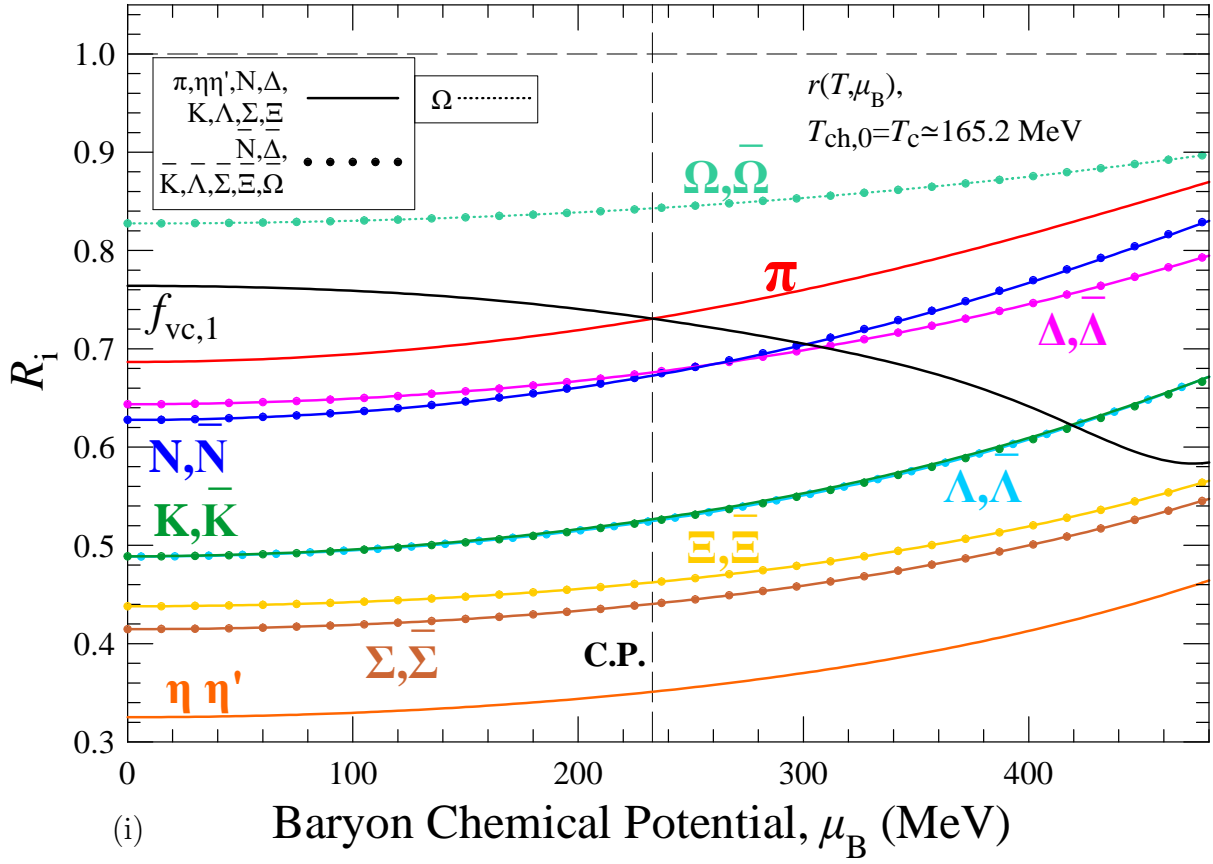
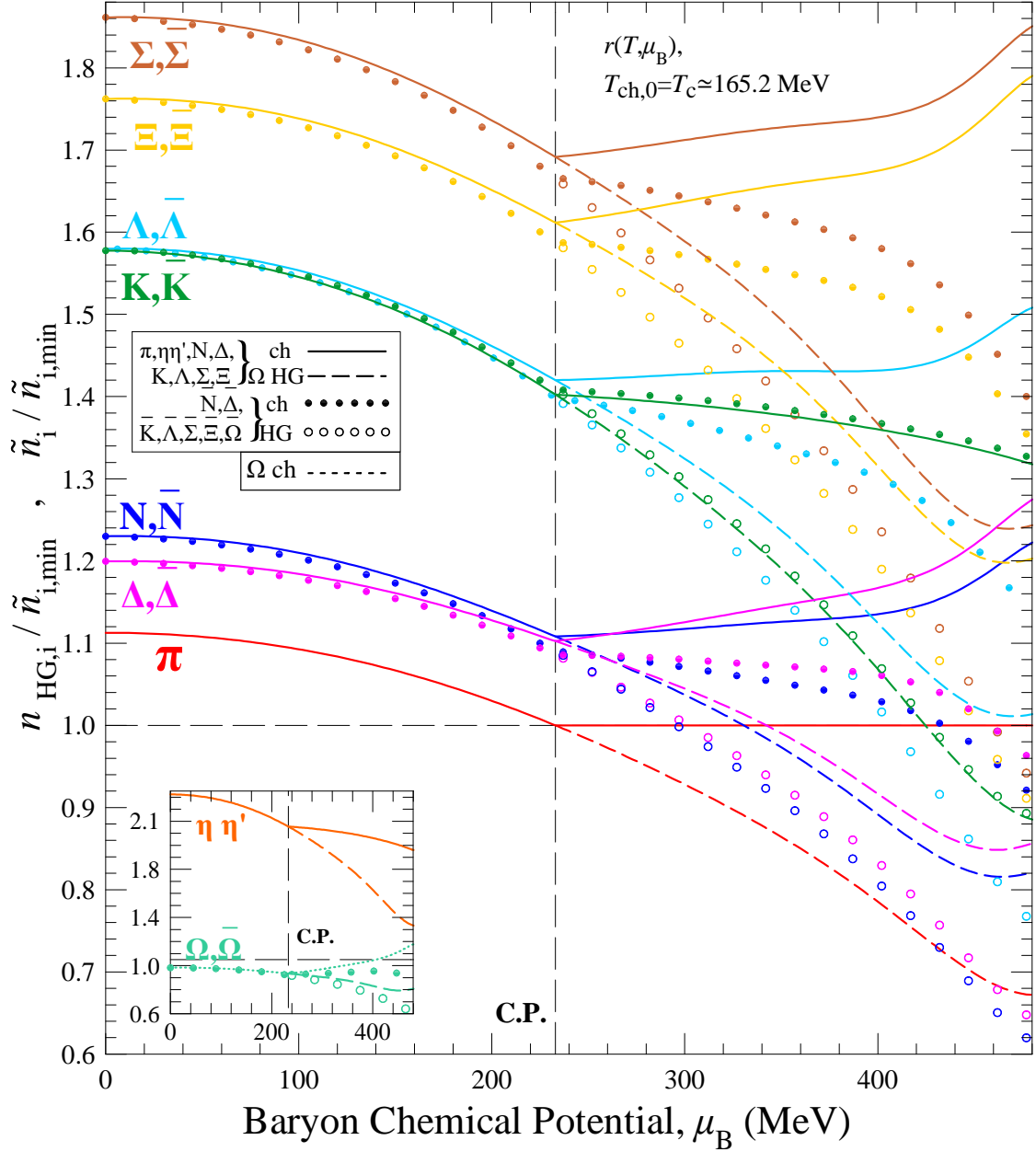


Figure 18: Graph similar to Fig. 10. Calculations are carried out in the interval $T_c \simeq (161.0-168.7)$ MeV. and involve common hadron radius which depends on temperature and baryon-chemical potential, $r(T, \mu_B)$, determined by the lattice pressure at $\mu_S = 0$ (volume model (d)). In (v) the freeze-out curves which correspond to the maximum value of $T_c = 168.7$ MeV, the minimum value of $T_c = 161.0$ MeV and the value of $T_c = 165.20$ MeV which produces the C.P. depicted with triangle are shown. In all graphs with triangles we present the critical point which additionally fulfils the criterion of section 6.





(iii)

Figure 19: Graph similar to Fig. 11. Calculations are carried out for $T_c = T_{ch,0} \simeq 165.16$ MeV and common hadronic radius $r_m(T, \mu_B)$, determined by the lattice pressure for $\mu_S = 0$. In (i) the shown volume correction factor for the pion family, $f_{vc,1}$, intersects with R_1 at $\mu_B \simeq 232.97$ MeV to produce at this location the critical point.

Eq. (87) acquires the same form as eq. (65), where we now identify $v = v(T, \mu_B)$. The derivative $\frac{\partial v}{\partial \mu_B}$ can be provided numerically from the values of r at adjacent points evaluated through eq. 85.

We present solutions for the critical point in the same manner as in the previous subsections (5.1-5.3) in Figs. 18(i)-(vi). We find that for $T_c = T_{ch,0} \gtrsim 161.0$ MeV there is positive solution for the chiral pion mass and that for $T_c \simeq 168.7$ MeV the position of the critical point is located at zero baryon chemical potential, thus, the values of T_c between these values produce acceptable solutions for the critical point. We note that the rather high values of T_c in the interval (166-168.7) MeV stay within the limit of the freeze-out temperature at low baryon-chemical potential $T_f = 166 \pm 3$ MeV recorded in [38]. Also, in Figs. 18(i)-(vi) we show by triangle the critical point which further

fulfils the criterion that the densities of q and s quarks which are contained in mesons and baryons are equal (described in the next Section 6). This corresponds to $T_c \simeq 165.2$ MeV and it is located at $\mu_B \simeq 233.0$ MeV and $T \simeq 157.6$ MeV.

Next we can evaluate the thermodynamic variables on the crossover and the 1st order transition curve, for a specific value of T_c which we choose to be the aforementioned one $T_c = 165.2$ MeV. The results are shown in Figs. 19(i)-(iii). We observe in Fig. 19(ii) that for some families the antibaryon chiral masses, at high values of μ_B rise above their maximum allowed values. On this effect we have to comment that: 1) The calculations are carried out at high $\mu_B \sim 480$ MeV and relative low $T \sim 130$ MeV where the Lattice QCD calculations may not be so precise. 2) Only one volume parameter is used for all hadrons. An introduction of a separate volume parameter for the baryons and antibaryons families may remedy the result. 3) The problem appears on antibaryon species existing in large positive μ_B , where their density is highly suppressed. Therefore, their presence is expected to have a minor effect on the system.

We end this section by presenting some further characteristics of the models we analysed. We utilise the solution for each model which further satisfies the criterion of the equality of the densities of q and s quarks contained in mesons and baryons (described in the next section).

In Fig. 20 we present for the models (a)-(d) the solution on the transition curve (crossover-1st order) for the hadron radius. For model (c) there are two separate radii for mesons and baryon-antibaryons. We, also, present the solution for model (c) for the derivative of r_b and for model (d) for the derivative of r with respect to the baryon chemical potential on the transition curve.

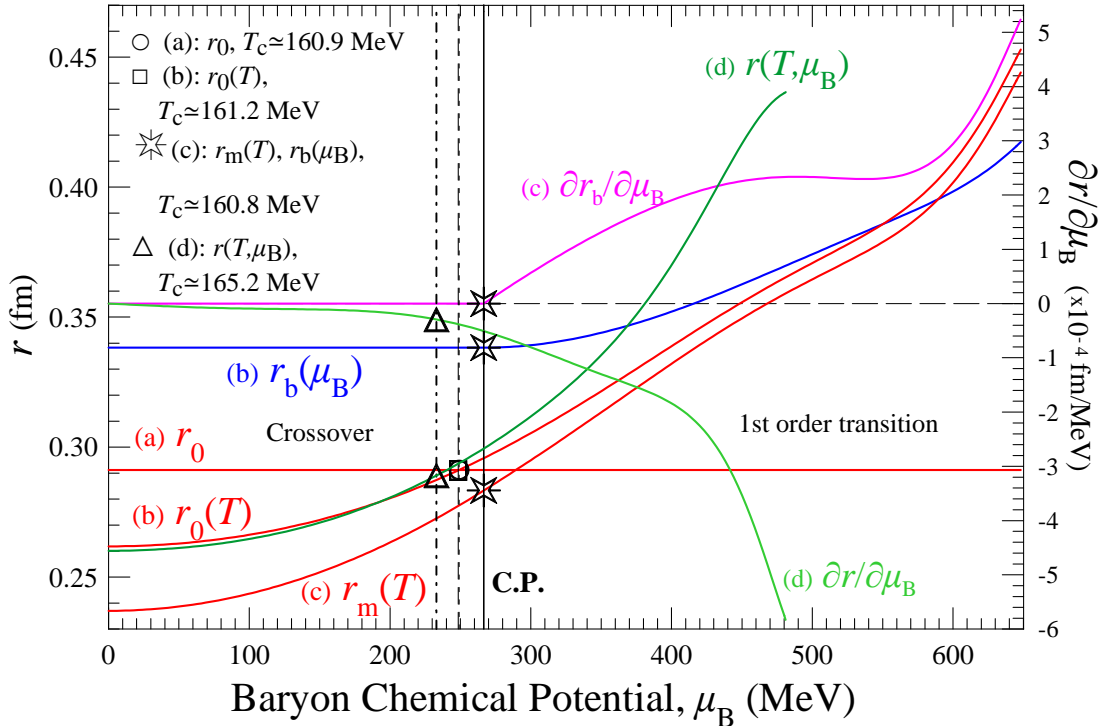


Figure 20: The hadronic radius r_0 (volume model (a)), for the calculations of Fig. 11, the hadronic radius $r_0(T)$ (volume model (b)), for the calculations of Fig. 13, the meson $r_m(T)$ and the baryon $r_b(\mu_B)$ radii (volume model (c)) for the calculations of Fig. 15 and the hadronic radius $r(T, \mu_B)$ (volume model (d)), for the calculations of Fig. 19 (along the respective transition curves), as function of the baryon-chemical potential μ_B (left axis). Also, shown the derivative of the baryon radius $\frac{\partial r_b}{\partial \mu_B}$ for model (c) and the derivative of the common hadron radius $\frac{\partial r}{\partial \mu_B}$ for model (d) with respect to the baryon-chemical potential (right axis). All cases fulfil the additional criterion of section 6.

In Fig. 21 we show for all four models of subsections 5.1-5.4 the volume expansion ratio v_{er} for the same values of T_c as in Fig. 20. We, also, show the corresponding transition curves in the $T - \mu_B$ plane, as well as, the relevant critical points.

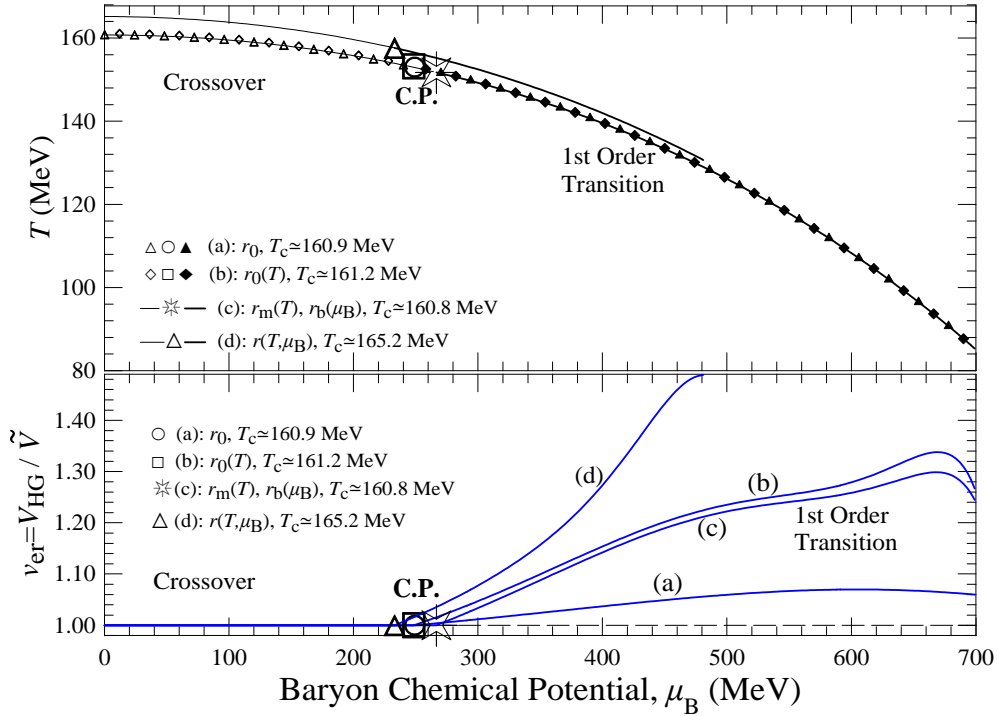


Figure 21: *Lower*: The volume expansion ratio, v_{er} , as function of μ_B for the calculations of Fig. 11, Fig. 13, Fig. 15 and Fig. 19 (volume models (a),(b), (c) and (d) respectively). *Upper*: The transition curve (crossover and 1st order region) with the respective critical point for the calculations of Figs. 11, 13, 15 and 19 in the T, μ_B plane.

6 A criterion for the Critical Point

At the transition line and at low baryon density (crossover region) Hadron Gas consists mainly of mesons. At high baryon density (1st order transition) Hadron Gas consists mainly of baryons. Also, the temperature of the chiral phase transition at zero baryon-chemical potential is of the order of the mass of the lightest meson, the pion. The transition baryon-chemical potential of the chiral phase transition at zero temperature is of the order of the mass of the lightest baryon, the proton. We, therefore, postulate that the attributes of the crossover region are mainly due to mesons, while the attributes of the region of the 1st order transition are mainly due to baryons.

For this reason we calculate the density of quarks (u , d named collectively as q quarks and s quarks) contained in mesons and baryons. We note that both q and s quarks carry baryon number. So, since we are seeking the critical point at positive baryon density, we have to take into account the total density of both q and s quarks which are contained in hadrons, which is

$$n_{qs,m} = n_{HG,mesons} = n_{HG,1} + n_{HG,2} + n_{HG,5} \quad (88)$$

$$n_{qs,b} = 3n_{HG,baryons} = 3(n_{HG,3} + n_{HG,4} + n_{HG,6} + n_{HG,7} + n_{HG,8} + n_{HG,9}), \quad (89)$$

where the index i in the densities $n_{HG,i}$ refers to the respective family of hadrons.

We evaluate the densities $n_{qs,m}$ and $n_{qs,b}$ for the critical points determined through the models (a) (r_0 fixed), (b) ($r_0(T)$), (c) ($r_m(T)$ and $r_b(\mu_B)$) and (d) ($r(T, \mu_B)$). Our results are shown in

Fig. 22. We observe that for model (a) the critical point, which additionally satisfies the equality of the densities of the quarks contained in mesons and baryons, is located at $\mu_{B,cr} \simeq 249$ MeV. The model (b) gives almost equal $\mu_{B,cr} \simeq 248$ MeV, while model (c) evaluates this position at $\mu_{B,cr} \simeq 267$ MeV and model (d) at $\mu_{B,cr} \simeq 233$ MeV.

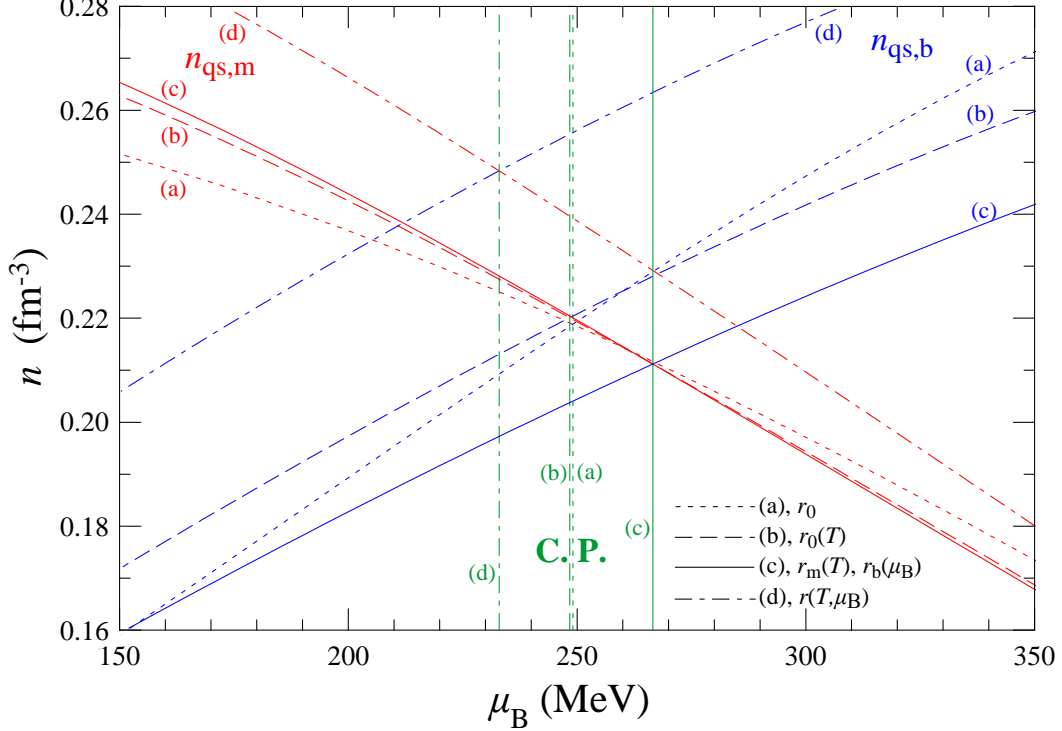


Figure 22: The densities of quarks (up, down q and strange s) contained in mesons m and baryons b of the Hadron Gas as function of the baryon-chemical potential calculated for the different conditions of Fig. 10 (model (a), dotted line), Fig. 12 (model (b), slashed line), Fig. 14 (model (c), continues line) and Fig. 18 (model (d), slashed-dotted line), as function of μ_B . The intersection of the two densities for each model determines a critical point which additionally fulfils $n_{qs,m} = n_{qs,b}$. This occurs for model (a) at $\mu_B \simeq 249.08$ MeV, for model (b) at $\mu_B \simeq 248.41$ MeV, for model (c) at $\mu_B \simeq 266.56$ MeV and for model (d) at $\mu_B \simeq 232.97$ MeV.

It is, also, possible to calculate and compare the densities of q quarks, as well as, the densities of s quarks alone, which are contained in mesons and baryons. However, this entails the exact knowledge of the factors c_1, c_2 for certain hadrons of family 2 with hidden strangeness and content $c_1(u\bar{u} + d\bar{d}) + c_2s\bar{s}$. Also, by dealing with higher densities, that is inclusive densities of q and s quarks instead of separate densities, our results are less affected by any lack of knowledge of the mass spectrum of hadrons.

We remark, further, on the density of the antiquarks \bar{q}, \bar{s} . The density of antiquarks contained in mesons is always equal to the density of quarks contained in the same mesons. However, the density of antiquarks contained in anti-baryons is significantly less than the density of the quarks contained in baryons, since we are in the positive baryon density region. Thus, nowhere in this region the density of antiquarks contained in mesons can become equal to the density of antiquarks contained in anti-baryons.

7 Conclusions

Guided by the lattice calculations which suggest that the QCD chiral restoration is completed, as temperature rises, well before the completion of deconfinement, we develop an effective description of the QCD state for temperatures near and above the chemical freeze-out curve. For temperatures in the region below the chemical freeze-out curve we adopt the hadronic resonance gas with the Bose/Fermi statistics and thermodynamically consistent volume corrections. The chiral phase consists of a few quark condensates, each of which shares the same quark content with a group of hadronic resonances with different masses. Between the two phases the particle number conservation is imposed as a minimum requirement of a phase transition, a condition which leads to the variation of the chiral masses along the transition curve.

We find that the pion particles with their partner resonances play the leading role in transforming the order of the transition from higher order to first order and in developing a critical point. The second family which may affect this transition is the family of nucleons. Thus, the exact knowledge of the specific spectrum of the rest of the hadronic particles is of secondary importance.

The position of the critical point is sensitive to the value of the radii of hadrons. For this reason, we use the Lattice calculations with three quark flavours for the pressure and entropy density below the critical temperature T_c and fit it with the Hadron Gas equation of state in order to determine the hadronic volumes. We, also, link the lattice critical temperature T_c with the freeze-out curve which we consider as our transition curve. We use four models for the hadron volumes, (a) which uses the same radius for all hadrons, constant for all temperatures, (b) which uses a common hadronic radius, which depends on temperature, (c) which uses different radius values for mesons and baryons, depending on temperature and baryon-chemical potential, respectively and (d) which uses a common hadronic radius, which depends on temperature and baryon-chemical potential. Our findings are summarised in Table 2. We observe that the critical point is limited by a maximum value of chemical potential which gradually diminishes from ~ 701 MeV to ~ 382 MeV as we move from model (a) to (d).

	Model (a)	Model (b)	Model (c)	Model (d)
	r_0	$r_0(T)$	$r_m(T), r_b(\mu_B)$	$r(T, \mu_B)$
General solutions				
$T_{ch,0} = T_c$ (MeV)	161.5-155.7	164.4-156.5	163.6-157.5	168.7-161.0
T_{cr} (MeV)	161.5-84.8	164.4-125.0	160.9-137.4	168.7-141.7
$\mu_{B,cr}$ (MeV)	0-701.0	0-497.6	141.5-403.6	0-382.3
$r_{m,cr}$ (fm)	0.301-0.157	0.298-0.253	0.292-0.262	0.294-0.275
$r_{b,cr}$ (fm)	$= r_{m,cr}$	$= r_{m,cr}$	0.343-0.321	$= r_{m,cr}$
Solution which additionally satisfies $n_{qs,m} = n_{qs,b}$				
$T_{ch,0} = T_c$ (MeV)	160.84	161.04	160.73	165.16
T_{cr} (MeV)	153.00	153.21	151.74	157.61
$\mu_{B,cr}$ (MeV)	249.08	248.41	266.56	232.97
$r_{m,cr}$ (fm)	0.2912	0.2911	0.2833	0.2891
$r_{b,cr}$ (fm)	$= r_{m,cr}$	$= r_{m,cr}$	0.3383	$= r_{m,cr}$

Table 2: Summary of the critical point's thermodynamic parameters for the four models of the hadronic volumes considered in this paper.

We, also, calculate for the solutions of the critical point the densities of the quarks which are contained in mesons and baryons, motivated by the gradual increase of baryon density and decrease of meson density, as we move along the transition curve towards higher values of baryon chemical

potential. We find that for all four models which we have used, the solution of the critical point which additionally satisfies equality of the two densities is located at $\mu_{B,cr} \simeq (233-267)$ MeV and $T_{cr} \simeq (152-158)$ MeV. Also, in this case, the hadronic volumes acquire realistic values. In models (a), (b) and (d) where a common volume is used, the hadronic radius is $r \simeq 0.29$ fm. In model (c) this radius is $r_m \simeq 0.28$ fm for mesons and $r_b \simeq 0.34$ fm for baryons.

The group of the chiral QCD states, considerably fewer than the abundance of the hadronic states existing at lower temperatures, can be taken as starting point for the effective description of the EoS at higher temperatures, where quark deconfinement is completed.

References

- [1] J. Cleymans, H. Satz, Z. Phys. C **57** (1993) 135; J. Letessier, A. Tounsi, J. Rafelski, Phys. Lett. B **292** (1992) 417; J. Letessier, A. Tounsi, U. Heinz, J. Sollfrank, J. Rafelski, Phys. Rev. D **51** (1995) 3408; F. Becattini, M. Gaździcki, A. Keränen, J. Manninen, R. Stock, Phys. Rev. C **69** (2004) 024905; J. Cleymans, K. Redlich, Phys. Rev. Lett. **81** (1998) 5284.
- [2] A. Bazavov et. al., (HotQCD Collaboration), Phys. Rev. D **90** (2014) 094503; arXiv:1407.6387 [hep-lat].
- [3] K. Fukushima and T. Hatsuda, Rept. Prog. Phys. **74** (2011) 014001; arXiv:1005.4814 [hep-ph].
- [4] Sz. Borsányi, Z. Fodor, C. Hoelbling, S.D. Katz, S. Krieg, C. Ratti and K.K. Szabó, JHEP (2010) 2010: 73; arXiv:1005.3508 [hep-lat].
- [5] A. Bazavova, N. Brambillab, H.-T. Dingd, P. Petreczkye, H.-P. Schadlere, A. Vairob and J.H. Weber, Phys. Rev. D **93** (2016) 114502; arXiv:1603.06637 [hep-lat].
- [6] A.S. Kapoyannis, A.D. Panagiotou, Eur. Phys. J. C **77** (2017) 736-1.
- [7] T. Hatsuda and M. Prakash, Phys. Lett. B **224** (1989) 11.
- [8] G. Aarts, C. Allton, D. De Boni, S. Hands, B. Jager, C. Prakia and J.-I. Skullerud, JHEP06 (2017) 034.
- [9] L. McLerran and R. D. Pisarski, Nucl. Phys. A **796** (2007) 83; arXiv:0706.2191 [hep-ph].
- [10] A.S. Kapoyannis, Eur. Phys. J. C **51** (2007) 135; *idid* Eur. Phys. J. C **51** (2007) 1013.
- [11] S. Borsányi, Z. Fodor, J.N. Guenther, R. Kara, S.D. Katz, P. Parotto, A. Pásztor, C. Ratti, K.K. Szabó, Phys. Rev. Lett. **126** (2021) 232001; arXiv:2102.06660 [hep-lat].
- [12] A. Bazavov, H.-T. Ding, P. Hegdea, O. Kaczmarek, F. Karsch, E. Laermann, Y. Maezawa, S. Mukherjee, H. Ohno, P. Petreczky, H. Sandmeyer, P. Steinbrecher, C. Schmidt, S. Sharma, W. Soeldner and M. Wagner, Phys. Rev. D **95** (2017) 054504; arXiv:1701.04325 [hep-lat].
- [13] R.V. Gavai and S. Gupta, Phys. Rev. D **78** (2008) 114503.

- [14] S. Datta, R.V. Gavai and S. Gupta, Nucl. Phys. A **904-905** (2013) 883c.
- [15] P. de Forcrand and O. Philipsen, J. High Energy Phys. JHEP01 (2007) 077.
- [16] M.P. Lombardo, J. Phys. G: Nucl. Part. Phys. **35** (2008) 104019.
- [17] G.D. Yen, M.I. Gorenstein, W. Greiner, S.N. Yang, Phys. Rev. C **56** (1997) 2210.
- [18] Sz. Borsányi, G. Endrődi, Z. Fodor, S.D. Katz and K.K. Szabó, JHEP **1207** (2012) 056; arXiv:1204.6184 [hep-lat].
- [19] L. Giusti and M. Pepec, Phys. Lett. B **769** (2017) 385; arXiv:1612.00265 [hep-lat].
- [20] M. Albright, J. Kapusta and C. Young, Phys. Rev. C **90** (2014) 024915; arXiv:1404.7540 [nucl-th].
- [21] M. Tanabashi *et al.* (Particle Data Group), Phys. Rev. D **98** (2018) 030001.
- [22] P.A. Zyla *et al.* (Particle Data Group), Prog. Theor. Exp. Phys. **2020** (2020) 083C01 and 2021 update.
- [23] M. Albaladejo and J.A. Oller, Phys. Rev. D **86**, (2012) 034003.
- [24] J. Cleymans, H. Oeschler, K. Redlich and S. Wheaton, Phys. Rev. C **73** (2006) 034905.
- [25] V. Vovchenko, V.V. Begun and M.I. Gorenstein, Phys. Rev. C **93** (2016) 064906; *ibid* Journal of Physics: Conf. Series **779** (2017) 012080.
- [26] A. Andronic, P. Braun-Munzinger, J. Stachel and M. Winn, Phys. Let. B **718** (2012) 80.
- [27] P. Braun-Munzinger, D. Magestroa, K. Redlich and J. Stachel, Phys. Let. B **518** (2001) 41.
- [28] A. Andronic, P. Braun-Munzinger and J. Stachel, Nucl. Phys. A **772** (2006) 167.
- [29] A. Bohr, B. Mottelson, Nuclear Structure, vol. **1**, Benjamin, New York, 1969, p. 251.
- [30] L.D. Roper, R.M. Wright, B.T. Feld, Phys. Rev. **138** (1964) 190.
- [31] P. Braun-Munzinger, I. Heppe and J. Stachel, Phys. Lett. B **465** (1999) 15.
- [32] M. Marczenko, D. Blaschke, K. Redlich, C. Sasaki, arXiv:1805.06886 [nucl-th]; *ibid*, *ibid* talk at the CPOD-2018 Conference, Corfu, 23-26 September 2018.
- [33] S. Mukherjee, “QCD phase-diagram: searching for criticality”, talk at “Critical Point and Onset of Deconfinement”, Corfu, 2018. <https://indico.cern.ch/event/731446/>.
- [34] K.A. Bugaev, A.I. Ivanytskyi, V.V. Sagun, B.E. Grinyuk, D.O. Savchenko, G.M. Zinovjev, E.G. Nikonov, L.V. Bravina, E.E. Zabrodin, D.B. Blaschke, A.V. Taranenko, L. Turko, Universe **5** (2019) 63.
- [35] V. Vovchenko, M. Gorenstein, C. Greiner, H. Stoecker, Phys. Rev. C **99** (2019) 045204; arXiv:1811.05737 [hep-ph].

- [36] R. Bellwied, C. Ratti, S. Borsányi, P. Parotto, Z. Fodor, J. N. Guenther, S.D. Katz, A. Pásztor, D. Pesznyák, K.K. Szabó, Phys. Rev. D **104** (2021) 094508; arXiv:2102.06625 [hep-lat].
- [37] S. Borsányi, Z. Fodor, J.N. Guenther, R. Kara, S.D. Katz, P. Parotto, A. Pásztor, C. Ratti, K.K. Szabó, Phys. Rev. Lett. **125** (2020) 052001.
- [38] F. Becattini, M. Bleicher, T. Kollegger, T. Schuster, J. Steinheimer, R. Stock, Phys. Rev. Lett. **111** (2013) 082302.